

UV-curable acrylate metal oxide nanocomposite coatings

Citation for published version (APA):

Posthumus, W. (2004). *UV-curable acrylate metal oxide nanocomposite coatings*. [Phd Thesis 1 (Research TU/e / Graduation TU/e), Chemical Engineering and Chemistry]. Technische Universiteit Eindhoven.
<https://doi.org/10.6100/IR575148>

DOI:

[10.6100/IR575148](https://doi.org/10.6100/IR575148)

Document status and date:

Published: 01/01/2004

Document Version:

Publisher's PDF, also known as Version of Record (includes final page, issue and volume numbers)

Please check the document version of this publication:

- A submitted manuscript is the version of the article upon submission and before peer-review. There can be important differences between the submitted version and the official published version of record. People interested in the research are advised to contact the author for the final version of the publication, or visit the DOI to the publisher's website.
- The final author version and the galley proof are versions of the publication after peer review.
- The final published version features the final layout of the paper including the volume, issue and page numbers.

[Link to publication](#)

General rights

Copyright and moral rights for the publications made accessible in the public portal are retained by the authors and/or other copyright owners and it is a condition of accessing publications that users recognise and abide by the legal requirements associated with these rights.

- Users may download and print one copy of any publication from the public portal for the purpose of private study or research.
- You may not further distribute the material or use it for any profit-making activity or commercial gain
- You may freely distribute the URL identifying the publication in the public portal.

If the publication is distributed under the terms of Article 25fa of the Dutch Copyright Act, indicated by the "Taverne" license above, please follow below link for the End User Agreement:

www.tue.nl/taverne

Take down policy

If you believe that this document breaches copyright please contact us at:

openaccess@tue.nl

providing details and we will investigate your claim.

UV-curable acrylate metal oxide nanocomposite coatings

Willem Posthumus

Druk: Universiteitsdrukkerij Technische Universiteit Eindhoven
Kaftontwerp: Willem Posthumus / Paul Verspaget

CIP-DATA LIBRARY TECHNISCHE UNIVERSITEIT EINDHOVEN

Posthumus, Willem

UV-curable acrylate metal oxide nanocomposite coatings / by Willem Posthumus. –
Eindhoven : Technische Universiteit Eindhoven, 2004.

Proefschrift. – ISBN 90-386-2985-0

NUR 913

Trefwoorden: deklagen; mechanische en elektrische eigenschappen /
composietmaterialen / nanocomposieten / acrylic polymers; morfologie / UV-
uitharding / silanen / silica / antimoontinnoxide; ATO / tinnoxide

Subject headings: coatings; mechanical and electrical properties / composite materials /
nanocomposites / acrylaatpolymeren; morphology / UV-curing / coupling agents;
silanes / silica / antimony tin oxide; ATO / tin oxide

UV-curable acrylate metal oxide nanocomposite coatings

PROEFSCHRIFT

ter verkrijging van de graad van doctor aan de
Technische Universiteit Eindhoven, op gezag van de
Rector Magnificus, prof.dr. R.A. van Santen, voor een
commissie aangewezen door het College voor
Promoties in het openbaar te verdedigen
op donderdag 6 mei 2004 om 16.00 uur

door

Willem Posthumus

geboren te Wijnjeterp

Dit proefschrift is goedgekeurd door de promotoren:

prof.dr. R. van der Linde

en

prof.dr. G. de With

Copromotor:

mw.dr. J.C.M. Brokken-Zijp

Table of contents

Chapter 1

Introduction	9
1.1. General introduction	10
1.2. Nanocomposite coatings	11
1.3. Composition of the nanocomposites studied	11
1.4. Scope of this thesis	13

Chapter 2

Grafting of silane coupling agents on the filler nanoparticles	17
2.1. Introduction	18
2.2. Grafting reactions	19
2.3. Experimental	21
2.3.1. Materials	21
2.3.2. Grafting reactions	21
2.3.3. Kinetics measurements	22
2.3.4. Characterisation and quantification of the grafted MPS	23
2.4. Colloidal stability of the particles	23
2.5. Kinetics study by ^{29}Si -NMR	24
2.6. Characterisation of the grafted particles	28
2.6.1. Quantification of the MPS load	28
2.6.2. Solid state ^{29}Si -NMR	32
2.7. Conclusions	33

Chapter 3

Practical aspects of the coating preparation	35
3.1. Introduction	36
3.2. Colloidal stability – theory	36
3.2.1. Thermal energy	37
3.2.2. Particle-particle interactions	37
3.2.3. Particle-matrix interactions	39
3.3. Colloidal stability – consequences for the systems studied	40

3.4.	Consequences of colloidal (in)stability for the preparation of the coatings	41
3.5.	Drying of the coatings	43
3.6.	Adhesion	43
3.7.	Selection of the acrylate resins	44
3.8.	Example of the preparation of ATO filled coatings	45

Chapter 4

UV-curing of the coatings 49

4.1.	Introduction	50
4.2.	Theory of the UV curing kinetics	51
4.2.1.	General kinetics	51
4.2.2.	The effects of crosslinking	52
4.2.3.	Copolymerisation of acrylates and methacrylates	52
4.3.	Experimental	53
4.3.1.	Materials	53
4.3.2.	Characterisation techniques	54
4.4.	Cure of pure acrylates	55
4.5.	Copolymerisation of PEGDA and MPS	56
4.6.	Influence of the particles on the curing kinetics	58
4.6.1.	Absorption of the UV-light by the oxides	58
4.6.2.	Curing of silica filled coatings	59
4.6.3.	Curing of ATO and tin oxide filled coatings	62
4.6.4.	Proposed mechanisms for the retardation of the curing	64
4.7.	Conclusions	66

Chapter 5

Electrical resistivity of the coatings 69

5.1.	Introduction	70
5.2.	Experimental	70
5.3.	Results	73
5.3.1.	Electrical resistivity of ATO filled coatings	73
5.3.2.	Electrical resistivity of tin oxide filled coatings	78
5.4.	Models for the resistivity of composite materials	79
5.4.1.	Model for type I behaviour	79

5.4.2. Type II behaviour	83
5.5. Conclusions	84
Chapter 6	
Mechanical properties of the coatings	87
6.1. Introduction	88
6.2. Experimental	89
6.3. Hardness and elasticity	90
6.3.1. Coatings with a PEGDA matrix	92
6.3.2. Coatings with a TMPTA matrix	95
6.4. Abrasion resistance	97
6.5. Conclusions	99
Epilogue	103
7.1. Aims of this study	103
7.2. Preparation and composition of the coatings	103
7.3. Properties of the coatings	104
7.4. Suggestions for further research	105
Appendix I	
Derivation of the curing rate equation	107
Appendix II	
Electron tunneling	109
Summary	113
Samenvatting	115
Dankwoord	117
Curriculum Vitae	118

Chapter 1

Introduction

1.1. General introduction

Composites are used when a combination of properties is required that cannot be found in a single material. Particularly interesting are combinations of organic polymers and inorganic materials as the properties of the pure components are very distinct. In general organic polymers are flexible, tough, and are easy to process, but they can also be relatively easily damaged, either chemically or mechanically. In contrast, inorganic materials are typically much harder, have better barrier properties, and have a good chemical stability, but are also brittle and are difficult to process. Organic-inorganic composites may yield a combination of these properties, resulting in a hard, tough, and chemically stable and durable material that is still easy to process. However, the combination of organic and inorganic materials may also give a composite that is soft, brittle, unstable, and totally useless.

The properties of a composite are not simply the average properties of its components. Besides the volume fractions of the components, also their size, shape, and the distribution are important. In a composite one component may be enclosed by another component that forms a continuous phase, but it is also possible that the components form continuous phases resulting in interpenetrating networks. Properties like heat conductivity and electrical conductivity are controlled by transport processes through one of the components; consequently a continuous network of the conducting component is highly advantageous. The interactions between the different components may induce changes in the chemical or physical structure of the components, especially in the first few nanometers from the interface⁽¹⁻³⁾. These effects become particularly important when the interfacial area between the different components is large⁽³⁾. The interfacial area increases with decreasing domain size in the composite, and consequently also the properties may change by altering the domain size in a composite. For nanocomposites, with domain sizes of about 10 nm, 1 cm³ of composite may contain several hundred square meters of interface, hence structural changes due to interface effects may affect a large portion of the material⁽³⁾. The addition of a third component that concentrates at the interface and alters the interactions can have strong effects on the composite properties⁽²⁻⁶⁾. The third component may be a surfactant that assembles at the interface by physical adsorption, or it may be a reactive species that is grafted on the surface of the filler or it may even react with both phases forming a chemical bond between the two phases⁽⁵⁾. This modification of the interface is often used to improve the mechanical properties of composites.

1.2. Nanocomposite coatings

The tailoring of properties is especially important for functional coatings. Therefore composites are commonplace in the coatings field. For instance, the addition of inorganic nanoparticles, typically silica or aluminium oxide, to organic coatings can result in a strong increase of the scratch and abrasion resistance^(4,7-12). Although many examples of abrasion resistant nanocomposite coatings can be found (especially in patents), explanations for their good performance are rarely given⁽⁴⁾. For the friction coefficient both increasing⁽¹⁰⁾ and decreasing⁽⁴⁾ values with increasing filler fraction are reported. More agreement is found for the modulus and the toughness that are generally reported to increase with the addition of nanoparticles. In comparison with micrometer-sized particles, a lower volume fraction of nanoparticles is needed to enhance the abrasion resistance and at optimal loadings the performance is considerably better⁽⁴⁾.

Inorganic semiconductor nanoparticles like CdS, TiO₂, and SnO₂ are used for tailoring of optical properties, for instance for increasing the refractive index of coatings or for reflection of UV and IR radiation while remaining transparent in the visible region⁽¹³⁻¹⁵⁾. For optical transparency of composites the domain sizes of regions with different refractive index are extremely important: when the size of these domains is larger than the wavelengths of the light, the light will be scattered and the composites become opaque, but with domains considerably smaller than the wavelengths of the light, the local variation in refractive index is averaged out and the composites are still transparent⁽¹⁶⁾.

Electrically conductive fillers are used for coatings with anti-static or electromagnetic shielding properties^(14,17-19) and for sophisticated materials utilised in a range of electronic devices like pressure and temperature dependent resistors, solar cells, and gas sensors⁽¹⁹⁻²¹⁾. For a high conductivity carbon black and metallic fillers are preferred, but for some of the devices and for transparent materials semi-conductor fillers are required.

1.3. Composition of the nanocomposites studied

In this thesis nanocomposite coatings based on UV curable acrylate matrices with inorganic nanoparticles are studied. The fillers that are used are silica (silicon oxide), tin oxide, and antimony doped tin oxide, with primary particle sizes of about 15, 5, and 7 nm, respectively. Silica is by far the most used nanofiller, both in academic research and in industrial applications; as such it is also the filler for which most literature data are available. Tin is in the same group in the periodic table as silicon, thus one may

expect strong similarities between the chemical behaviours of their oxides. This enables the application of the same preparation procedures for composites containing silica or tin oxide. An interesting difference between tin oxide and silica is that the band gap in tin oxide is only 3 eV, which makes it a semiconductor, whereas silica has a band gap of 9 eV, which makes it an insulator. By doping tin oxide with antimony the number of electrons in the conduction band is enlarged resulting in an increased electrical conductivity, whereas optical transparency is retained⁽²²⁾. This makes antimony doped tin oxide (ATO) a very interesting filler for lowering the electrical resistivity of insulating matrices^(22,23).

The used inorganic fillers are very hydrophilic and cannot be dispersed directly in low-polar acrylate resins. To improve the compatibility of the fillers with the acrylate matrix, the surface of the fillers can be treated with silane coupling agents⁽⁵⁾. In this thesis the silane coupling agents 3-methacryloxypropyltrimethoxysilane (MPS) and *n*-octyltrimethoxysilane (OTS) are used. MPS has reactive groups for both the filler and the matrix and may form a chemical link between the two phases. OTS is used as a reference as it has only a reactive group for the filler particles, but it cannot react with the matrix.

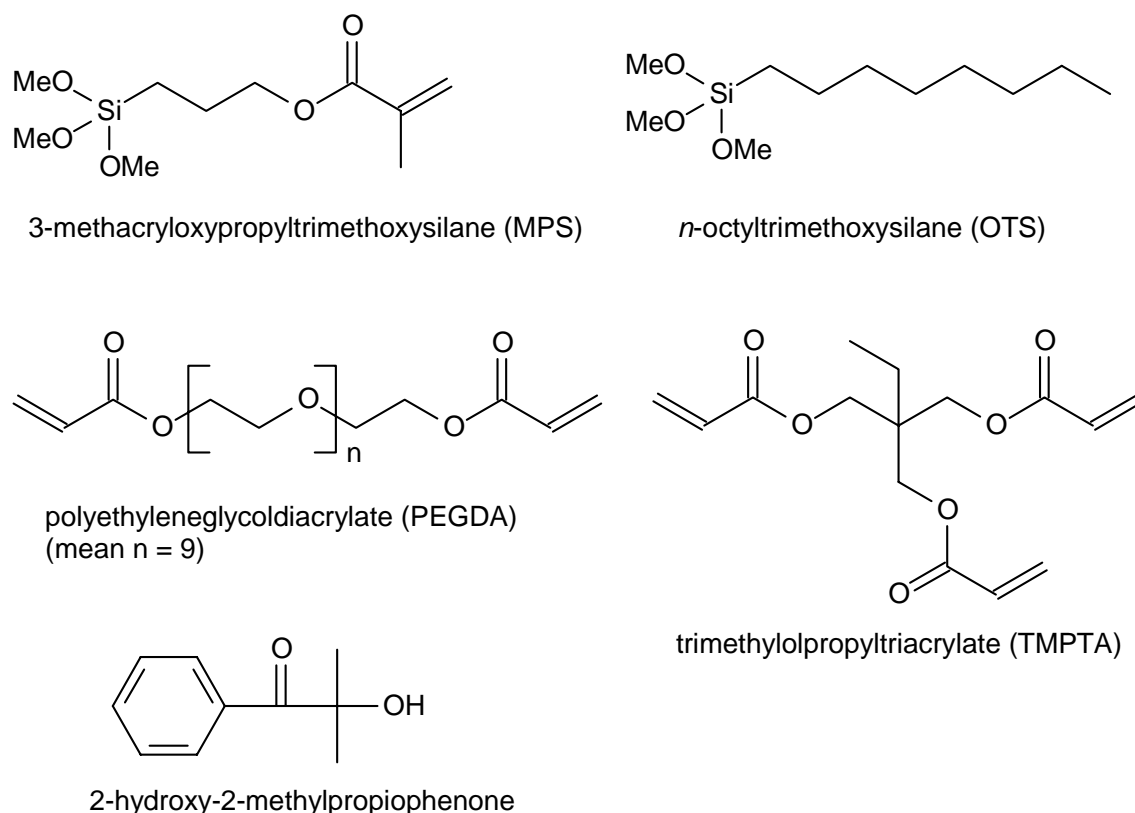


Figure 1.1 Chemical structures of components used in the coating formulations.

For the matrix three different acrylate resins are used: PEGDA, TMPTA, and Ebecryl 745, all with 2-hydroxy-2-methylpropiophenone as photoinitiator. The choice for these resins is based on mainly practical grounds. PEGDA is a diacrylate with a polyethylene glycol spacer that gives a rubbery matrix after curing. TMPTA is a triacrylate with a very small spacer that gives a highly cross-linked glassy matrix after curing. Ebecryl 745 is a commercial acrylate resin based on an acrylate backbone with unsaturated acrylate side-groups diluted with 25 % HDDA and 25 % TPGDA; also this resin gives a glassy matrix after curing and has a good overall performance. The curing of the resins takes place by a free radical polymerisation that is initiated by the photoinitiator upon exposure to UV light. The use of this curing mechanism has the advantage that during the preparation and application of the coating mixtures (in the absence of UV light) no reaction takes place.

A coating needs a substrate; in this study polycarbonate (Lexan 9030, GE Plastics) was used. This substrate was selected as adhesion of the coatings on polycarbonate is achieved relatively easy, and because there is a strong commercial interest in this coating-substrate combination. Polycarbonate is an interesting material to replace glass in numerous applications as it is highly transparent, flexible, has a high impact resistance, and is easy to process. However, polycarbonate has also unwanted properties like a low scratch and abrasion resistance and accumulation of electrostatic charge. The coatings that are described in this thesis are intended to correct these undesired properties.

1.4. Scope of this thesis

The central subjects in this thesis are the surface modification of the filler particles and the effects of this surface modification on the composite properties. The grafting of the silane coupling agents on the filler particles is described in chapter 2. Attention is paid to the kinetics of the reactions involved and the analysis of the amount and structure of the groups grafted on the surface of the particles. In chapter 3 the practical problems that are encountered during the preparation of the coatings are described. Also a short introduction in colloidal stability of nanoparticles is given as this is the main parameter that determines experimental success or failure, and it also influences some of the final coating properties. Chapter 4 deals with the curing of the coatings by means of a UV-initiated radical polymerisation. The involvement of silane coupling agents in the curing and the influence of the particles on the curing kinetics are discussed. The effect of electrical conducting fillers on the electrical resistivity of the

coatings and the effect of the fillers on the mechanical properties of the coatings are described in chapters 5 and 6. For both properties the relationships with filler fraction and with the amount of grafted silane coupling agents are discussed.

Reference List

1. P. S. Theocaris, *Colloid and Polymer Science*, 263, 863-872 (1985).
2. R. Rethon, Particulate-filled polymer composites (Longman Scientific & Technical, Harlow), pp. XII, 375 (1995).
3. N. S. Enikolopyan, M. L. Fridman, I. O. Stalnova, V. L. Popov, *Advances in Polymer Science*, 96, 1-67 (1990).
4. M. Z. Rong, M. Q. Zhang, G. Shi, Q. L. Ji, B. Wetzell, and K. Friedrich, *Tribology International*, 36, 697-707 (2003).
5. E. P. Plueddemann, Silane coupling agents (Plenum Press, London), pp. IX, 235 (1982).
6. J. W. ten Brinke, V. M. Litvinov, J. E. G. J. Wijnhoven, J. W. M. Noordermeer, *Macromolecules*, 35, 10026-10037 (2002).
7. D. R. Olson, and K. K. Webb, Method of preparing curable coating composition from alcohol, colloidal silica, silylacrylate and multiacrylate monomer. *US4491508*, General Electric Company (1985).
8. S. Sepeur, N. Kunze, B. Werner, H. Schmidt, *Thin Solid Films*, 351(1,2), 216-219 (1999).
9. J. Gilberts, and A. H. A. Tinnemans, *RAD news*, 24, 7-10 (1998).
10. S. Frings, Organic-inorganic hybrid coatings, thesis, TU Eindhoven (1999).
11. V. A. Soloukhin, Nanocomposite hybrid coatings on polycarbonate, thesis, TU Eindhoven (2003).
12. M. Misra, A. Guest, M. Tilley, *Surface Coatings International*, 594-595 (1998).
13. L. L. Beecroft and C. K. Ober, *Chemistry of Materials* 9, 1302-1317 (1997).
14. J. Sun, L. F. Francis, L. F. Francis, *Journal of Polymer Science part B-Polymer Physics*, 41, 1744-1761 (2003).
15. J. E. Mark, *Polymer Engineering and Science*, 36(24), 2905-2920 (1996).

16. G. Mie, *Annalen der Physik*, 25(3), 377-445 (1908).
17. J. Texter, and M. Lelental, *Langmuir*, 15(3), 654-661. (1999).
18. S. Radhakrishnan, *Polymer Communications*, 26, 153-157 (1985).
19. R. Strumpler, and J. Glatz-Reichenbach, *Journal of Electroceramics*, 3(4), 329-346 (1999).
20. F. Carmona, and J. Ravier, *Carbon*, 40, 151-156. (2002).
21. D. Y. Godovsky, *Advances in Polymer Science*, 153, 163-205 (2000).
22. K. L. Chopra, S. Major, and D. K. Pandya, *Thin Solid Films*, 102(1), 1-46 (1983).
23. C. C. Anderson, Y. Wang, and M. D. DeLaura, Imaging element comprising an electrically-conductive layer. *US5912109*, Eastman Kodak Company (1999).

Chapter 2

Grafting of silane coupling agents on the filler nanoparticles*

Synopsis

In this chapter the grafting of silane coupling agents on the filler nanoparticles is described. For 3-methacryloxypropyltrimethoxysilane (MPS) the kinetics of the involved reactions as well as the amount and structure of the groups grafted on the surface of the particles were studied. The grafting of MPS on the fillers was followed with ^{29}Si -NMR. It was found that the hydrolysis of the methoxy groups of MPS is the rate-determining step. As the hydrolysis is base-catalysed, the reactions proceed faster in dispersions with a high pH. The kinetics measurements also revealed that reaction of MPS with ATO is faster than homocondensation. Solid state NMR revealed that chemical bonds are formed between the MPS and the particles. Quantification of the amount of MPS on the particles by FTIR revealed that the maximum amount of MPS bonded to silica or tin oxide corresponds to a monolayer with a parallel orientation to the surface of the particle, whereas for ATO a 30-50 % lower value was found. When MPS to particle ratios are lower than the amount needed for monolayer coverage of the particles, the majority of the MPS is bonded to the particles.

* *The contents of this chapter are published in the Journal of Colloid and Interface Sciences 269 109-116 (2004)*

2.1. Introduction

In this chapter the grafting of silane coupling agents on the silica, tin oxide, and antimony doped tin oxide (ATO) nanoparticles is described. These metal oxides have polar surfaces and therefore they have poor interactions with the acrylates that are used as matrix material for the coatings. Due to this large difference in polarity, the fillers are not compatible with the acrylates and it is not possible to make homogeneous coatings. The compatibility between the fillers and the acrylate can be enhanced by grafting organic groups on the surface of the fillers. For this purpose a special class of chemicals is available: silane coupling agents. Silane coupling agents have a silicon centred group that can form chemical or physical bonds with a metal oxide surface, and they have an organic group for a good compatibility with organic materials. The organic group may be a simple alkyl chain but it may also contain a functional group, such as an amine, an epoxy, or a methacrylate group. This organo-functional group can be used for further reaction with other organic materials. A silane coupling agent that is effective in stabilising metal oxide fillers in an UV curable acrylate matrix is 3-methacryloxypropyltrimethoxysilane (MPS). The methacrylate group of the MPS can participate in the curing reaction of the acrylate matrix; consequently MPS can form a chemical link between the filler and the matrix. This link may be beneficial for the mechanical properties of the coatings. Furthermore MPS has become one of the most important commercially available silane coupling agents; it is relatively inexpensive and a considerable amount of literature data is available for this compound. Therefore MPS was selected for the surface modification of the metal oxide fillers used in this work.

An important question is how much MPS is required to cover the surface of the particles. Theoretical calculations⁽¹⁾ yield two estimates, depending on the orientation of the MPS molecules (see figure 2.1). If the molecule is considered as a rod with a

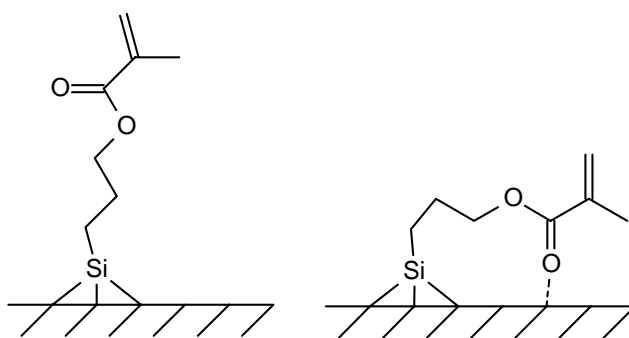
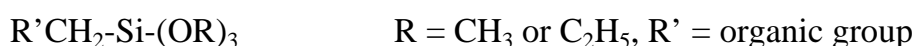


Figure 2.1 Grafted MPS with perpendicular and parallel orientation.

perpendicular orientation to the surface, it is estimated that $6.9 \mu\text{mol}/\text{m}^2$ of MPS is needed for a monolayer. If the MPS is oriented parallel to the surface, which might be induced by hydrogen bonding between the MPS-carbonyl and a hydroxyl group of the oxide, only $3.0 \mu\text{mol}/\text{m}^2$ is needed for a monolayer. However, these estimates are based on one completely filled monolayer. The real values can deviate from these estimates due to incomplete coverage or as a result of the formation of multilayers. In literature most studies describe the modification of silica while only a few consider the modification of other metal oxides. Only a part of these studies mention the quantitative amount of grafted molecules⁽²⁻⁸⁾. The experimentally determined maximum values for the surface coverage of oxides by MPS range from $2.8 \mu\text{mol}/\text{m}^2$ to $7.5 \mu\text{mol}/\text{m}^2$, depending on the type of metal oxide. Miller and Ishida⁽¹⁾ reported a coverage of $2.8 \mu\text{mol}/\text{m}^2$ for lead oxide and clay, while Abboud *et al.*⁽⁹⁾ obtained a surface coverage of $4.6\text{-}7.5 \mu\text{mol}/\text{m}^2$ for aluminium oxide and titanium oxide particles. For silica Nishiyama *et al.*⁽⁶⁾ reported a value of $3.8 \mu\text{mol}/\text{m}^2$. Gellermann *et al.*⁽³⁾ prepared core-shell particles with a silica core and a tin oxide shell on which they grafted $1.0 \mu\text{mol}/\text{m}^2$ MPS with an efficiency of $\sim 85\%$. Unfortunately they did not describe grafting with higher MPS loadings. Quantitative information regarding the maximum amount of MPS that can be grafted on tin oxide or antimony doped tin oxide particles is not available in literature.

2.2. Grafting reactions

MPS and the other silane coupling agents that are used in this study are represented by the general formula:



The C-Si bond is relatively stable and will not react under ambient conditions. The Si-OR bond, however, is easily hydrolysed with the formation of a silanol group and an alcohol as a result:



The hydrolysis reaction is reversible, and the reverse reaction can also proceed with other alcohols. However, typically these reactions are performed with a large excess of water and in this case virtually all alkoxy groups on the silane are hydrolysed. The hydrolysis reaction is catalysed both by acid and base and the minimum hydrolysis rate is found at pH 7⁽²⁾. The silanol group can react further in condensation reactions with

hydroxyl or alkoxy groups that belong to a metal oxide surface (M-OH) or to another silane unit:



As the used silanes have three alkoxy groups they can react with up to three other molecules and form oligomers or polymers. The condensation reactions are also catalysed by acid and base. For the homocondensation of two silane monomers the minimum rate is found at pH 4.5, which is the isoelectric point of the silanol group⁽²⁾.

A simplified reaction scheme for the grafting of MPS on the particles is given in figure 2.2. Scheme A shows the hydrolysis of MPS; this reaction can take place for each Si-OCH₃ group irrespective the reactions the MPS unit has already undergone. Scheme B shows the grafting on the oxide. Not only MPS monomers, but also dimers and higher oligomers of MPS may react with the oxide surface. Scheme C shows the

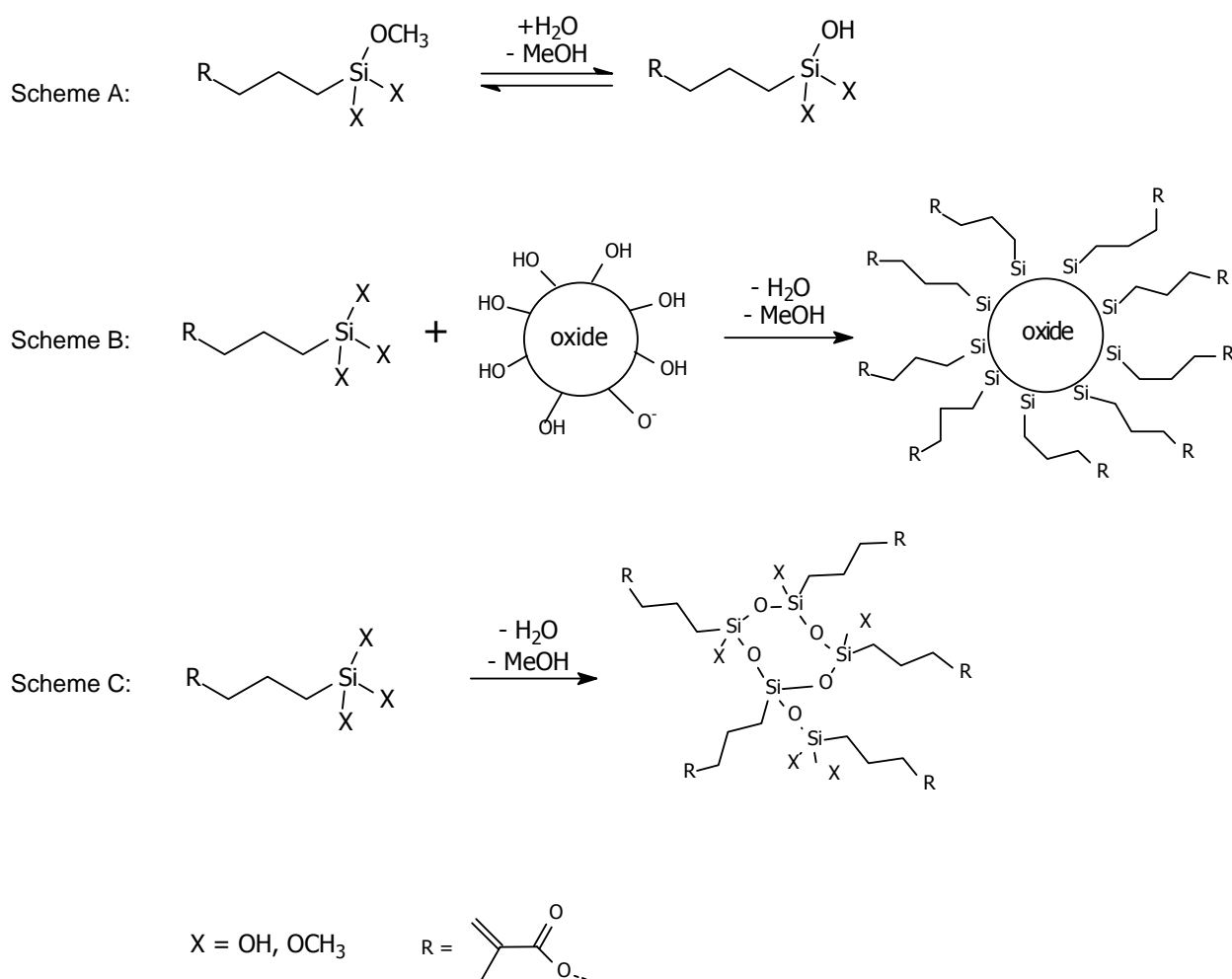


Figure 2.2 Reaction schemes for the grafting of MPS onto metal oxide particles.

homocondensation of MPS, with the intermediates omitted. The grafting (scheme B) and the homocondensation (scheme C) compete with each other for the hydrolysed MPS. Moreover, if the homocondensation is faster than the grafting reaction, the MPS may no longer be available for reaction with the inorganic surface. Methods to suppress this homocondensation, such as working under anhydrous conditions or working at pH 4.5 where the condensation of trifunctional silanes is negligible⁽²⁾, cannot always be used as they may be in conflict with the colloidal stability of dispersed inorganic particles. Consequently, it is possible that a major part of the MPS forms homocondensates and that only a fraction of the added MPS is grafted on the inorganic surface.

2.3. Experimental

2.3.1. Materials

The tin oxide (TO) dispersion in water was donated by Nyacol (USA). This dispersion (SN-15CG) is amine-stabilised at pH 10, and has a solid content of 15 wt%. TEM images showed spherical particles of about 5 nm in rather open secondary aggregates. The antimony doped tin oxide (ATO) dispersion in water was obtained from LWB-Eindhoven (the Netherlands). This dispersion has a solid content of 12 wt% and a pH of 7, the doping level is 16 mol%. TEM images showed spherical particles of 5-10 nm in rather open secondary aggregates. The amine-stabilised silica dispersion in water (Ludox AS-30) was obtained from Aldrich. This dispersion has a solid content of 30 wt%, and a pH of 9.5. TEM images showed spherical particles of about 15 nm. 3-Methacryloxypropyltrimethoxysilane (MPS) was supplied by ABCR. Methanol and *n*-propanol (both of AR grade) were obtained from Biosolve. All materials were used as received.

2.3.2. Grafting reactions

In a typical modification reaction the aqueous dispersion, containing ATO, TO or silica, was mixed with methanol or a mixture of water and methanol (see table 2.1) to ensure colloidal stability of both the modified and unmodified particles. The desired amount of MPS was added after which the mixture was heated to reflux (approx. 70 °C) for at least 4 hours. At the end of the reaction, the mixture was allowed to cool down and was split into two parts for analysis.

One part of the reaction mixture was dried by solvent evaporation at 40-50 °C at reduced pressure, resulting in a mixture of the particles and all the added MPS (grafted, monomers, homocondensates, see figure 2.2). These samples are further re-

	TO	ATO	Silica
Dispersion (g)	20	20	10
Water (g)	40	-	-
Methanol (g)	150	50	25
Reflux time (hrs)	4	24	4
MPS (g/g particle)	0.03 – 0.58	0.04 – 0.36	0.10 – 0.85

Table 2.1 Overview of the different types of experiments.

ferred to as the ‘dried’ samples. The other part of the reaction mixture was 4-5 times diluted with *n*-propanol to improve the solubility of the homocondensates. This sample was centrifuged at 20.000 rpm for 2 hours at room temperature. The clear supernatant, with the homocondensates and possible unreacted MPS, was decanted from the solid deposit comprising the particles with the grafted MPS. These samples of solid deposit are further referred to as ‘centrifuged’ samples. Subsequently both types of samples were dried at 40 °C in vacuo for at least 16 hours.

2.3.3. Kinetics measurements

²⁹Si-NMR spectroscopy was used to study the kinetics of the reactions given in figure 1. To the reaction mixtures as given in table 1, 0.6 wt% chromium acetylacetonate (Aldrich) was added as a relaxation agent, 5 wt% DMSO-d₆ was added as a deuterium source to lock the signal, and trimethylsilylethanol (supplied by ABCR, 33 wt% of the MPS content) was added as an internal reference. To enable increasing the MPS concentration without changing the MPS / ATO ratio, the aqueous ATO dispersions were concentrated to 25 wt% solid content. This increased concentration was needed to improve the signal to noise ratio to a level where the reactions could be followed quantitatively.

A Varian 500 MHz broadband NMR spectrometer with a 10 mm probe was used to collect the spectra. Spectra were continuously recorded and scans were averaged in blocks of 5 minutes up to 12 hours collecting time. The middle of each block was taken as the spectrum time. The size of a block was a compromise between the desired signal to noise ratio and the reaction progress in that time. To ensure that sufficient data points were taken, the block size was always shorter than the half-life time ($t_{1/2}$) of the hydrolysis of the MPS.

2.3.4. Characterisation and quantification of the grafted MPS

The grafted MPS was characterised using FTIR measurements and solid state ^{29}Si -MAS-NMR spectroscopy. For both techniques the ‘dried’ and ‘centrifuged’ samples as described in subsection 2.3.2 were used. The solid state ^{29}Si -MAS-NMR measurements were performed on a Bruker DMX500 spectrometer equipped with a 7 mm MAS probe head. For FTIR measurements KBr pellets were prepared using the ‘dried’ and ‘centrifuged’ samples and IR spectra were taken on a BIORAD FTS6000 spectrometer.

For the quantification of the grafted MPS the ratio between the surface area of the peaks associated to MPS and of the peak of the oxide was determined ($[A_{\text{MPS}}/A_{\text{oxide}}]_{\text{exp}}$). This ratio was measured as a function of the MPS concentration (g MPS / g oxide) in the initial reaction mixture. The peaks relevant for analysis are illustrated in figure 2.6. The ‘dried’ samples were used to make a calibration line for determination of the amount of MPS that was present in the centrifuged samples. The slope of this calibration line (C), a straight line, was used for the calculation of the amount of MPS in the ‘centrifuged’ samples.

To calculate the surface coverage, in $\mu\text{mol}/\text{m}^2$, the specific surface area of the untreated particles was determined with BET surface area analysis using a Micromeritics Tristar, with N_2 as the adsorbent gas. The obtained values for ATO, tin oxide, and silica were respectively 121, 182, and 191 m^2/g , with an experimental error of about 8%. Assuming perfect spheres with a density of 6.9 g/cm^3 for ATO and tin oxide and 2.2 g/cm^3 for silica, these values would represent pore-free particles with a size of 7, 5, and 14 nm, respectively. TEM pictures showed particles of similar size.

The surface coverage of the particles was calculated using:

$$\Gamma = \frac{[A_{\text{MPS}} / A_{\text{oxide}}]_{\text{exp}}}{C \cdot M_{\text{MPS}} \cdot \text{BET}} \cdot 10^6 \quad [1]$$

where Γ is the surface coverage in $\mu\text{mol}/\text{m}^2$, $[A_{\text{MPS}}/A_{\text{oxide}}]_{\text{exp}}$ is the ratio of the surface area of the peaks associated to MPS and of the peak of the oxide, C is the slope of the calibration line in g oxide / g MPS, M_{MPS} is the molar mass of MPS (248.35 g/mol), and BET is the measured BET surface area in m^2/g .

2.4. Colloidal stability of the particles

The nanoparticles that were used in this study were already dispersed in water when they were supplied. However, pure water is not a good solvent for the silane

coupling agents that are used in this study. For a successful grafting of the silane coupling agents on the particles a one phase system is desired. Moreover, after the grafting, the particles have an apolar surface with the consequence that also the particles are no longer compatible with water. Thus the polarity of the water had to be lowered to enhance the solubility of the silane coupling agents and to increase the colloidal stability of the grafted particles. This can be done by the addition of alcohols like methanol, ethanol, and propanol. However, if too much alcohol is added the stability of the dispersion is affected and the particles start to gel. The maximum amount of methanol that can be added to the dispersions before gellation occurs is considerably larger than the maximum amount of ethanol that can be added, and the maximum amount of ethanol is higher than the maximum amount of propanol. In the case of the tin oxide dispersion as supplied, the amount of alcohol that can be added is too low to enable dissolving the silane coupling agents. The required alcohol concentration for dissolving the silane coupling agents can only be reached by decreasing the tin oxide concentration. At lower tin oxide concentrations colloidal stability is also maintained at higher alcohol to water ratios. In practice, after threefold dilution of the tin oxide dispersion, sufficient methanol can be added to dissolve the silane coupling agents.

2.5. Kinetics study by ^{29}Si -NMR

To gain more insight into the competition between the grafting reactions and the homocondensation, and to ensure that the reaction conditions and reaction time were sufficient to complete the grafting process, a kinetics study was performed by ^{29}Si -NMR. To distinguish between the different hydrolysis and condensation states that MPS can have during the whole process the notation MPS(x,y) is used, where x represents the number of hydroxy groups on the silicon and y represents the number of Si-O-Si bonds formed by condensation with another MPS unit. As the ^{29}Si -NMR signal is weak and the MPS concentrations are low, many scans have to be combined and averaged to get a reasonable signal to noise ratio. For the MPS(0,0) (unreacted) this implied that blocks of 5 to 10 minutes of scanning time were needed to observe a significant signal. These blocks were short enough to enable following the disappearance of MPS(0,0) in all experiments with silica and ATO. For the intermediates 30 minutes to several hours of scanning time was needed as they appeared in lower concentrations or yielded broader peaks. Consequently, only for the experiments where the reactions were relatively slow the formation processes of the intermediates and final products could be monitored.

The experiment that gave the most accurate data was the modification of ATO at 25 °C. In this experiment the reactions were very slow which permits the use of scanning blocks of 12 hours. Due to the large number of scans acceptable integrals over all peaks could be obtained. Figure 2.3 shows the averaged spectrum taken between 48 and 60 hours after the start of the reaction. The starting material MPS(0,0), the intermediates, and the homocondensates are all visible in this stage of the reaction. Figure 2.4a shows the progress of the hydrolysis of the MPS(x,0). The MPS(0,0) disappears with an exponential decay, which suggests pseudo-first order kinetics for the first hydrolysis step. The half-life time ($t_{1/2,ATO}$) for this decay is found to be 16.4 hours. The product of this first hydrolysis step, MPS(1,0), is visible in the NMR-spectra, but never reaches a high concentration. Also the MPS(2,0) and MPS(3,0) are only present in small quantities. This implies that at least one of the next steps, the grafting or the condensation, is faster than the hydrolysis.

The progress of the condensation is shown in figure 2.4b. It can be observed that also in the case of condensation, the concentrations of the intermediates, MPS(x,1) and MPS(x,2), remain low. As the intermediates never reach a high concentration, it is concluded that the first step of the reaction, the hydrolysis of MPS(0,0), is the rate-determining step.

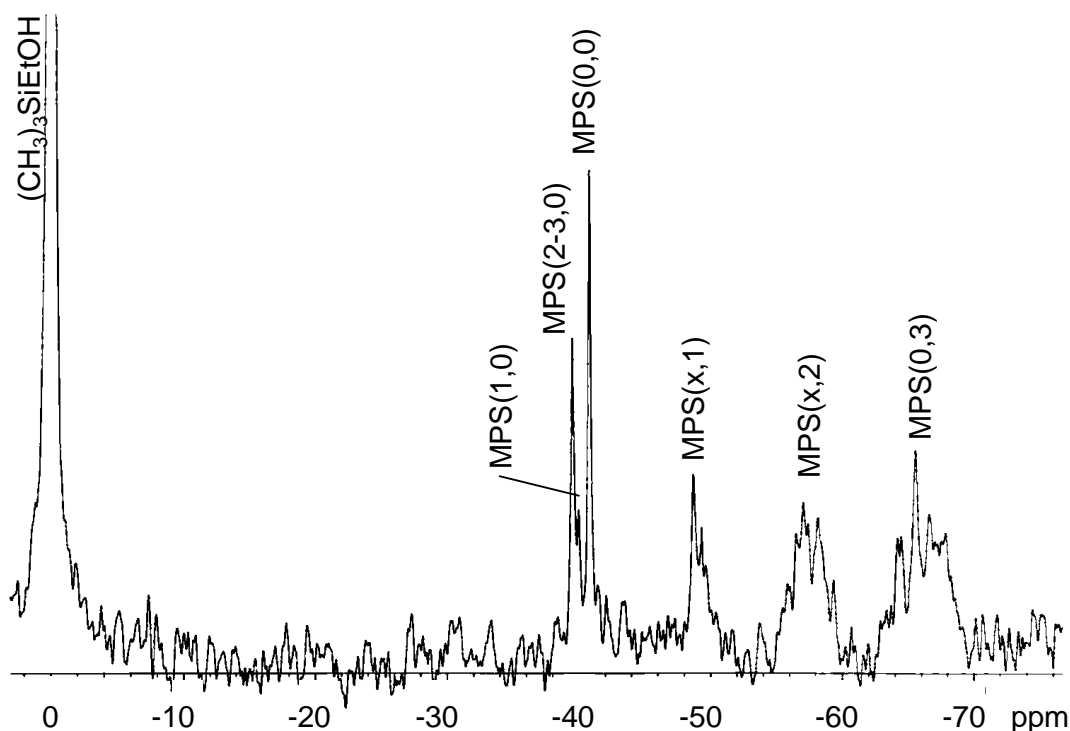


Figure 2.3 ^{29}Si -NMR spectrum taken between 48 and 60 h reaction time during the grafting of MPS onto ATO at 25 °C, ratio MPS/ATO = 0.21 g/g.

When the MPS is grafted to a particle, it becomes immobile and consequently it will give a much weaker NMR-response. As a result, the sum of MPS related signals will decrease. Such a decrease in the sum of the signals gives an indication for the amount of grafted MPS. In figure 2.4b one can see that the sum of the signals decreases by about 30 % in the first 30 hours and then remains more or less constant. This implies that the grafting of the particles takes place in the first stages of the reaction, thus the grafting proceeds faster than the homocondensation of the MPS. In this

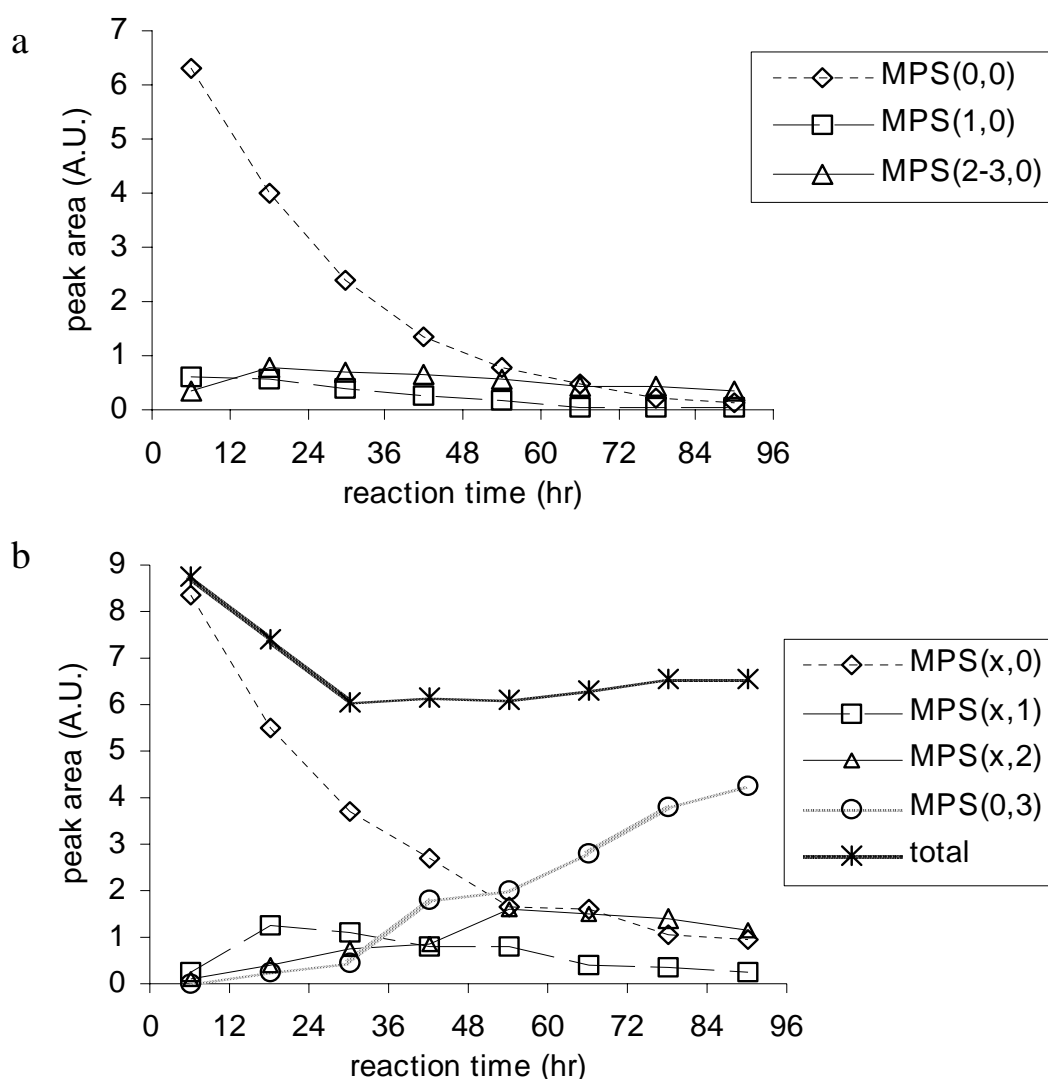


Figure 2.4 Quantification of starting material, intermediates and products during the modification of ATO at 25 °C, divided in hydrolysis of the MPS monomer (a) and the formation of homocondensates (b). Grafted MPS gives no signal in this experiment and is consequently quantified by the decrease of the sum of the signals.

experiment 0.21 g MPS / g ATO was used, thus the 30 % decrease equals an amount of 0.06 g MPS / g ATO. Using a specific surface area of 121 m²/g, that was determined with BET adsorption measurements for ATO, a coverage of 2 μmol MPS per m² ATO surface is calculated.

For the modification reactions of silica and TO, the reactions proceeded much faster when compared to the ATO modification. Consequently, the scanning time per block had to be reduced resulting in spectra with a lower signal to noise ratio. A good quantification of the intermediates is not possible, but verification of the general trends was still possible. As the peaks for MPS(1,0), MPS(2,0), MPS(3,0), and MPS(x,1) are rather sharp, relative low concentrations of these intermediates would also give a significant signal. However, significant signals of these intermediates were not observed in any of the experiments, which indicates that in all experiments the hydrolysis was the rate determining step and not the condensation.

As a reference experiment the reactions of MPS in the typical reaction mixture at pH 9.5 but without particles were followed. The concentration of MPS could be taken relatively high as it was not linked to the concentration of particles. The formation of the intermediates and of the homocondensates showed the same course as in the experiment with ATO. Only the relative intensity of the homocondensate signals was higher as no MPS was consumed by particles.

As the first hydrolysis of MPS is the rate determining step, the decay of the MPS(0,0) signal can be used to give an estimate of the overall progress of the reactions. Moreover, as only one peak is followed, it is allowed to use peak height instead of peak area for the quantification of the MPS(0,0). Peak height determination is less sensitive to noise than the peak area determination; therefore the block times could be reduced to 5 minutes. The MPS(0,0) consumption in the experiments with silica particles showed also an exponential decay, but now with a half-life time ($t_{1/2, \text{silica}}$) of approximately 38 times shorter than $t_{1/2, \text{ATO}}$. However, for the hydrolysis of MPS the temperature dependence of the reaction rate was the same, as illustrated by the slopes in the Arrhenius-plots (see figure 2.5). The difference in reaction rate might be explained by the pH of the particle dispersion used. It is known that OH⁻ catalyses the hydrolysis of MPS, thus the higher pH of the silica dispersion probably caused the faster hydrolysis. Increasing the pH of the ATO dispersions should result in a higher overall reaction rate for the grafting of MPS on ATO. Experiments to test this theory unfortunately failed as addition of base caused coagulation of the ATO. The reflux temperature of the reaction mixtures is 70-75 °C. Extrapolation of the fitted lines in the

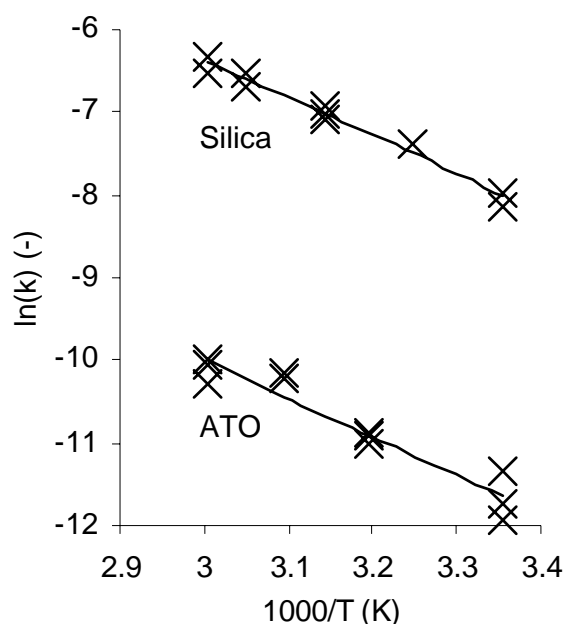


Figure 2.5 Arrhenius plots of MPS hydrolysis in the presence of ATO or silica.

Arrhenius plots gives half-life times at reflux temperature of approximately 4 minutes for the hydrolysis of MPS(0,0) in silica dispersions and 2½ hours for the hydrolysis in ATO dispersions. Both fitted lines correspond to an activation energy of 37.8 kJ/mol.

Monitoring the reactions in the TO dispersion was not possible due to the low concentration of the reactants and the high reaction rates. Only a rough estimation at 25 °C could be made, resulting in a half-life time ($t_{1/2,TO}$) of 15-30 minutes. Considering the effect of the pH found on the reaction rates in the silica and ATO dispersions this estimated half-life time is in line with expectations.

2.6. Characterisation of the grafted particles

2.6.1. Quantification of the MPS load

The signals of TO and ATO in the infrared spectra are well separated from the peaks associated with MPS(x,y). The TO and the ATO have a large peak at 600 cm^{-1} and some small peaks at 1400 and 1630 cm^{-1} , the latter ones can be assigned to associated water. The MPS has several well-separated peaks in the range of 800 - 1800 cm^{-1} of which most are assigned to groups that do not participate in the grafting or condensation reactions (figure 2.6). The intensity of the used peaks is only dependent on the concentration of MPS, irrespective whether MPS has reacted with the particles, has formed homocondensates, or has not reacted at all. With increasing MPS concentration the selected peaks (assigned * in figure 2.6) of MPS should grow linearly relative to

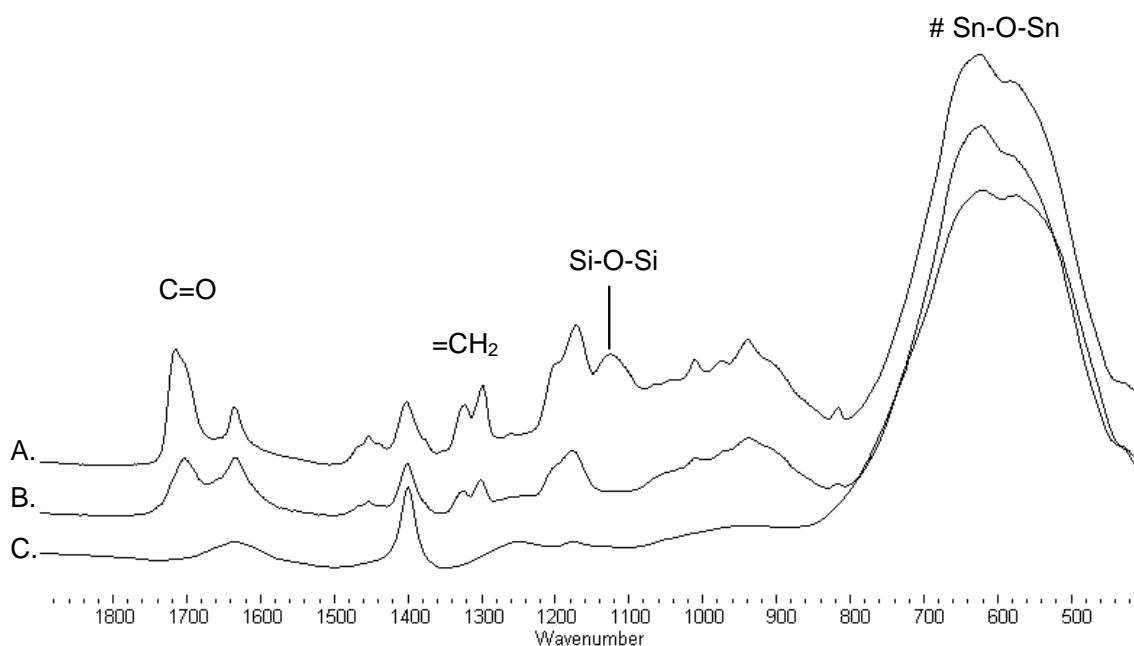


Figure 2.6 FTIR-spectra of TO treated with 0.16 g MPS / g TO.

A: 'dried' sample, B: 'centrifuged' sample, C: untreated tin oxide,

* MPS peaks used for quantification, # TO peak

the peak of the oxide (assigned #). This linear relation was found for the 'dried' samples (dried reaction mixture, consisting of the particles with the grafted MPS and the homocondensates). Consequently, a reliable calibration line for the measurement of the MPS concentration in the 'centrifuged' samples (deposit of the centrifuged reaction mixture, consisting of the particles with the grafted MPS but without the homocondensates) can be made. The main peak of silica (1100 cm^{-1}) is positioned in the middle of the MPS spectrum, thus only a few peaks do not overlap with this silica peak. However, with the remaining peaks still a good calibration line for the MPS / silica ratio could be made.

When a large amount of MPS was added to the reaction mixtures containing TO or ATO particles, a new peak appears at 1120 cm^{-1} in the 'dried' samples. This peak is assigned to the Si-O-Si bonds that are present in MPS-homocondensates⁽¹⁰⁾. In the spectra of the 'centrifuged' samples this peak is not observed. Apparently, these homocondensates are not bound to the particles. In addition, the carbonyl peak in the spectra of the dried samples is found at 1730 cm^{-1} with a shoulder at 1700 cm^{-1} . In the 'centrifuged' samples the carbonyl peak only appears at 1700 cm^{-1} . This indicates that after grafting, a hydrogen bond between the oxide and the MPS-carbonyl is formed⁽¹⁾.

Miller and Ishida⁽¹⁾ calculated the amounts of MPS needed to build a monolayer. Depending on the orientation of the MPS molecule, they proposed two estimates for

surface coverage. Considering the MPS molecule as a rod with a perpendicular orientation to the surface $6.9 \mu\text{mol}/\text{m}^2$ is needed for a monolayer. When parallel orientation is considered, only $3.0 \mu\text{mol}/\text{m}^2$ is needed. This parallel orientation can be induced by hydrogen bonding of the MPS-carbonyl and the hydroxyl group of the oxide. The formation of hydrogen bonds is envisaged in the infrared spectra by the presence of a peak at 1700 cm^{-1} .

Figure 2.7 shows the calculated surface coverage (Γ , Eq. [1]) of MPS for different amounts of MPS initially added to the particles. The solid lines are the calibration lines that were determined using the ‘dried’ samples. The dashed lines in the plot represent the theoretical amount of MPS that Miller and Ishida⁽¹⁾ calculated for a completely filled monolayer. The lower dashed line in figure 2.7 represents a parallel orientation of the MPS to the surface and the upper dashed line represents a perpendicular orientation. From figure 2.7 it becomes clear that for silica and TO the maximum amount of MPS bound to the particles corresponds to one completely filled monolayer with for the most part a parallel orientation. This orientation is consistent with the presence of a hydrogen bond between the oxide surface and the carbonyl peak as found in the spectra of the centrifuged samples. These results are in line with the results that Miller and Ishida obtained for the grafting of MPS on lead oxide and clay.

The maximum amount of bound MPS onto ATO is only $2 \mu\text{mol}/\text{m}^2$, or about 50-70 % of a completely filled monolayer. It should be noted that this value is consistent with the result obtained in the kinetics experiments (see figure 2.5.). This low value can be explained in two ways. It is expected that the ATO-surface is enriched with antimony(III)⁽⁷⁾ and a bond between the MPS and this antimony might not be possible. The number of reactive sites on the ATO surface might be lower than the number needed for a full surface coverage. Another explanation might be that a part of the measured surface consists of pores in which the MPS cannot penetrate and consequently that part of the surface is not covered. However, the measured surface area of ATO corresponds to massive particles with a diameter of 7 nm, and this size was confirmed with TEM measurements. As porous particles with the same diameter will have a larger specific surface area, the latter hypothesis is less likely.

If the amount of MPS added to the particles is about equal to or lower than the amount needed to fill a monolayer, then most of the MPS is bonded to the particles. This confirms the observation in the kinetic experiment that the grafting to the particles is favoured over the formation of homocondensates.

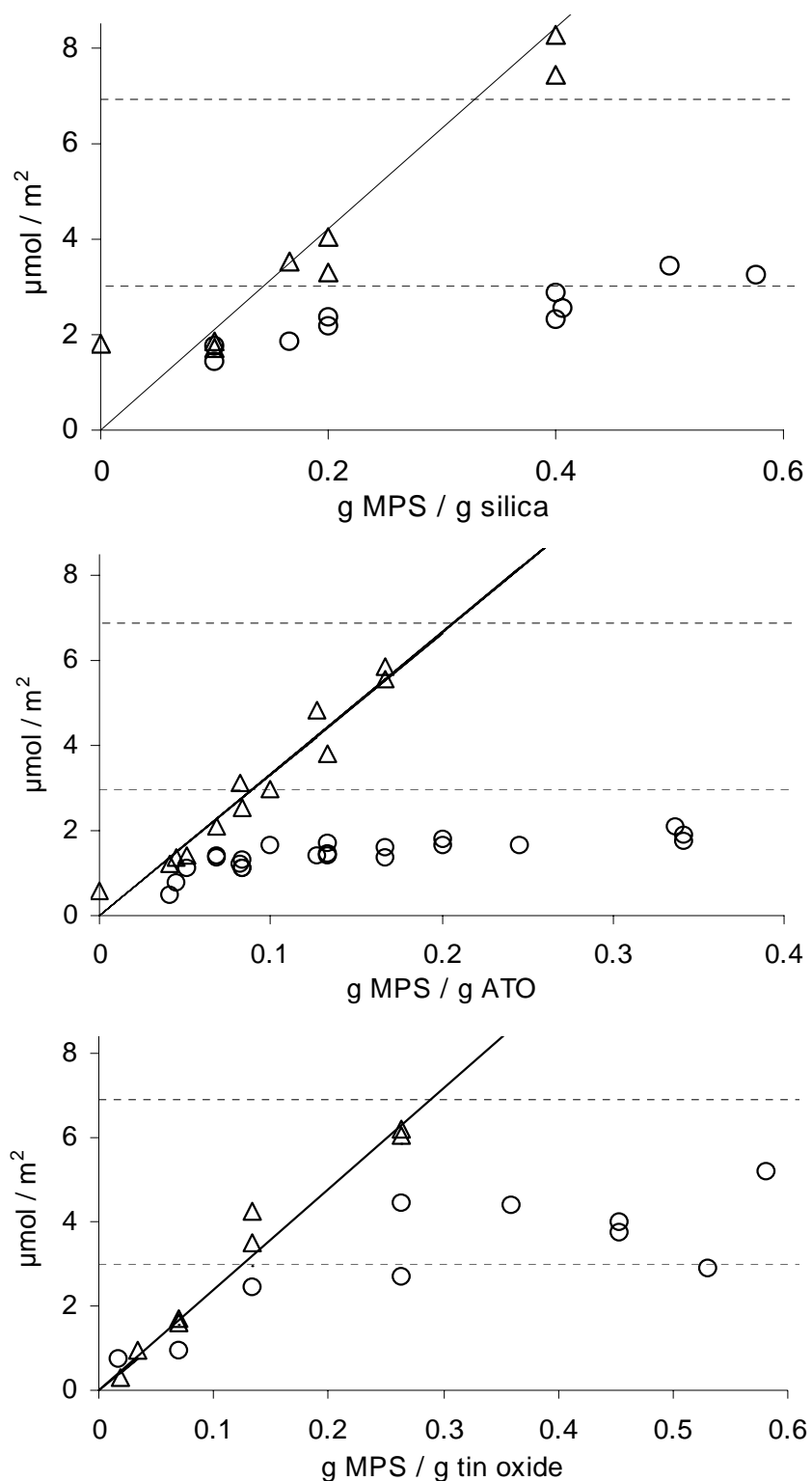


Figure 2.7 Surface coverage of modified particles as determined by FTIR. (Δ) 'dried' samples; (\circ) 'centrifuged' samples; the solid line is the calibration line; the dashed lines are the theoretical amounts needed for a monolayer of MPS, where the upper line represents perpendicular oriented MPS and the lower line represents parallel oriented MPS.

2.6.2. Solid state ^{29}Si -NMR

To determine the existence of a chemical bond between the MPS and the oxide particles solid state ^{29}Si -NMR measurements on ‘dried’ and ‘centrifuged’ samples were performed. In the case of untreated silica particles, NMR signals were found at -112 ppm, from $(\text{SiO})_4\text{Si}$ groups in the bulk of the particles, and at -102 ppm, from the surface $(\text{SiO})_3\text{SiOH}$ groups⁽⁴⁾. After the grafting of the MPS the signal at -102 ppm became much weaker as a large portion of the surface $(\text{SiO})_3\text{SiOH}$ groups had reacted with MPS and was converted to $(\text{SiO})_3\text{SiOSi}$ groups. Determination of the grafting of MPS to silica by the position of the ^{29}Si -NMR peaks that originate from MPS is not possible due to overlap of peaks. MPS grafted onto silica or MPS bound to another MPS moiety both are characterised by the formation of a Si-O-Si bond and these peaks will overlap.

In the case of TO and ATO particles, obviously no ^{29}Si -NMR signals from the particles can be expected. Consequently, determination of grafting of MPS to the particles had to be performed by studying the signals of the silicon atom in MPS. In the reactions of MPS with TO or ATO Si-O-Sn or Si-O-Sb bonds are formed which may give a different peak position compared to the peak positions of the homocondensates. In the spectrum of a ‘dried’ sample of grafted TO three peaks were observed: at -43.9, -58.8, and -68.3 ppm. In the spectrum of the ‘centrifuged’ TO however, only the peak at -43.9 ppm was found (figure 2.8). Consequently this peak was assigned to the MPS grafted TO. As the signals at -58.8 and -68.3 ppm were only present in the ‘dried’ samples, they are attributed to the homocondensates. The chemical shifts are in good agreement with values that are reported⁽⁵⁾ for $\text{MPS}(x,2)$ and $\text{MPS}(0,3)$. In the ^{29}Si -NMR spectra of the ATO samples no clear signal for the MPS grafted to the particles could be found. However, in the range from -40 to -70 ppm an elevation of the baseline appeared. A possible explanation is that the electric conductivity of the ATO causes strong broadening of ^{29}Si NMR signals of the attached MPS, e.g., similar to the ^{13}C NMR line broadening observed for ^{13}CO on platinum⁽⁸⁾. Another possibility is that the doping of the oxide yields a broad surface heterogeneity on the ATO particles with correspondingly different MPS binding sites. This will yield a broad, inhomogeneous ^{29}Si NMR signal of the attached MPS.

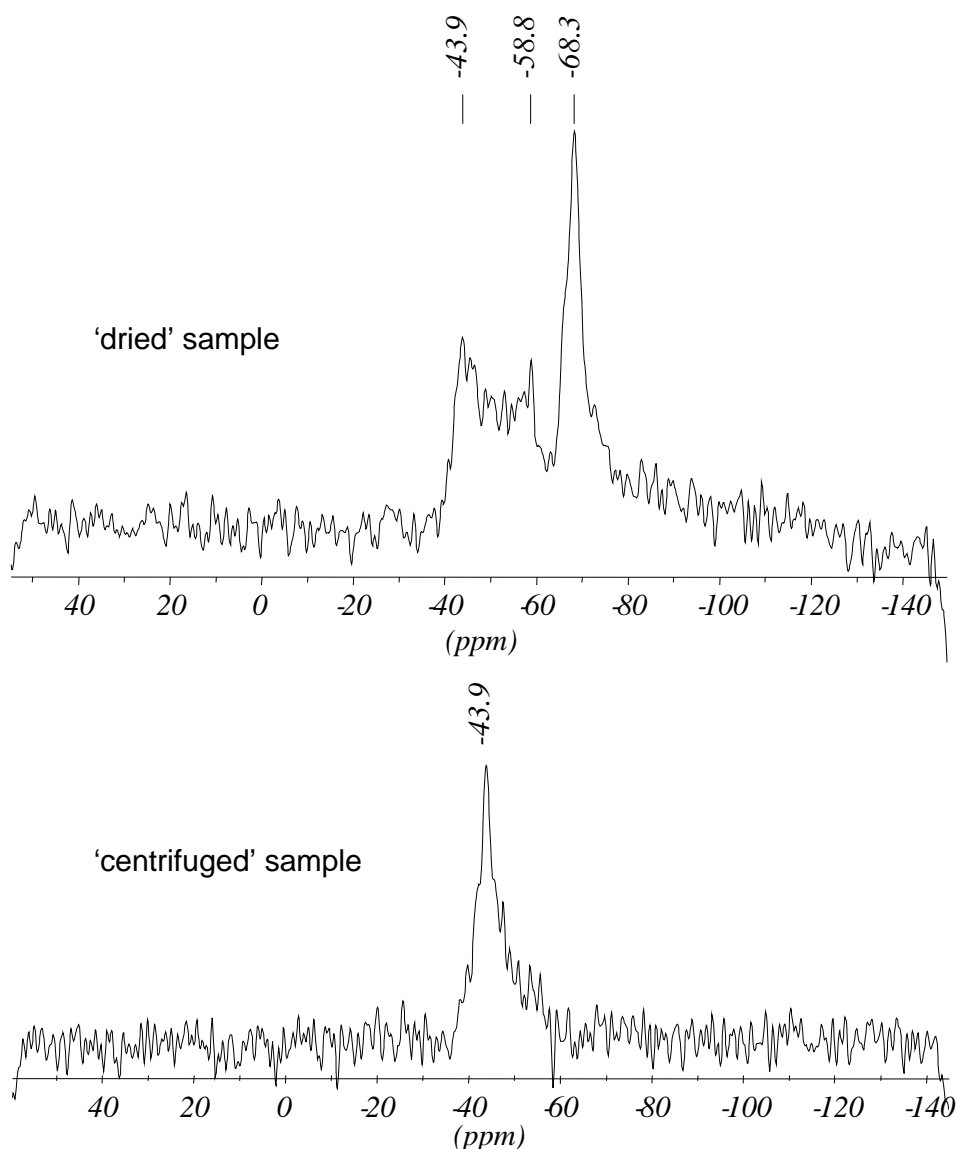


Figure 2.8 ^{29}Si MAS NMR spectra of 'dried' and 'centrifuged' samples of an experiment in which MPS was reacted with TO (0.27 g/g).

2.7. Conclusions

The treatment of TO and silica particles with sufficient MPS results in a closed monolayer of grafted MPS on the particles surfaces. The MPS has a parallel orientation towards the oxide surface and a hydrogen bond between the MPS-carbonyl and the oxide surface is formed. For ATO the maximum amount of grafted MPS is about 30-40% lower than the minimum amount required to form a closed monolayer. When the maximum surface coverage is reached excessive MPS does not bind to the particles but forms homocondensates. Both the NMR and the infrared data show that the grafting of MPS onto the studied particles is preferred over the formation of homoconden-

sates. The kinetic experiments with the silica and ATO dispersions show that the rates of the grafting and the homocondensation are limited by the hydrolysis of the MPS(0,0). Although the reaction rates change when using another oxide, the oxide itself is probably not involved in this difference since the observed differences can easily be correlated to the differences in pH.

Reference List

1. J. D. Miller and H. Ishida, *Surface Science*, 148, 601-622 (1984).
2. M. W. Daniels, J. Sefcik, L. F. Francis, A. V. McCormick, *Journal of Colloid and Interface Science*, 219, 351-356 (1999).
3. C. Gellermann, H. Wolter, W. Storch, *Materials Research Society Symposium Proceedings 520(Nanostructured Powders and Their Industrial Applications)*, 185-190 (1998).
4. U. Goerl, A. Hunsche, A. Mueller, H. G. Koban, *Rubber Chemistry and Technology*, 70(4), 608-623 (1997).
5. N. Nishiyama, K. Horie, *Journal of Applied Polymer Science*, 34, 1619-1630 (1987).
6. N. Nishiyama, R. Shick, H. Ishida, *Journal of Colloid and Interface Science*, 143(1), 146-156 (1991).
7. B. Slater, C. R. A. Catlow, D. H. Gay, D. E. Williams, V. Dusastre, *Journal of Physical Chemistry B*, 103(48), 10644-10650 (1999).
8. Y. Y. Tong, E. Oldfield, A. Wieckowski, *Faraday Discussions*, 121, 323-330 (2002).
9. M. Abboud, M. Turner, E. Duguet, M. Fontanille, *Journal of Materials Chemistry*, 7(8), 1527-1532 (1997).
10. J.D. Miller, H. Ishida, *Journal of Chemical Physics*, 86(3), 1593-1600 (1987).

Chapter 3

Practical aspects of the coating preparation

Synopsis

In this chapter an extensive description of the preparation procedure of the coatings is given. The colloidal stability of nanoparticles is discussed, as this is the main parameter that determines experimental success or failure, and it also influences some of the final coating properties. It appears that for the colloidal stability of the used nanoparticles the polarity of the solvents is an important factor. The used nanoparticles are dispersed in water when supplied and these dispersions become unstable when the polarity of the solvent is lowered. However, after the grafting of silane coupling agents on the particle surfaces, stable dispersions can only be obtained in low polar matrices. Furthermore the adhesion of the coatings and its consequences for the selection of the acrylate resins are discussed.

3.1. Introduction

The ultimate object of this thesis is to investigate the influence of the coating composition on the electrical and mechanical properties of the coatings. It is evident that before studying the coating properties, the coatings need to be prepared. However, the preparation of usable coatings was not straightforward for all desired compositions. The most critical factors for experimental success were the colloidal stability of the filler particles and the adhesion of the coatings; both are strongly affected by the composition of the coating formulations.

The basic components of the coatings are metal oxide nanoparticles, an acrylate resin with photoinitiator, and a silane coupling agent that is present in two forms: grafted on the particle surface and as homocondensate (see chapter 2). Both the type and the relative amounts of these components are varied extensively, resulting in a large number of different coating compositions. During the preparation also solvents, water, methanol, and propanol are needed to enhance the colloidal stability of the nanoparticles, or to lower the viscosity of the formulation. With this large number of components, and with the large number of variations therein, a fundamental study of colloidal stability and adhesion was not possible. Hence, the preparation procedure was established on basis of educated trial and error. In order to give the reader more feeling for the critical parameters, the basics of colloidal stability and adhesion are discussed and an example of the preparation procedure is given. Furthermore the selection of the acrylate resins is discussed as this selection was partly determined by the adhesion of the coatings.

3.2. Colloidal stability - theory

Colloidal stability is determined by several types of attractive and repulsive interactions between the particles, by interactions between the particles and the dispersing medium, and by the thermal energy of the system. The interactions include Van der Waals, electrostatic, steric, and solvation/structural interactions. The relative importance of any of these interactions depends on the composition of the system and on the size of the particles. Extensive general descriptions of the various interactions can be found in many textbooks, where especially the book of Israelachvili is renowned⁽¹⁻⁴⁾. A short but very comprehensive overview of the particle size effects on the interactions in colloidal dispersions is given by Miller and Zukoski⁽⁵⁾.

3.2.1. Thermal energy

Nanosized particles in a low viscous liquid continuously move due to thermal energy. The mean kinetic energy of these particles is $\frac{3}{2} kT$, where T is the absolute temperature and k is Boltzmann's constant. If a particle encounters an energy barrier higher than its thermal energy, its movements are blocked effectively. This may, for instance, prevent breaking up of aggregated particles, or it may prevent the opposite, the aggregation of particles. As $\frac{3}{2} kT$ is the mean energy, a considerable part of the particles have a higher thermal energy, thus to restrict the movements of virtually all particles also the energy barrier has to be considerably higher. This is especially important if the interaction between two particles is strongly attractive at contact, but repulsive at a small separation (a very common situation). When the repulsive barrier is high, the particles will not come into contact and the dispersion is stable. If the repulsive barrier is low (less than $10\text{-}20 kT$), however, the dispersion is unstable as in a non-negligible part of the encounters between particles the barrier will be passed and the dispersed particles can aggregate, with a rate depending on the barrier height.

3.2.2. Particle-particle interactions

Particles attract each other through Van der Waals forces. These forces are strong at very short distances, but their strength decreases with increasing distance. The Van der Waals interaction energy (V_A) between two spheres at short distance can be written as^(1,2):

$$V_A = -\frac{a}{12 \cdot d} \cdot \left(\sqrt{A_m} - \sqrt{A_p} \right)^2 \quad [1]$$

where A is the Hamaker constant, the suffixes m and p indicate the matrix and the particle, a is the radius of the particles, and d is the distance between the particles. Table 3.1 shows the calculated Hamaker constants, the distance where the Van der Waals attraction equals the thermal energy, and the Van der Waals interaction energies at minimum separation for the fillers used in this study. A minimum separation distance of 0.165 nm was used in these calculations; this separation distance was also used in calculations of the surface energy on basis of the Van der Waals interactions leading to remarkable accurate results for a wide range of liquids and solids⁽²⁾. In a crude estimation the maximum attraction between two nanoparticles at minimum separation in a typical coating is about $2.6 kT$ for silica, $20 kT$ for tin oxide, and $29 kT$ for ATO. Equation 1 shows that the medium between the particles influences the Van der Waals attraction. If the medium has the same Hamaker constant as the particles, the net at-

	Particle size (nm)	Hamaker constant ($\times 10^{-20}$ J)	d where $V_A = \frac{3}{2} kT$ (nm)	V_A at con- tact** (kT)
Silica	15	6.4	0.3	2.6
Tin oxide	5	21*	2.2	21
ATO	7	21*	3.2	29
Water		3.6		
Propanol		4.7		
Acrylate		6*		

* estimated value on basis of the Lifshitz theory ⁽²⁾

** average distance at contact is about 0.165 nm ⁽²⁾

Table 3.1 *Estimates of the Van der Waals attraction.*

traction between the particles is zero. This situation can be encountered for instance with silica particles in an acrylate matrix.

As the attractive Van der Waals forces are only strong at small particle separations, aggregation of the particles can be prevented by repulsive forces between the particles. One type of repulsive force is electrostatic repulsion. Inorganic particles that are dispersed in polar solvents typically have an electrical charge, with a value usually depending on the pH of the system. A cloud of oppositely charged ions around the particle balances this charge leading to an electrical double layer. The thickness of this layer is determined by the ion concentration, ionic charge, temperature, and the dielectric constant of the medium. When two particles approach to a distance where their ion clouds overlap they experience the interaction of their charges. As two particles of the same material will be equally charged, their interaction will be repulsive. For large particles dispersed in polar media this force can be quite large and is an important stabilisation mechanism. However, small particles (10 nm) have also a small surface, which limits the charge of the particles and thus limits the magnitude of the repulsion to about $5 kT$ ⁽⁵⁾.

Another type of repulsive force that prevents the approach of two particles is steric stabilisation by an adsorbed or grafted layer of (organic) molecules on the particle surface. These molecules are literally in between the particles, preventing the particles from approaching each other at distances smaller than the size of the attached molecules. To effectively stabilise the dispersion, the attached molecules should have

properties distinctively different from the particles so they do not contribute to the particle-particle attraction. The size of the attached molecules should be larger than the distance at which the particle-particle attraction becomes effective. As for nanoparticles a steric barrier of only a few nanometer is sufficient for stabilisation, attachment of relatively small groups is sufficient to effectively counteract the particle-particle Van der Waals attraction. The groups on the surface can be intentionally added compounds that may be grafted or adsorbed to the surface, but the groups may also be adsorbed solvent molecules.

3.2.3. Particle-matrix interactions

The relevance of particle-matrix interactions for the colloidal stability is increasingly recognised in colloid chemistry. However, the exact interpretation of these interactions and the nomenclature are not yet established. The interactions can be divided in two groups: those due to unfavourable packing of the matrix molecules and those due to interaction energies of the matrix components with the filler surface.

Upon close approach of two particles, the matrix molecules may no longer be able to completely fill the space between the two filler surfaces, as schematically shown in figure 3.1. The unfavourable packing of the matrix molecules results in an additional pressure in the direction of a more favourable packing. This pressure has an oscillatory dependency on the distance between particles, with a periodicity close to the diameter of the matrix molecules⁽²⁾. At increasing distance this pressure effect fades out and at about 4-5 times the molecular diameter, which typically is about 1-2 nm, the effect has faded away. For 'rough' surfaces and for matrices with a heterogeneous composition the packing effect will be less pronounced.

Particles with a hydrophobic surface that are immersed in water experience a considerable stronger attraction than expected on basis of the particle-particle interactions and the oscillatory pressure. The exact origin of this interaction is still unknown, but entropically unfavourable orientation of water molecules in the vicinity of surfaces

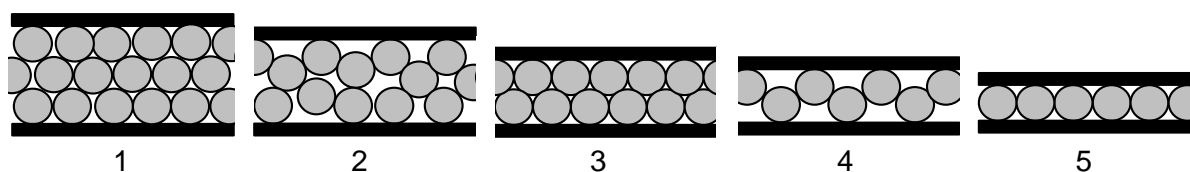


Figure 3.1 *Schematic illustration of the filling of the gap between two approaching surfaces by matrix molecules; the resulting pressures between the surfaces are alternating repulsive (1-3-5) and attractive (2-4).*

that cannot form hydrogen bonds is believed to play a major role⁽²⁾. The magnitude of this hydrophobic interaction energy (W) has been found to correlate with the solid-liquid interfacial energy γ_{SL} of the particle surface with the matrix by⁽²⁾:

$$W = -2 \cdot \gamma_{SL} \cdot e^{-d/d_0} \quad [2]$$

where d is the particle-particle separation and d_0 is the decay length (typical 1-2 nm). The interfacial energy between water and hydrophobic surfaces is typical 10-50 mJ/m², or 2-12 kT/nm^2 , which makes the hydrophobic interactions a major factor for colloidal (in)stability. Particles with a hydrophilic surface are found to be more stable in water and other hydrogen bond forming solvents than expected on basis of the particle-particle interactions and the oscillatory pressure^(6,7). Upon contact between two particles, the liquid-particle interface at the contact area (several nm²) is replaced by particle-particle interface. The contact between two solids is typically imperfect due to surface roughness, thus interface energy between solids at contact will remain higher than zero, unlike in the case of two contacting liquid droplets, where the interface disappears. When the interface energy between two contacting filler particles is higher than that of a corresponding filler surface wetted by the matrix, the contact energy will be positive and the colloidal stability will be enhanced⁽⁷⁾.

3.3. Colloidal stability – consequences for the systems studied

Colloidal (in)stability during the preparation of a coating has a large effect on the final distribution of the particles in the coating, and consequently has a large effect on the properties of the coating. A good stabilisation of the particles during the whole preparation procedure results in a homogeneous distribution in the final coating (figure 3.2). If the particles loose colloidal stability somewhere during the preparation procedure, this may lead to aggregation. This aggregation may result in segregation of the particles from the matrix, leading to extremely inhomogeneous coatings. Such aggregation may also result in a particle gel leading to coatings that are homogeneous on a macroscopic scale, with properties very different from coatings with well-dispersed fillers. Whether gelation or segregation takes place depends on factors like particle concentration, particle size, bond strength between particles, and process time.

Acrylate matrices generally are poor dispersing media for metal oxide fillers. The difference in surface energy between acrylates and metal oxide fillers is typically very large. Additionally, in acrylates with a low matrix polarity the ion dissociation is low leading to poor electrostatic stabilisation. Stabilisation of the fillers, however, is possi-

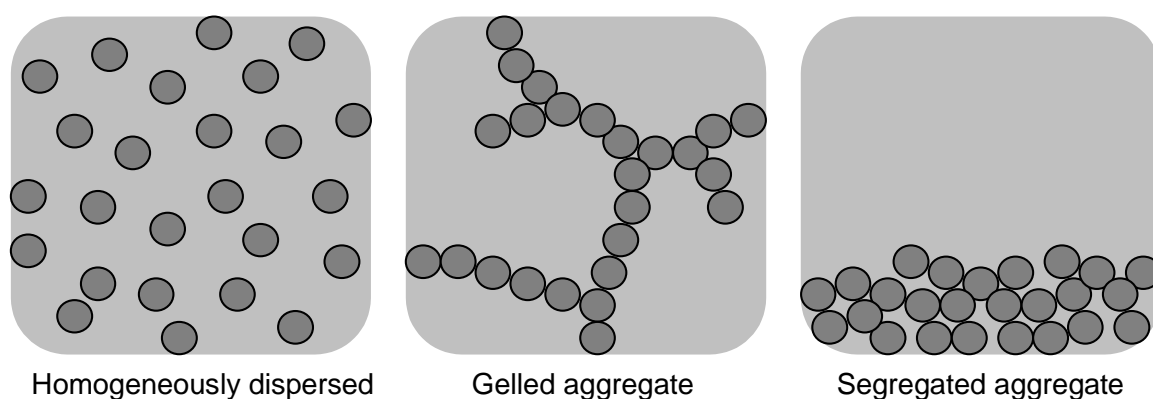


Figure 3.2 *Different modes of filler distribution.*

ble by attachment of organic groups that lower the interface energy and provide steric stabilisation. In this study organic groups are provided by silane coupling agents that react with the metal oxide surface (see chapter 2). This surface modification can be sufficient to provide a stable dispersion in an acrylate matrix, depending on the amount and the type of silane coupling agent used, and on the type of matrix. For coating formulations with still insufficient filler stabilisation, the stability of the filler can be improved by the addition of solvents that lower the filler concentration and increase the polarity of the medium. Upon drying of such coatings, the stabilisation contribution by the solvents will be lost and the insufficiently stabilised fillers will aggregate. With partial filler stabilisation (for example when using a small amount of silane coupling agent) instead of no stabilisation, the moment of aggregation can be postponed and aggregation may result in a homogeneous particle gel instead of segregation.

Addition of solvents may also be needed for coating formulations with well-stabilised fillers with large repulsive barriers. For the rheological properties, repulsive barriers enlarge the effective radius of the particles; consequently the effective volume fraction of the particles is considerably higher than the real volume fraction. If the effective volume fraction exceeds levels of about 50 % (the real volume fraction might be below 10 %), the system solidifies into a colloidal crystal or glass⁽⁵⁾. To obtain in such a case a liquid coating formulation, the effective volume fraction of the filler has to be lowered by the addition of solvents.

3.4. Consequences of colloidal (in)stability for the preparation of the coatings

The coating preparation starts with the surface modification of the inorganic fillers. The fillers (silica, tin oxide, and antimony doped tin oxide (ATO)) were supplied as aqueous dispersions. The silane coupling agents (3-methacryltrimethoxysilane

(MPS) and *n*-octyltrimethoxysilane (OTS)), which were used for the surface modification of the particles, are not soluble in water; in order to dissolve them in the filler dispersions the aqueous filler dispersions were mixed with methanol in a 1:2 (for MPS) or 2:5 (for OTS) w/w ratio. Other alcohols like ethanol or propanol could also be used, but only in smaller amounts as decreasing the polarity of the dispersing medium also decreases the stability of the unmodified particles. This problem appeared particularly severe for the tin oxide dispersions; to avoid aggregation they had to be diluted with water (from 15 to 5 w%) before methanol could be added.

After mixing methanol with the filler dispersion, the silane coupling agent was added and the mixture was heated to reflux. During the reaction the filler particles became more hydrophobic, and thus required a less polar dispersing medium. In the chosen water-methanol mixture typically both the unmodified and the modified particles were colloidally stable at the reflux temperature (about 70 °C). Depending on the amount and type of the silane coupling agents used, upon cooling to room temperature some dispersions became unstable and extra alcohol (*n*-propanol) had to be added. The resulting dispersions were very dilute (0.3-5 vol% filler) and needed to be concentrated (by solvent evaporation) before they could be used for coating applications.

During evaporation of the solvents (in a rotational evaporator), methanol disappeared first, which could result into loss of colloidal stability and aggregation of the particles into a gel. By the addition of propanol the particle gel could be redispersed. In the case of silica and tin oxide this appeared only successful as long as the gel was wet, for ATO even dried particles could be redispersed. Without surface modification, aggregation of the silica and tin oxide particles was irreversible whereas ATO could be redispersed with water. After the methanol had been removed, the acrylate resin was added and the mixture was further concentrated. In this stage both water and propanol evaporate together (as they form an azeotrope). When needed, additional propanol or water was added to maintain colloidal stability. At the point that a viscosity suitable for coating application was reached, the last component, the photoinitiator, was added. The solvent content (water + propanol) of the coating formulations at this stage was typically 30-50 w%, 70-85 w%, and 60-75 w% for the silica, tin oxide, and ATO filled coating formulations, respectively.

With this procedure the control over the amount of solvents and the ratio between the solvents in the coating formulation is poor. The amount of solvents added is relevant for the rheology during application of the coatings, for which a high precision is not needed. However, the amount of solvents is not expected to have a significant in-

fluence on the structure of the coatings after drying. The water to propanol ratio may be more important, but is more difficult to control. The relative evaporation rates of water and propanol depend on pressure and temperature, and on their chemical activities in the coating formulation, which are also influenced by the other coating components. For the formulations that are on the limit of stability the poor control over the water to propanol ratio during evaporation can cause lack of reproducibility. For the formulations that are clearly stable or unstable the influence of the solvent ratio on the final coating structure is considerably smaller. The coating property that is most sensitive to the filler distribution is the electrical conductivity. For most coating compositions the reproducibility of the electrical conductivity is reasonable, but for some compositions it is rather poor, as is further described in chapter 5.

3.5. Drying of the coatings

The next step in the preparation of the coatings was the application of a layer of the coating formulation on the substrate with a doctor blade (gap 100 or 200 μm) and placing the samples in a well-ventilated place to allow the solvents to evaporate. During the solvent evaporation the filler particles may lose colloidal stability and aggregate into a particle gel. If the gelation starts in an early stage where the amount of solvents is still high, further drying results in mechanical stresses in the gel and cracks may appear in the coating. Another problem that may arise after the application is demixing of the solvents and the acrylate resin. As most acrylate resins are not compatible with water, a sufficiently high alcohol/water ratio is needed during all stages of the drying. Methanol and ethanol evaporate considerably faster than water and consequently are not useful in the drying stage. With 1-propanol this problem does not arise; hence this is the preferred cosolvent for the drying stage. After the drying, the acrylate matrix was cured by a short and intense exposure to UV irradiation, which fully fixed the particles in the matrix.

3.6. Adhesion

A coating can only fulfil its functions as long as it is fixed well to the substrate. As such, adhesion is the most important requirement of a coating-substrate system. Adhesion is realised by a range of forces, like chemical bonding, Van der Waals forces, mechanical interlocking, etc⁽⁸⁾. For plastic substrates, adhesion can be enhanced by moderate diffusion of the coating binder in the substrate^(9,10). Delamination is

mainly caused by mechanical stresses that may be applied either externally or may be built up in the coating during curing.

To achieve an optimal adhesion, the contact area between the coating and substrate has to be as large as possible, which means that the coating should follow the micro-roughness of the substrate. The extent to which this occurs depends on the surface energies of the substrate and the applied coating formulation. The coating will completely wet the substrate if the sum of the surface energy of the coating formulation and the coating-substrate interface energy is lower than the surface energy of the substrate. With a higher sum the coating will not completely fill the micro-roughness valleys.

During UV-curing of acrylate coatings Van der Waals bonds between acrylate groups are replaced by (shorter) chemical bonds, resulting in shrinkage of the coating film. The shrinkage is about 20 ml for each mol of reacted acrylate groups⁽⁹⁾, for commonly used acrylate monomers this equals a few percent up to 25 % of the coating volume⁽¹¹⁾. As the coatings are attached to the substrate, shrinkage in lateral directions is not possible and the stresses that are built up can become large. With flexible substrates this commonly results in upwards bending of the sample. The stresses are lower for coatings with lower concentrations of reactive groups as well as for coatings with a low T_g as those can dissipate the stresses more easily by reorientation of the polymer chains. As the internal stresses are a bulk property of the coatings and the adhesive forces between the coatings and the substrate only act at the interface, the net adhesion decreases with increasing coating thickness.

3.7. Selection of the acrylate resins

Several acrylate resins were tested as matrix material for the nanocomposite coatings. The main issue was their performance on a polycarbonate substrate, as the studied nanocomposite coatings are expected to find their main applications on this type of substrate. Monoacrylates and to a lesser extent (linear) diacrylates do swell the polycarbonate substrate, whereas branched acrylates and methacrylates hardly do so. This swelling of the polycarbonate by the acrylate resin is very beneficial for the adhesion of the coatings^(9,10), but excessive swelling is not desired as it results in a turbid interphase. The addition of fillers was found to reduce the swelling drastically. Consequently, acrylate resins that, when applied without filler, give coatings with a good adhesion, can have insufficient adhesion when the filler level is increased; at high filler levels these coatings delaminate already during curing. On the other hand acrylate res-

ins that give coatings with a good adhesion at high filler levels, generally swell the polycarbonate excessively at low filler fractions resulting in highly turbid systems. None of the tested acrylate resins has an excellent performance with both high and low filler fraction.

The three acrylate resins that were used for the experiments described further on in this thesis are PEGDA, TMPTA, and Ebecryl 745. These examples of a rubbery, a glassy, and a commercial resin have in general sufficient adhesion for the performed tests without excessive swelling of the polycarbonate substrate.

PEGDA is made of a polyethylene glycol oligomer ($n = 10.5$) with two acrylic endgroups. PEGDA coatings without fillers swell the polycarbonate moderately, resulting in some turbidity. However, with 10 vol% filler, or more, the coatings are transparent as apparently the swelling of the polycarbonate is weaker. As cured PEGDA is a rubber (T_g at -30°C), internal stresses will be relatively low thus also thick coatings can have good adhesion. The polyethylene glycol oligomer has a relatively good compatibility with polar materials, which lowers the need for surface modification of the used fillers. As the viscosity is rather low and the surface tension is relatively high, the (undesired) flow of the coatings after application is extensive.

TMPTA is made of three acrylic groups connected by trimethylolpropane. It forms relatively hard coatings with a very high crosslink density. The swelling of polycarbonate even by low-filled coatings is relatively small and all coatings are transparent. Notwithstanding the extremely high shrinkage of TMPTA upon curing, the adhesion is sufficient for the tests applied in this study, except for very high filler fractions and very thick layers. The compatibility of TMPTA with polar materials is relatively poor thus proper mixing with the fillers used in this study is not possible without surface modification.

Ebecryl 745 is a commercial acrylate resin based on an acrylate backbone with unsaturated acrylate side-groups diluted with 25 % HDDA and 25 % TPGDA. From the tested acrylate resins it offers the best compromise between adhesion, rheology, and compatibility with a wide range of fillers. Disadvantages are poor adhesion at high filler fractions and lack of knowledge concerning the composition of the resin.

3.8. Example of the preparation of ATO filled coatings

For the modification of the ATO surface 20.0 g of ATO dispersion (12 wt% ATO in water, thus 2.4 g ATO) was mixed with 50 g methanol and 0.20 g MPS (3-methacryloxypropyltrimethoxysilane), and the mixture was heated to reflux (appr. 70

°C) during 24 hours. After cooling the mixture the methanol was evaporated using a rotatory evaporator at 350 mbar and while slowly decreasing the pressure to 100 mbar the mixture was further concentrated to about 10 g, leading to coagulation of a major part of the ATO. Subsequently 20 g propanol and 0.71 g PEGDA were added and the mixture was stirred until all ATO was redispersed. The mixture was again concentrated to 17.2 g with a rotatory evaporator at 100 mbar, now no coagulation was observed. Adding 0.037 g 2-hydroxy-2-methylpropiophenone as photoinitiator completed the coating formulation for a coating with 30 vol% ATO. In order to make a coating with 5 vol% ATO, 2.00 g of the 30 vol% ATO coating formulation was diluted with 0.72 g propanol, 0.69 g PEGDA, and 0.022 g 2-hydroxy-2-methylpropiophenon. Note that the density of ATO is more than 6 times higher than the density of PEGDA, thus the volume fraction does not equal the weight fraction.

The coating formulations were applied on a polycarbonate substrate using a doctor blade with an opening of 100 μm . Due to rheology, substrate wetting, and other effects, the wet film thickness was typically considerably lower than 100 μm . Next the samples were placed for one hour in a well-ventilated area to allow the solvents to evaporate. The coatings were cured by exposure to UV (20 mW/cm²; 60 seconds; N₂ atmosphere). Both coatings were homogeneous and transparent. The thickness of the coatings was 8 μm for the coating with 30 vol% ATO, and 20 μm for the coating with 5 vol% ATO.

Reference List

1. R. J. Hunter, Introduction to modern colloid science (Oxford University Press, Oxford, ed. Repr. with corr. 1996).
2. J. N. Israelachvili, Intermolecular and surface forces (Academic Press, London, ed. 2nd ed., 1991).
3. D. F. Evans and H. Wennerstroem, The colloidal domain : where physics, chemistry, biology, and technology meet (VCH, New York, 1994).
4. J. Lyklema, Fundamentals of interface and colloid science (Academic Press, London, 1991).
5. K. T. Miller, C. F. Zukoski, *Studies in Surface Sciences and Catalysis. D.*, 103 (Semiconductor nanoclusters), 23-55 (1996).
6. S. R. Raghavan, H. J. Walls, S. A. Khan, *Langmuir*, 16(21), 7920-7930 (2000).

7. V. V. Yaminsky and B. W. Ninham, *Advances in Colloid and Interface Science*, 83, 227-311 (1999).
8. Z. W. Wicks, F. N. Jones, S. P. Pappas, *Organic coatings: science and technology* (Wiley-Interscience, Chichester, 1992).
9. A. Priola, G. Gozzelino, F. Ferrero, *Advances in Organic Coatings Science and Technology Series*, 11, 156-163 (1989).
10. A. Priola, G. Gozzelino, F. Ferrero, *International Journal of Adhesion and Adhesives*, 11, 255-259 (1991).
11. F. McGill, *Polymer Paint Colour Journal*, 186, 10-14 (1996).

Chapter 4

UV-curing of the coatings

Synopsis

In this chapter the curing by means of UV-initiated radical polymerisation of the acrylate matrix is described. An important issue is whether chemical links between the filler and the matrix are established. The UV curing of the coatings was followed by real-time FTIR. Silica and ATO did not interfere directly with the curing reactions, although ATO can retard the curing due to strong absorption of the UV light. Tin oxide however interferes directly with the curing reactions, resulting in a strong retardation of the curing. Tin oxide is suspected of catalysing the termination of the radical polymerisation by disproportionation. The methacrylate groups of the MPS react faster than the acrylate groups of the matrix; this indicates that the intended copolymerisation between the MPS and the matrix takes place, thus the intended chemical links between the filler and the matrix are formed.

4.1. Introduction

In this chapter the curing of the acrylate-metal oxide nanocomposite coatings is described. The coatings are composed of an acrylate resin, photoinitiator, silica, metal-oxide nanoparticles (silica, tin oxide or antimony doped tin oxide), and silane coupling agents that are mainly grafted on the nanoparticles (see chapter 2). The curing takes place by means of an UV-initiated radical polymerisation of the (meth)acrylate groups in the coating formulation. General descriptions of UV initiation and radical polymerisations can be found in many textbooks and review articles⁽¹⁻⁷⁾. An important issue in this chapter is whether chemical links between the filler and the matrix are established. These links should be established by copolymerisation of the acrylate matrix with the methacryl group of 3-methacryloxypropyltrimethoxysilane (MPS) that is grafted on the metal oxide fillers. Typically, methacrylates and acrylates copolymerise, however, in this system it cannot be taken for granted because the methacrylate is grafted on the filler surface and consequently it is not completely mixed with the acrylate. Furthermore hydrogen bonding between the methacrylate carbonyl and the filler surface may restrict the spatial orientation of the methacrylate group and consequently may affect its reactivity.

The addition of metal oxide nanoparticles may influence the curing in many ways. A typical problem is absorption of UV light by the metal oxide fillers. Consequently, the intensity of the UV light in the deeper layers of coatings may be very low and therefore the curing of the deeper layers may be very slow. Physical interactions between the filler and the matrix may affect the mobility of the reactive groups and consequently affect the curing rate. Furthermore, the fillers used in this study are known to catalyse many reactions, like oxidation of unsaturated hydrocarbons and other organic compounds^(8,9), and other semiconductor nanoparticles are found to initiate radical polymerisations⁽¹⁰⁾. Hence, unexpected side reactions may occur.

No literature regarding radical polymerisations in the presence of tin oxide or antimony doped tin oxide (ATO) could be found and also detailed studies concerning the copolymerisation of grafted MPS with acrylate resins were not found. To determine to what extent the mentioned potential problems occur, the curing kinetics of the coatings with the different fillers in various amounts were studied.

4.2. Theory of the UV curing kinetics

4.2.1. General kinetics

The curing starts when UV light activates the photoinitiator: the photoinitiator splits up into two radicals that may react with the (meth)acrylate groups and consequently initiate the free radical polymerisation. The polymer chain continues growing until it meets another free radical with which it forms a stable chemical bond or until it abstracts a H-atom from another molecule that consequently forms a new radical. The polymerisation may be strongly retarded or completely inhibited if the radicals are consumed in competing reactions with other compounds, which are referred to as inhibitors. When present in small quantities an inhibitor will be completely consumed in the first moments of the curing, once consumed it plays no further role. However, atmospheric oxygen also acts as an inhibitor and may be replenished from the air; to prevent this oxygen inhibition radical polymerisations are commonly performed under a nitrogen atmosphere.

For a system with ideal behaviour the relationship between the curing rate R_p and the intensity of the UV-light and the concentration and reactivity of the photoinitiator and (meth)acrylate is given by:^{(11)*}

$$R_p = k_p \cdot [M] \cdot \sqrt{1000 \cdot \Phi \cdot I_0 \cdot \left(1 - 10^{-\varepsilon[PI] \cdot d}\right) / (d \cdot k_t)} \quad [1]$$

where k_p is the propagation rate constant in s^{-1} , $[M]$ is the concentration of (meth)acrylate in mol/L, Φ is number of initiated polymer chains per absorbed photon, I_0 is the intensity of the incident light in Einstein $cm^{-2} s^{-1}$, ε is the extinction coefficient in $L mol^{-1} cm^{-1}$, $[PI]$ is the photoinitiator concentration in mol/L, d is the thickness of the sample in cm, and k_t is the termination rate constant in s^{-1} and with R_p expressed in $mol L^{-1} s^{-1}$. Important factors like absorption of the light by other components than the photoinitiator, the effects of the light gradient over the coating, differences in reactivities in monomer mixtures, and changes of the mobility of reactive groups during the curing are not taken into account. Hence, the given equation is useful for getting a feeling for the importance of some process parameters, but the model is too crude for allowing the equation to be used for fitting of experimental data.

* Unfortunately in literature^(4,7,15,23,24) an erroneous equation persistently appears:

$R_p = k_p \cdot [M] \cdot \sqrt{1000 \cdot \Phi \cdot I_0 \cdot \left(1 - 10^{-\varepsilon[PI] \cdot d}\right) / k_t}$. This equation predicts that thicker coatings give faster curing, which is opposite to general experimental observations. The theoretical derivation of Eq. [1] is given in appendix I.

4.2.2. The effects of crosslinking

Coating formulations typically contain starting compounds with two or more (meth)acrylate groups in order to form a densely crosslinked polymer network⁽¹²⁾. During the formation of the network the mobility of the reactive groups decreases, which may strongly affect the curing rate. The decreased mobility of the (meth)acrylate groups may decrease the curing rate. Furthermore, a considerable fraction of the radicals and the (meth)acrylate groups may become occluded in the polymer network and may not be available for reaction anymore. In free radical polymerisations a strong increase of the polymerisation rate is often observed at intermediate or high conversions, also known as the ‘gel’ or the ‘Trommsdorff’ effect. A common explanation is that decreased mobility of the radicals results in a lower recombination rate and consequently in a higher radical concentration, which subsequently may result in an increase of the curing rate⁽¹³⁾. The net result of all effects may be either faster or slower curing.

An important indicator for the mobility is the glass transition temperature (T_g); at temperatures higher than the T_g polymer segments are mobile and below T_g the system is vitrified. The T_g is determined by the composition of the polymer, the length of the polymer chains, and the degree of crosslinking⁽¹⁴⁾. The influence of the length of the polymer chain is approximately described by:⁽¹⁴⁾

$$T_g = T_g(\infty) - C / M_n \quad [2]$$

where $T_g(\infty)$ is the limiting value of the T_g at high molecular weight, C is a constant, and M_n is the average molecular weight of the polymer. The influence of the crosslinking is approximately given by:⁽¹⁴⁾

$$T_g = T_g(l) + C' / M_c \quad [3]$$

where $T_g(l)$ is the T_g for the polymer without crosslinks; C' is a constant and M_c is the average mass between two crosslinks. During the curing the average polymer chain length and the degree of crosslinking increase, both resulting in an increase of the T_g . When the T_g becomes significantly higher than the curing temperature, the system vitrifies and the curing virtually stops.

4.2.3. Copolymerisation of acrylates and methacrylates

In most of the coatings studied both acrylate and methacrylate groups are present. The difference between acrylates and methacrylates is only one methyl group that is attached to the vinyl group (figure 4.1); this methyl group does not affect the basic mechanism of the radical polymerisation, and acrylates and methacrylates do copoly-

merise. The kinetics of the radical polymerisation, however, is affected. The methyl group enhances the stability of the radical, and consequently lowers its reactivity. In homopolymerisations this lower reactivity results in lower polymerisation rates for methacrylates compared to acrylates. In the case of copolymerisation, also the cross-reactivity between the acrylate and methacrylate groups and their radicals has to be considered. Both the methacrylate radical and the acrylate radical react faster with the methacrylate monomer than with the acrylate monomer. Consequently, in a copolymerisation the methacrylates react faster than the acrylates whereas in a homopolymerisation methacrylates react slower than acrylates.

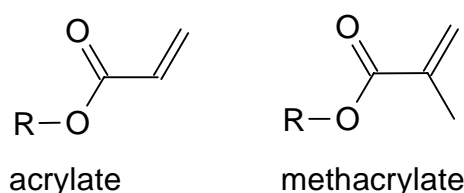


Figure 4.1 General structures of acrylate and methacrylate.

4.3. Experimental

4.3.1. Materials

The matrix material for the coatings was either PEGDA (polyethyleneglycoldiacrylate Mw 575, Aldrich) or TMPTA (trimethylolpropanetriacrylate, UCB). 3-Methacryloxypropyltrimethoxysilane (MPS (ABCR)), propyltriethoxysilane (Aldrich), and methyltrimethoxysilane (Aldrich) were grafted on the silica, tin oxide, and ATO fillers following the procedure as described for MPS in chapter 2. 2-Hydroxy-2-methylpropiophenone (Aldrich) was used as photoinitiator. All materials were used as received.

The coating mixtures were prepared starting from a dispersion of the filler with grafted silane coupling agent (and a small quantity of silane coupling agent oligomers, see chapters 2 and 3) in a water/n-propanol solvent mixture. To this dispersion the desired amounts of acrylate and photoinitiator were added. The amount of photoinitiator was 3 wt% of the organic components (acrylate + MPS) in the coatings. The amounts of water and propanol were adjusted to get the best compromise between colloidal stability of the filler, the solubility of the acrylate, and the rheology of the coating formulation.

4.3.2. Characterisation techniques

The curing kinetics was studied by real-time FTIR⁽¹⁵⁾. Hence, the uncured coatings were applied on a diamond ATR crystal that was mounted in a BIORAD Excalibur FTIR unit (figure 4.2). This unit was operated at up to three IR-spectra per second. The thickness of the coatings with silica, tin oxide, or without filler was 1-3 μm , for ATO filled coatings the thickness was less than 1 μm to compensate for the higher light absorption by the ATO particles. The curing experiments were started after the solvents had evaporated, which could be determined by the disappearance of the solvent signals from the IR-spectrum. The curing was monitored by measuring the decrease of the area of the peaks that are associated with the vinyl group. An UV light source, a Spectral Luminator from ORIEL instruments, was mounted over the ATR crystal. Light (305-325 nm) with an intensity of 2 mW/cm^2 was used. The curing was studied under constant illumination and under a nitrogen atmosphere.

The UV/VIS transmittance spectra of the silica, tin oxide, and ATO nanoparticles in dispersion were recorded with a Hewlett Packard 8453 spectrophotometer. Nanoparticles with an MPS treatment (0.1 g MPS / g oxide) were dispersed in a 2/1 methanol/water mixture, this solvent mixture was also used for the baseline measurement. The concentration of the nanoparticles was 0.01 vol% and the path length through the samples was 1 cm. The amount of silica, tin oxide, or ATO in the path of the measurement was equivalent to the amount in a 10 μm thick coating with a filler concentration of 10 vol%.

The T_g of the cured coatings was measured with a Perkin Elmer Pyris 1 DSC unit at a scanning rate of 10 $^\circ\text{C}/\text{min}$.

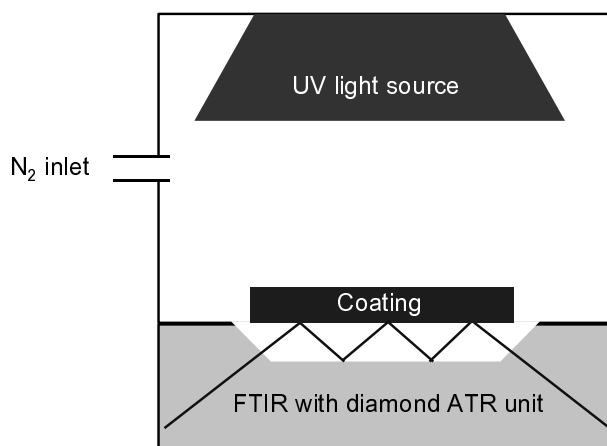


Figure 4.2 Experimental setup for real-time monitoring of the UV-curing.

4.4. Curing of pure acrylates

To get more insight into the curing behaviour of the matrix materials, first the curing of pure acrylates with 3 % photoinitiator but without fillers was studied. During the curing a large number of peaks disappeared from the IR spectrum, as can be seen in figure 4.3. In homopolymerisations of PEGDA and MPS the peaks listed in table 4.1 decreased at the same rate, indicating that the decrease of these peaks may be attributed to the same reacting group, which is the vinyl group that is part of the (meth)acrylate group. In this study only the peaks at 1636 cm^{-1} , 1410 cm^{-1} , and 1320 cm^{-1} were used to follow the conversion of the (meth)acrylate groups. As the carbonyl

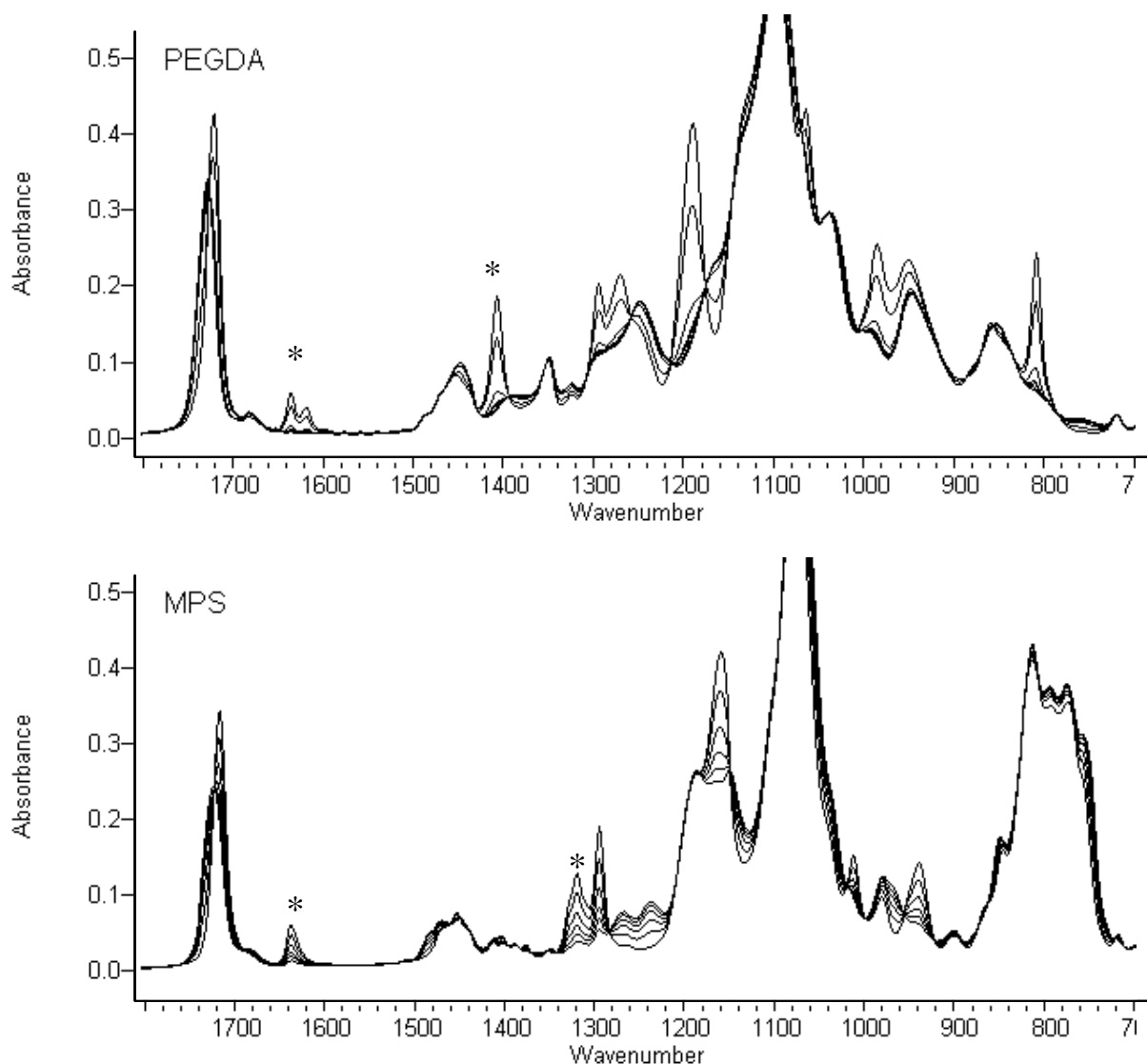


Figure 4.3 Changing IR-spectrum of PEGDA and MPS during curing; the asterisk's indicate peaks that were used to monitor the curing; other peaks that disappear at the same rate are given in table 4.1.

Disappearing peaks (cm ⁻¹)	
PEGDA	MPS
1636	1638
1620	1320
1408	1296
1296	1166
1271	1015
1191	940
980	
810	

Table 4.1 *IR-peaks that can be used to follow the curing.*

group within the (meth)acrylate group is conjugated with the vinyl group the change of the shape of the carbonyl peak at 1700 cm⁻¹ is likely also caused by the conversion of the vinyl groups during curing.

For PEGDA the vinyl groups completely disappeared in 10 seconds. For TMPTA the initial rate was almost as fast as for PEGDA, but after about 20 percent conversion a substantial slowdown of the reaction rate was observed and full conversion was not reached (see figure 4.4). This fits well with the theory that states that the reaction is retarded when the reactive groups are hindered in their movements. The best indication for the mobility of groups in a polymer is the glass transition temperature, or T_g . The T_g of completely cured PEGDA is -30 °C, thus at room temperature the reactive groups remain mobile. For TMPTA no T_g in the range from -60 to +150 °C could be found. A homopolymerisation of MPS was performed to determine the curing rate of the methacrylate group in this compound. This rate was approximately hundred times lower than the curing rate for pure PEGDA.

4.5. Copolymerisation of PEGDA and MPS

To study their copolymerisation, PEGDA and MPS were mixed without any filler and cured following the standard procedure using 3 % photoinitiator. With increasing MPS concentration also the time needed for complete curing increased (figure 4.5). For a pure PEGDA coating about 10 seconds of UV exposure was sufficient for complete curing, but for a coating with 30 w% MPS about 35 seconds was needed. The decrease of the curing rate is especially observed in the early stages of the curing. This observation is in line with the theory for copolymerisation of an acrylate (PEGDA) with a methacrylate (MPS) (section 4.2.3). A radical reacts more easily with a

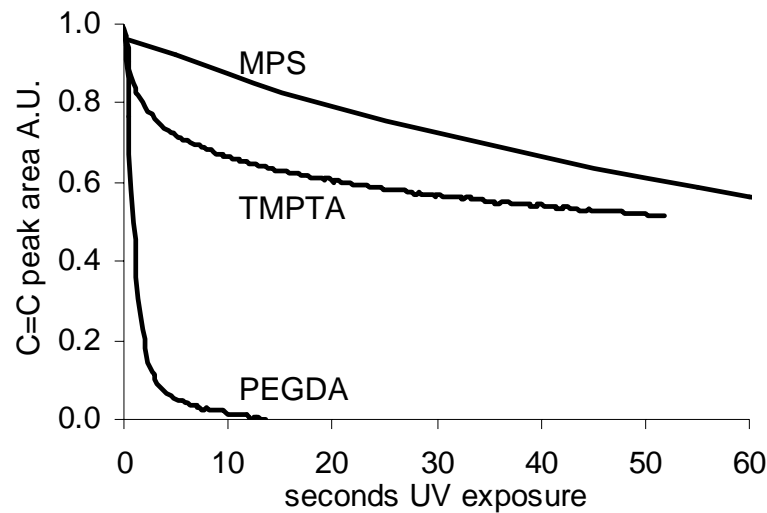


Figure 4.4 *Polymerisation of pure components.*

methacrylate group than with an acrylate group; therefore in the early stages of the polymerisation the methacrylate is consumed in excess and the acrylate is consumed mainly in the late stages of the polymerisation. Consequently, in the early stages the curing rate is closer to the curing rate of the MPS and in the late stages the curing rate is closer to the curing rate of the PEGDA.

By monitoring the peaks at 1636 cm^{-1} , 1408 cm^{-1} , and 1320 cm^{-1} the preferential addition of MPS in a copolymerisation with PEGDA can be observed directly. With the spectra from the homopolymerisation experiments the peak at 1636 cm^{-1} can be attributed to both PEGDA and MPS, whereas the peak at 1408 cm^{-1} is only attributed to PEGDA and the peak at 1320 cm^{-1} is only attributed to MPS. In all experiments the

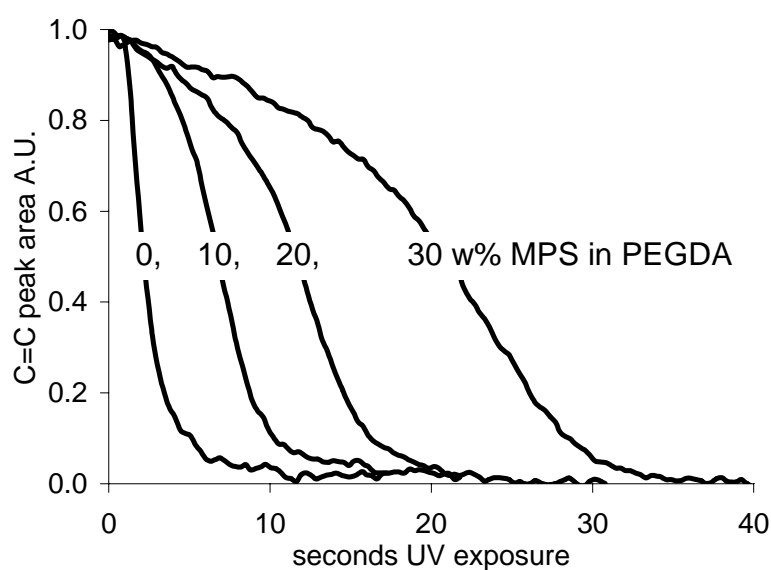


Figure 4.5 *Influence of MPS concentration on the curing kinetics (monitored at 1636 cm^{-1}).*

peak at 1320 cm^{-1} disappeared faster and the peak at 1408 cm^{-1} disappeared slower than the peak at 1636 cm^{-1} . Figure 4.6 shows the decay of these three peaks during the curing of PEGDA-MPS mixture with 30 w% MPS. Initially the relative decay of the MPS peak is three times faster than the decay of the PEGDA peak. This reactivity ratio corresponds well with the values that are typically found for copolymerisation of methacrylates with acrylates; typically the methacrylate is 1-10 times more reactive than the acrylate⁽¹⁶⁾.

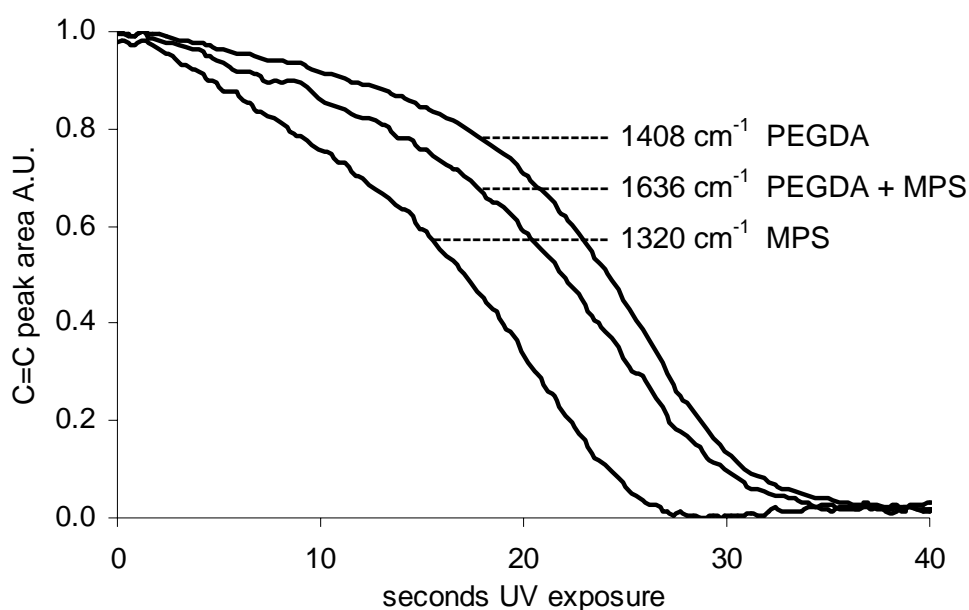


Figure 4.6 Copolymerisation of 30/70 ^{w/w} MPS and PEGDA.

4.6. Influence of the particles on the curing kinetics

4.6.1. Absorption of the UV-light by the oxides

As UV light is used to start the curing reactions it is important that the UV light is available through the whole coating. Absorption of UV light is a typical property of semiconductor materials, thus the use of tin oxide and ATO as filler may decrease the UV intensity in the deeper layers of the coating and consequently may hamper the curing.

Figure 4.7 shows the transmittance through dispersions of silica, tin oxide, and ATO nanoparticles that were treated with 0.1 g MPS per g filler. The amount of nanoparticles in the path of the measurement was equivalent with the amount in a 10 μm thick coating with 10 vol% of filler. For silica the transmittance is high at all measured wavelengths and problems for the curing are not expected. For tin oxide the

transmittance increases strongly between 290 and 320 nm. Especially the transmittance at 315 nm is important as at this wavelength a good efficiency of the photoinitiator is combined with a strong peak in the intensity of the emission spectrum of the UV-lamp used. At 315 nm 52 % of the light is transmitted through the tin oxide, which is sufficient for a reasonable curing rate. For ATO the transmittance is considerably lower, at 315 nm 17 %. This transmittance is sufficient for effective, although somewhat slower, curing, but for thick coatings or coatings with a high ATO concentration the transmittance will be very low and the curing in the deep layers will be strongly hampered.

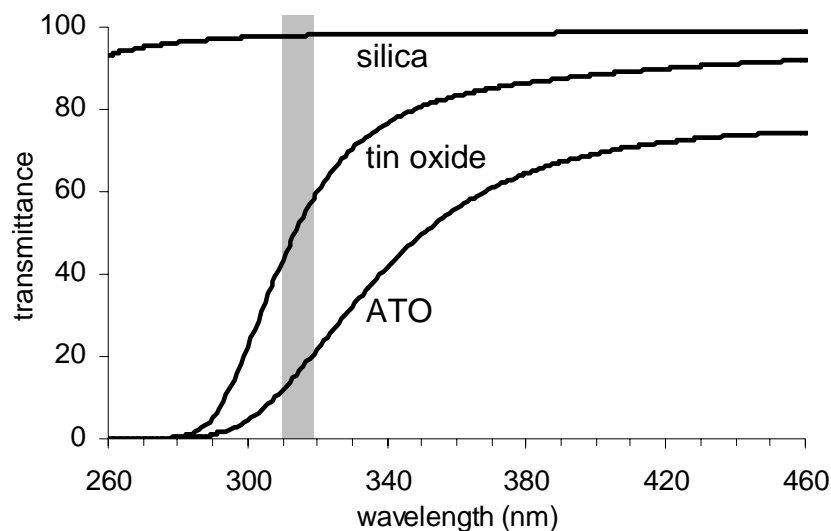


Figure 4.7 Light transmittance through silica, tin oxide, and ATO treated with 0.1 g MPS / g oxide; the grey bar indicates the range where the used photoinitiator and UV-lamps interact strongest.

4.6.2. Curing of silica filled coatings

The effect of silica nanoparticles on the curing of PEGDA coatings was studied with pure silica and with silica with grafted MPS or *n*-propyltriethoxysilane. Addition of pure silica or addition of silica with grafted *n*-propyltriethoxysilane did not affect the curing. Even at a silica concentration of 50 vol% the course of the curing did not change. The addition of silica with grafted MPS resulted in a small retardation, which increased with increasing filler concentration. Figure 4.8 shows the curing of silica filled PEGDA coatings with 0.2 g MPS per g silica. It is expected that more than half of the MPS is grafted on the silica and the remainder is mixed as oligomers with the PEGDA (chapter 2, figure 2.7). The retardation is smaller than might be expected on basis of the MPS-PEGDA ratio in the coatings (table 4.2), when compared to the cur-

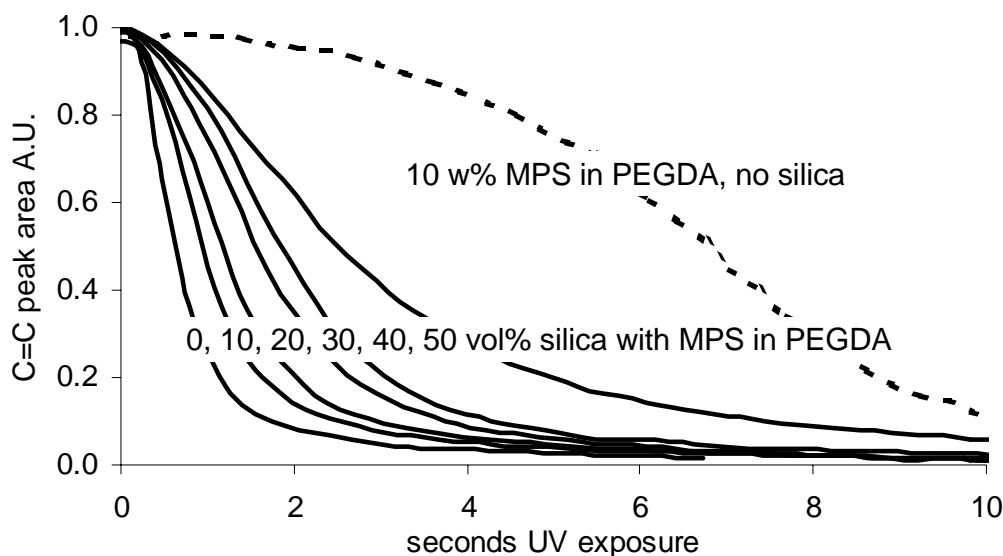


Figure 4.8 Curing of PEGDA coatings with MPS treated silica (0.2 g/g) and 10 w% MPS in PEGDA as reference (all monitored at 1636 cm^{-1}).

ing rates of corresponding MPS-PEGDA mixtures without particles. The coating with 50 vol% silica has an MPS-PEGDA ratio of 35-65, but the curing is faster than the curing of a 10-90 MPS-PEGDA mixture without particles, as shown in figure 4.5. This relative high curing rate for the silica filled coating implies that the silica affects the reactivity of the MPS or PEGDA, or it is possible that a part of the MPS does not participate in the curing. Due to peak overlap it is not possible to exactly determine the fraction of MPS that did react, but it is estimated to be more than 70%. Consequently, the observed curing rate cannot only be attributed to a low MPS participation, thus an increased reactivity of MPS or PEGDA due to interactions with silica has to be considered. Especially hydrogen bonds between silica hydroxyl groups and the carbonyl

vol% silica	weight ratio	
	MPS	PEGDA
0	0	100
10	4	96
20	10	90
30	17	83
40	25	75
50	35	65

Table 4.2 MPS-PEGDA ratio in silica filled coatings (0.2 g MPS / g silica).

groups of the MPS or PEGDA may affect the curing. An acceleration of the polymerisation rate due to hydrogen bonding is not uncommon for acrylates and methacrylates⁽¹⁶⁻¹⁸⁾.

An important question is whether the MPS that is grafted on the filler forms a copolymer with the acrylate matrix. This can be determined by comparing the conversion rates of MPS and PEGDA, as discussed in section 4.5. For all coatings containing silica with grafted MPS, the conversion of MPS was faster than the conversion of acrylate. This suggests that the MPS and the acrylate form a copolymer, thus a chemical link between the filler and matrix is formed. In figure 4.9 the conversion of MPS and PEGDA is shown for a coating with 50 vol% silica. The difference between the conversion rate of MPS and PEGDA is smaller than expected on basis of the experiments in section 4.5. Again the difference between the experiments may be explained by a lower MPS conversion or by interactions with the silica that may affect the reactivity ratios of MPS and PEGDA. Moreover, as the MPS is mainly located at the surface of the silica and to a minor extent in the bulk of the matrix, the degree of mixing of MPS and PEGDA is lower. The lower degree of mixing will shift the kinetics somewhat towards the homopolymerisation and consequently will increase the conversion rate of PEGDA and will decrease the conversion rate of MPS.

With TMPTA as acrylate matrix about 40% of the acrylate groups are not con-

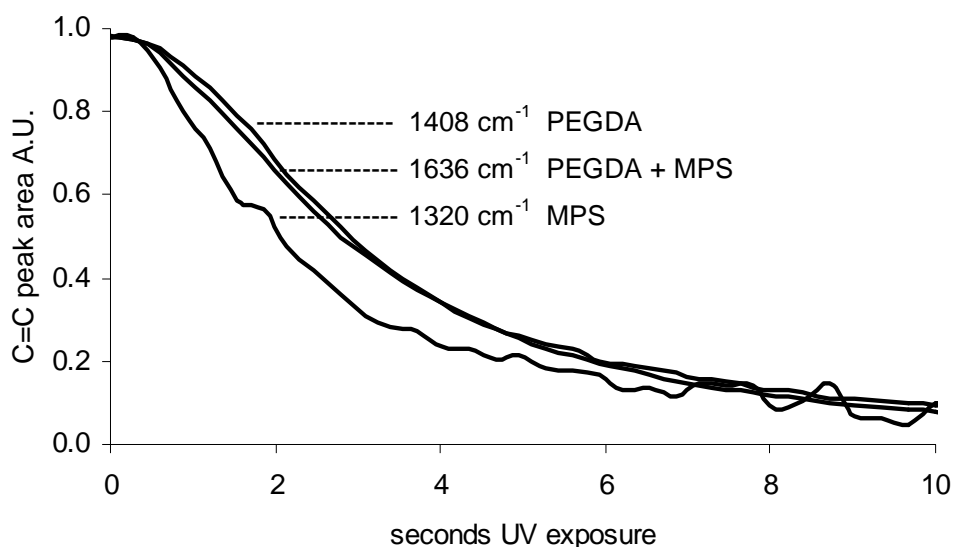


Figure 4.9 Curing of grafted MPS and PEGDA matrix in a coating with 50 vol% silica; the MPS/PEGDA ratio is 1/2 w/w .

verted during curing. Addition of up to 50 vol% silica with 0.2 g MPS / g silica does not result in a significant change of unreacted (meth)acrylate groups after curing. In the first stages a slowdown of the curing due to the MPS is observed like with the PEGDA, but in the stages where the curing rate is determined by the mobility of the reactive groups, the curing rate is not affected by increasing silica and MPS concentration.

4.6.3. Curing of ATO and tin oxide filled coatings

In very thin coatings, where the absorption of UV light by ATO is negligible, the effects found with ATO are similar as with silica. Addition of pure ATO does not affect the curing rate and addition of MPS modified ATO causes a small decrease of the curing rate (figure 4.10). In thick coatings the curing in the deeper layers is strongly

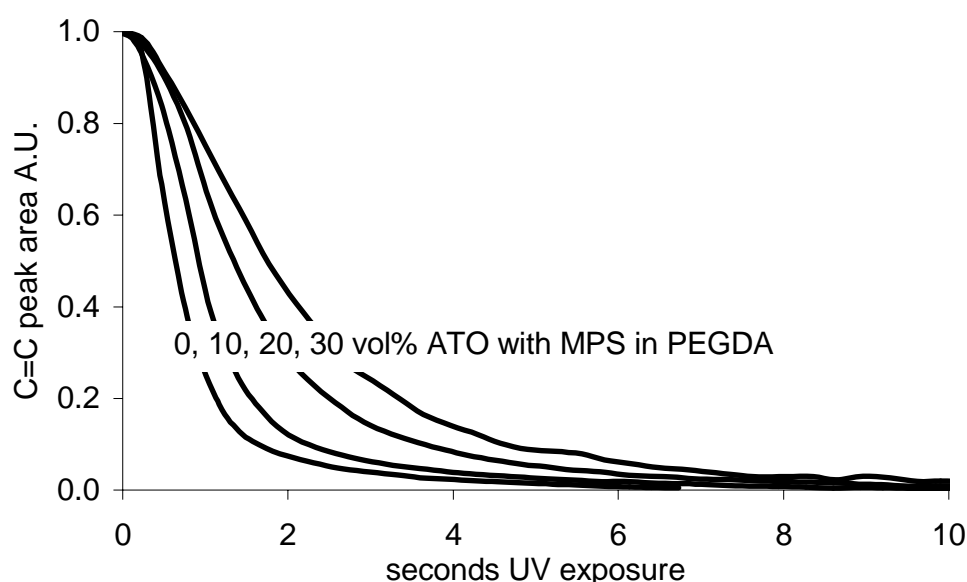


Figure 4.10 Curing of PEGDA coatings with MPS treated ATO (monitored at 1636 cm^{-1}).

retarded due to the lower UV intensity.

In contrast to silica and ATO, tin oxide has a strong effect on the curing. With increasing tin oxide concentration the curing becomes much slower, as shown in figure 4.11. The retardation is observed during all stages of the curing and consequently it cannot be attributed to a decreased mobility of the reactive groups. It has to be attributed to a lower propagation rate of the polymerisation or to a decrease of the radical concentration. Lowering of the propagation rate can occur when the radicals reversibly form complexes with other molecules. In the complex the radical may have a low reac-

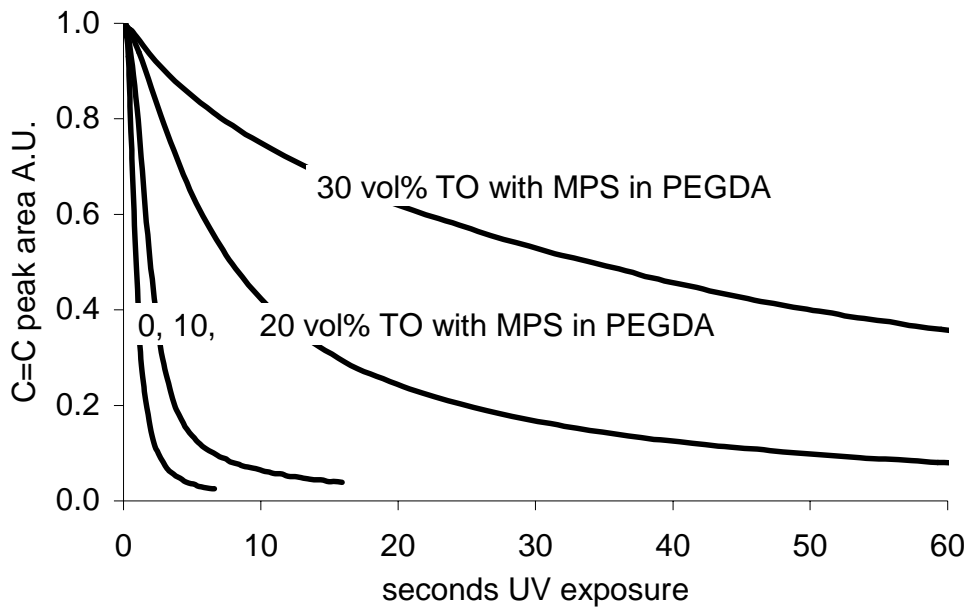


Figure 4.11 Curing of PEGDA coatings with MPS treated TO (monitored at 1636 cm^{-1}).

tivity or no reactivity at all, but when the complex is broken up the polymerisation can proceed⁽¹⁹⁾. With these complexes a strong post curing is expected, i.e. the curing after the UV exposure has stopped and no new radicals are generated. However, the post curing in coatings with tin oxide was smaller than the post curing in similar coatings with silica. Apparently the cause for the retardation has to be found in a lower radical concentration. This lower radical concentration can be due to a lower radical generation rate or due to excessive radical consumption. Lowering of the radical generation rate can be expected if the intensity of the UV light decreases due to absorption by a filler. However, the transmittance in the coatings with tin oxide is higher than in the ATO coatings whereas the curing rate is much slower. Moreover the retardation was found to depend only moderately on layer thickness. Consequently, the retardation of the curing is most likely caused by excessive radical consumption. The direct interactions between the reactive groups and the tin oxide surface may be an important factor for the retardation of the curing. To study these interactions reference coatings with pure tin oxide and with tin oxide that was treated with methyltrimethoxysilane (0.2 g/g) were made. With 5 or 10 vol% pure tin oxide the retardation of the curing was stronger than for comparable coatings with tin oxide with grafted MPS. Due to lack of colloidal stability of the pure tin oxide, the preparation of homogeneous coatings with more than 10 vol% tin oxide was impossible. With tin oxide that was treated with methyltrimethoxysilane the retardation of the curing was negligible; the curing rate was

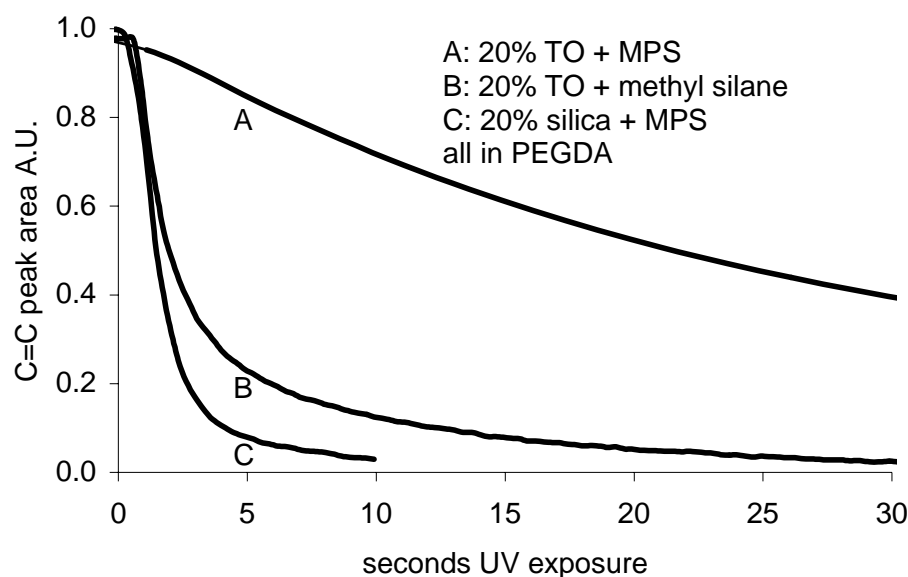


Figure 4.12 Effect of TO surface on the curing rate of PEGDA based coatings (monitored at 1636 cm^{-1}).

comparable to that of the coatings with silica (see figure 4.12). The methyltrimethoxysilane is likely to form a closed inert layer on the tin oxide surface that prevents direct contact of the acrylate groups and radicals with the tin oxide. The MPS also forms a closed layer, but with its methacrylate group folded back to the tin oxide surface (see chapter 2). The direct interaction of this methacrylate group, or an other (meth)acrylate group, with the tin oxide surface may be essential in the retardation mechanism.

4.6.4. Proposed mechanisms for the retardation of the curing

An important termination mechanism for polymerisation of (meth)acrylates is disproportionation, i.e. the transfer of one H-atom from one radical to another radical. A similar reaction might also be possible with tin oxide. The hydroxyl groups on tin oxide can donate a H-atom leaving a relatively stable Sn-O* radical. This new radical may not be able to initiate a new chain, but may combine with another (meth)acrylate radical. Thus, although the number of radicals remains the same, a large part of highly reactive (meth)acrylate radicals are replaced by stable Sn-O* radicals that do not participate in the curing. However, the Sn-O* radicals may still combine with another (methacrylate) radical.

Another possibility is the abstraction of a H-atom from a (meth)acrylate radical by means of an electrochemical process. Mulvani et al.⁽²⁰⁾ showed that tin oxide nanoparticles can abstract an electron from a 1-hydroxy-1-methylethyl radical, leaving

2-propanon and a proton. Subsequently the excess electrons in the tin oxide reduce the protons under formation of H_2 . Similar processes may also occur with (meth)acrylate radicals. Electron transfer from the (meth)acrylate radical to the tin oxide is possible if the redox potential of the tin oxide is higher than the redox potential of the (meth)acrylate radical. The redox potential of the conduction band of bulk tin oxide is close to 0 V vs. NHE (Normal Hydrogen Electrode), but for nanoparticles a somewhat lower value may be expected due to quantum size effects⁽²⁰⁾. The redox potential for the injection of one electron in methylmethacrylate is -1.1 V vs. NHE⁽¹⁰⁾. If a proton is added to this anion radical, the structure is the same as for a methacrylate radical in a free radical polymerisation. Due to the extra proton a somewhat higher redox potential for the methacrylate radical than the mentioned -1.1 V may be expected, but it may still be lower than the redox potential of the conduction band of tin oxide, thus transfer of an electron from the (meth)acrylate radical to tin oxide may be possible. Figure 4.13 shows the proposed mechanism for the electrochemical radical consumption by tin oxide. The methacrylate radical has two main resonance structures and the radical is partly situated on the carbonyl oxygen (figure 4.13 A). Due to the hydrogen bonding between this carbonyl and a hydroxy group on the tin oxide surface the distance between the radical and the tin oxide is small, which is important for the electron transfer. Together with the electron the methacrylate radical loses a proton; hence effectively a H-atom is lost. The H-atom may be lost from the methyl group, as depicted in figure 4.13 B, or it may be lost from the CH_2 group in the acrylate backbone. A small accumulation of protons in the matrix and electrons in the tin oxide may occur, but ultimately they have to disappear. This is possible by reduction of the protons under the formation of H_2 as observed by Mulvani *et al.* Furthermore it should be considered that the accumulated protons in the matrix increase the redox potential of the (meth)acrylate radicals and the accumulated electrons in the tin oxide lower the redox potential of tin oxide. Consequently the redox potential of the radicals may become higher than the redox potential of the tin oxide and electron transfer from the tin oxide to the (meth)acrylate radical may become possible. An equilibrium situation may be established in which both the reactions depicted in figure 4.13 B and C proceed and tin oxide effectively catalyses the termination by disproportionation.

As antimony doped tin oxide is also a semiconductor it is surprising that the same retardation of the curing was not found with this type of particles. However, the surface chemistry of ATO is very different from the surface chemistry of tin oxide. The surface of ATO is enriched with Sb(III)^(21,22) and may not contain many hydroxy

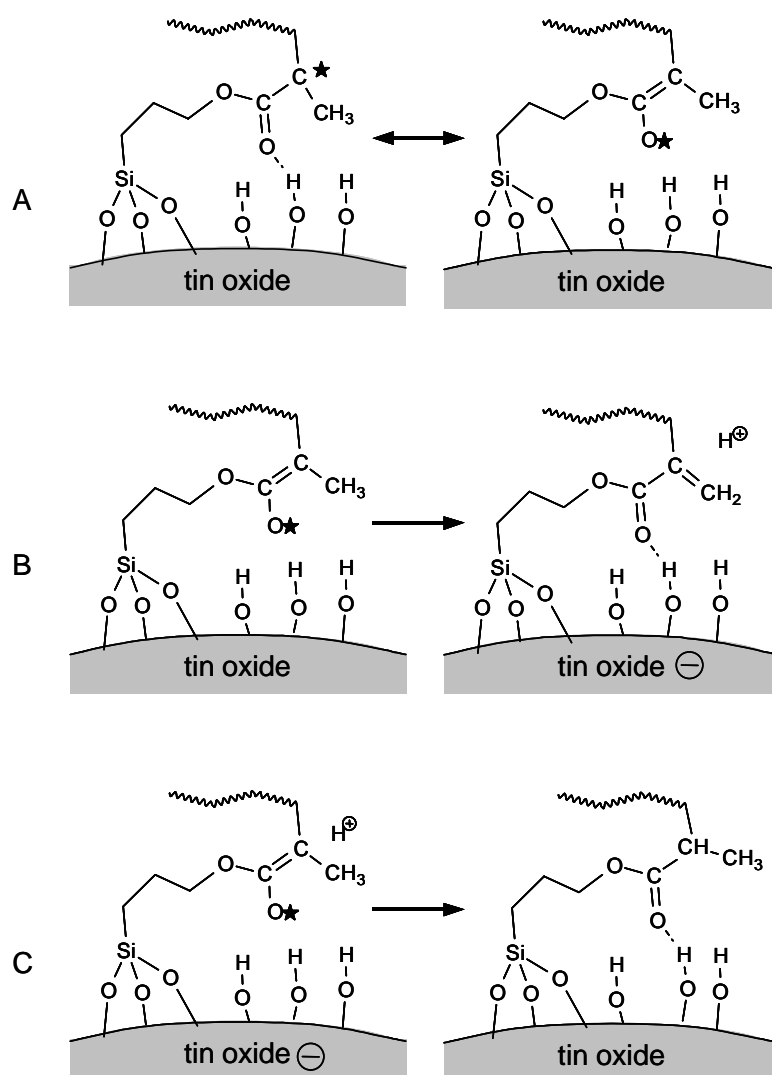


Figure 4.13 *Proposed mechanism for the retardation of the curing by tin oxide.*

groups. Furthermore the redox potential of ATO might be different from the redox potential of tin oxide.

4.7. Conclusions

Silica, tin oxide, and ATO have different effects on the curing of the acrylate matrix. Pure silica does not significantly influence the curing of the acrylate matrix. The PEGDA coatings with silica that was treated with MPS cured somewhat faster than equivalent PEGDA-MPS mixtures without silica. Tin oxide and especially ATO absorb UV light, which will slow down the curing in deeper layers. The MPS that is grafted on the fillers is thought to copolymerise with the acrylate matrix, thus the intended chemical links between the filler and the matrix are formed. As the polymerisa-

tion rate of MPS is considerably lower than the polymerisation rate of the pure acrylates, the presence of MPS in the coating formulations results in slower curing. Direct contact between the tin oxide and the (meth)acrylate results in a strong retardation of the curing; this effect is not found for silica and ATO. To explain the retardation a mechanism is proposed that involves catalysis by the tin oxide of the termination of the free radical polymerisation by disproportionation. However, for verification of this proposed mechanism further research is needed.

Reference List

1. C. Decker, *Macromolecular Rapid Communications*, 23, 1067-1093 (2002).
2. C. Decker, *Materials Science and Technology*, 18 (Processing of polymers), 615-657 (1997).
3. S. P. Pappas, *Radiation curing: science and technology* (Plenum, London, 1992).
4. J. P. Fouassier and J. F. Rabek, *Radiation curing in polymer science and technology* (Elsevier Science Publishers Ltd, Barking, ed. 1-4, 1993).
5. M. D. Goodner and J. Brandrup, *Chemical Engineering Science*, 57, 887-900 (2002).
6. R. Mehnert, A. Pincus, I. Janorsky, R. Stowe, A. Berejka, *UV & EB Curing Technology & Equipment* (John Wiley & Sons, London, 1998).
7. J. G. Kloosterboer, *Advances in Polymer Science*, 84, 1-61 (1988).
8. P. G. Harrison, in *Chemistry and Technology of Silicon and Tin*, 384-395 (1992).
9. B. R. Muller, S. Majoni, D. Meissner, R. Memming, *Journal of Photochemistry and Photobiology A: Chemistry*, 151, 253-265 (2002).
10. A. J. Hoffman, H. Yee, G. Mills, M. R. Hoffmann, *Journal of Physical Chemistry*, 96, 5540-5546 (1992).
11. G. R. Tryson and A. R. Shultz, *Journal of Polymer Science, Polymer Physics Edition*, 17, 2059-2075 (1979).
12. C. Decker, *Pigment & Resin Technology*, 30, 278-286 (2001).
13. G. A. O'Neil, M. B. Wisnudel, J. M. Torkelson, *Macromolecules*, 29, 7477-7490 (1996).
14. D. W. van Krevelen, *Properties of polymers : their correlation with chemical structure, their numerical estimation and prediction from additive group contributions* (Elsevier, Amsterdam, ed. 3rd, compl. rev. ed., 1990).
15. T. Scherzer and U. Decker, *Radiation Physics and Chemistry*, 55, 615-619 (1999).
16. J. Brandrup, *Polymer Handbook*, 4th edition, 1999).

17. J. F. G. A. Jansen, A. A. Dias, M. Dorschu, B. Coussens, *Macromolecules*, 36, 3861-3873 (2003).
18. K. Plochocka, *Journal of Macromolecular Science Reviews, Macromolecular Chemistry*, C20, 67 (1981).
19. R. J. Young and P. A. Lovell, *Introduction to polymers* (Stanley Thornes Ltd, 1991).
20. P. Mulvaney, F. Grieser, D. Meisel, *Langmuir*, 6(3), 567-572 (1990).
21. V. Dusastre, D. E. Williams, *Journal of Physical Chemistry B*, 102(35), 6732-6737 (1998).
22. B. Slater, C. R. A. Catlow, D. H. Gay, D. E. Williams, V. Dusastre, *Journal of Physical Chemistry B*, 103(48), 10644-10650 (1999).
23. G. Odian, *Principles of polymerization* (Wiley-Interscience, Chichester, ed. 3rd ed, 1991).
24. K. A. Berchtold, T. M. Lovestead, C. N. Bowman, *Macromolecules*, 35, 7968-7975 (2002).

Chapter 5

Electrical properties of the nanocomposite coatings

Synopsis

In this chapter the effect of the addition of antimony doped tin oxide (ATO) and tin oxide nanoparticles on the electrical resistivity of acrylate coatings is described. ATO and tin oxide are electrically conductive materials, hence when used as filler they lower the electrical resistance of a composite. To enable dispersing of these fillers in acrylate matrices, 3-methacryloxypropyltrimethoxysilane (MPS) was grafted on the surface of the fillers. However, the effect of this surface modification on the resistivity of the composite was unknown. It was found that the effect of the surface modification is twofold. By increasing the amount of (insulating) MPS on ATO a slight increase of the electrical resistance between the particles was found. Besides that, the surface modification was also found to have a strong effect on the distribution of the ATO in the acrylate matrix. Surface modification with a large amount of MPS resulted in stable dispersions of ATO, leading to a homogeneous distribution. Surface modification with small amounts of MPS led to instable ATO dispersions and aggregation of ATO into a fractal type network, which gives a much lower resistivity especially at low-volume fractions.

5.1. Introduction

In this chapter the effect of the addition of antimony doped tin oxide (ATO) and tin oxide nanoparticles on the electrical resistivity of acrylate coatings is described. As ATO and to a lesser extent tin oxide have a good electrical conductivity, the addition of these nanoparticles is expected to lower the electrical resistivity of the composite coatings. A complicating factor in this study is the presence of grafted 3-methacryloxypropyltrimethoxysilane (MPS) on the surface of the nanoparticles, which is needed for dispersing the nanoparticles in the acrylate matrix (see chapter 2 and 3). The grafted MPS forms a thin non-conducting layer on the conductive filler, which is, from the point of view of realising a high conductivity level in the nanocomposite coatings, an undesirable aspect. By varying the amount of MPS the effect of this layer on the electrical resistivity of the composites is studied.

The electrical resistivity of a coating with conducting filler particles is determined by the amount and the distribution of these fillers and by the effectiveness of electron transport between the particles⁽¹⁻³⁾. The electrical resistivity is most effectively lowered when the filler particles are in direct contact with each other and form a continuous network through the whole matrix. The formation of such a network depends on the filler fraction, but also on filler-filler, filler-matrix, and matrix-matrix interactions, the size and shape of the particles, and the preparation conditions⁽¹⁻⁸⁾. The number of parameters for electron transport and filler distribution is very large, and it is extremely difficult, if not impossible, to include all these parameters in a model describing the dependency of the electrical resistivity on the filler fraction. However, for different systems not all parameters are equally important and, depending on the system, some parameters may be omitted from the model. The many models that have been proposed in literature are all applicable to a part of the reported experimental results, but none of the individual models is applicable to all experimental results^(2,3,7,8). In this chapter first the experimental results are presented and subsequently a link with theory is made.

5.2. Experimental

3-Methacryloxypropyltrimethoxysilane (MPS) was grafted on the ATO and tin oxide particles as described in chapter 2. The amount of MPS that was used for the grafting was varied from 0 to 0.4 g per g of ATO or tin oxide. The solvent mixture used in the grafting procedure was replaced by a water / 1-propanol mixture; the ratio between water and propanol and the total amount of solvents was adjusted to obtain a stable dispersion in which also the acrylate resin could be dissolved. This resulted in a

typical water to propanol ratio of 1:1 to 1:2 by weight and a solvents to ATO or tin oxide ratio of typically 1:2 to 1:5 by weight. Variable amounts of this master batch were mixed with the appropriate amounts of matrix material and photoinitiator (2-hydroxy-2-methylpropiophenone, Aldrich) resulting in a concentration series from 0 to 30 vol% ATO or tin oxide (without solvents). As matrix material Ebecryl 745 (commercial acrylate mixture, UCB), PEGDA (polyethyleneglycoldiacrylate Mw 575, Aldrich), and TMPTA (trimethylolpropanetriacrylate, UCB) were used. For the calculation of the volume fractions, the MPS was considered as part of the matrix. The coating mixtures were applied on a polycarbonate substrate and subsequently the samples were placed for half an hour to one hour in a well-ventilated area to allow the solvents to evaporate. Next the coatings were cured by exposure to UV light (20 mW/cm²; 60 seconds; N₂ atmosphere). The thickness of the coatings ranged from 5 to 30 μm.

TEM images were collected with a JEOL 2000FX operated at 80 kV. The samples were prepared by microtome cutting; the thickness of the samples was approximately 70-100 nm.

The electrical resistance of the coatings was measured with a Keithley 237 electrometer using the direct current mode. The applied voltage ranged between 10 and 1000 V; in this range the coatings were found to have ohmic behaviour. On the coatings four electrodes were applied with highly conductive paint (graphite conductive adhesive 154, Electron Microscopy Sciences). The electrodes were applied as four parallel lines with a length and a separation of 1 cm. The resistance was measured over at least three sets of electrodes at three different spacings, as indicated in figure 5.1. To correct for the contribution of the contact resistance between the electrodes and the coating, the increase of the measured electrical resistance upon the increase of the elec-

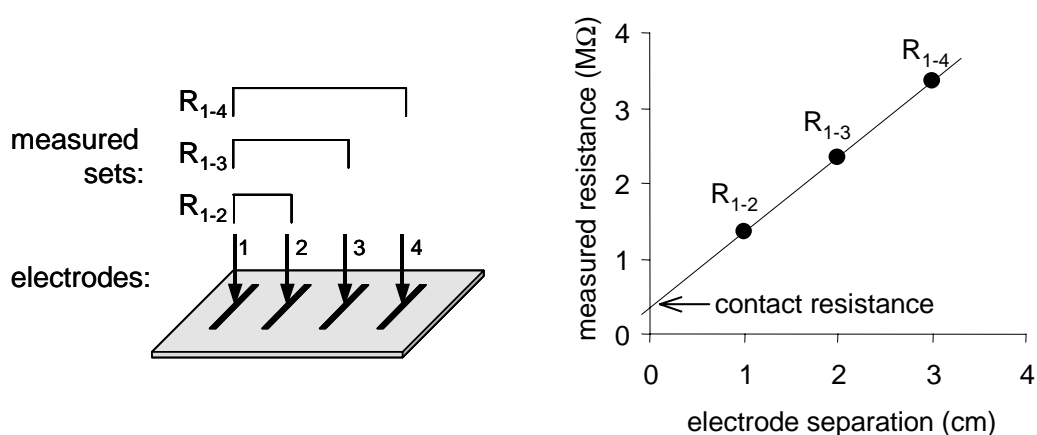


Figure 5.1 Schematic representation of the electrical resistance measurements.

trodes separation was used to calculate the electrical resistance of the coatings.

The reproducibility of the experiments depended on the accuracy of the resistivity measurements and on the reproducibility of coating preparation. The accuracy of the measurements was affected by variations in spacing and length (both $\pm 20\%$) of the painted electrodes and occasional variations in coating thickness, which could be recognised by differences in colour intensity. Measurements on different areas of a coating gave a variation of up to 50% in resistance values. The same variation caused that the increase of the measured resistance with increasing electrode spacing was somewhat irregular: ideally the steps in measured resistance should be equal, but in practice a variation of up to 50% in step size was observed. In the calculated coating resistivity the variation in step size is somewhat averaged out. Representative examples of experimental resistance series are given in table 5.1. In theory, the contact resistance between the electrodes and the coating can be calculated by extrapolation of the measured resistances to an electrode separation of zero. However, the variation in the step size also affects this extrapolation and the resulting error can be larger than the actual contact resistance itself. In practice the calculated contact resistance was in the same range as the variation in the step size. The resistance of the coating was converted to the bulk resistivity by multiplying the coating resistance with the coating thickness. The measured coating thickness ranged from 5 μm for coatings with high filler fractions to 30 μm for coatings with low filler fractions. The thickness of the coatings was measured with an accuracy of about 2 μm , which added an additional error of 20-40% to the calculated resistivity.

example	measured resistance (M Ω)			increase of resistance (M Ω)		ratio between step 1 and step 2
	R ₁₋₂	R ₁₋₃	R ₁₋₄	step 1	step 2	
1	10	19	27	9	8	1.13
2	2.5	4.6	8.2	2.1	3.6	0.58
3	25	44	65	19	21	0.90
4	16 *10 ²	26 *10 ²	37 *10 ²	1.0 *10 ²	1.1 *10 ²	0.91

1: TMPTA with 5 vol% ATO; 0.17 g MPS / g ATO

2: TMPTA with 10 vol% ATO; 0.08 g MPS / g ATO

3: Ebecryl 745 with 30 vol% ATO; 0.33 g MPS / g ATO

4: PEGDA with 20 vol% ATO; 0.21 g MPS / g ATO

Table 5.1 Examples of experimental resistance series.

The preparation of the coatings gave the largest variation for the reproducibility of the experiments. The resistivity values of different coatings prepared from one master batch varied up to 50%, which is about the error of measurement. Between different master batches, however, the resistivity levels varied about one decade. As the trend lines for the resistivities cover many orders of magnitude this large variation does not prohibit drawing useful conclusions. Repeating the resistance measurements with several months interval gave values within 20 % of the original measurement.

5.3. Results

5.3.1. Electrical resistivity of ATO filled coatings

The electrical resistivity of the ATO filled coatings was studied with three different matrix materials: Ebecryl 745, PEGDA, and TMPTA. For these three matrices the effects of ATO concentration and of on the filler surface grafted MPS were studied.

With Ebecryl 745 as the matrix, the dependence of the composite resistivity on the ATO concentration and the grafting of MPS on ATO is demonstrated most clearly. Ebecryl 745 coatings without filler have a resistivity higher than 10^{11} Ωcm , but by filling these coatings with ATO particles the resistivity can be reduced to values below 10^3 Ωcm . The resistivity of the composite depends both on the volume fraction of ATO and on the amount of MPS used to modify the ATO surface, as shown in figure 5.2. In the series with 0.04 and 0.08 g MPS / g ATO addition of only 1-2 volume per-

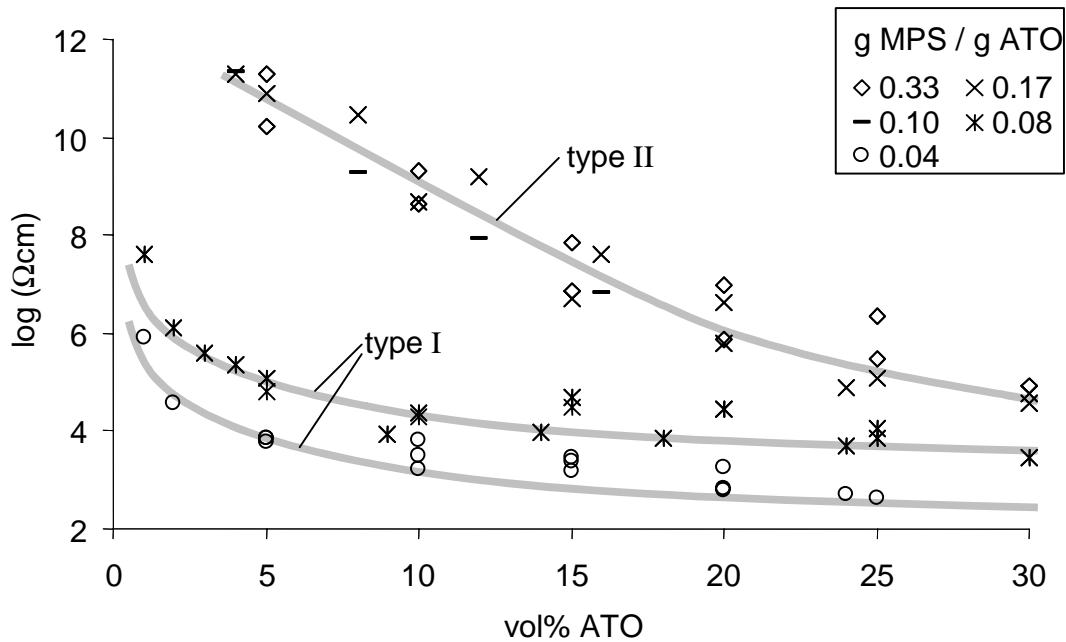


Figure 5.2 Resistivity of Ebecryl 745 coatings filled with ATO treated with 0.04 to 0.33 g/g MPS. Lines are guides to the eye.

cent of ATO results in a decrease of the electrical resistivity by several orders of magnitude. A further increase of the volume fraction of ATO has only a relatively small effect on the resistivity. A curve with this shape will further on be referred to as type I. For the whole ATO concentration range studied, the composites with 0.04 g MPS / g ATO have a somewhat lower resistivity than the composites with 0.08 g MPS / g ATO.

For the series with 0.10, 0.17, and 0.33 g MPS / g ATO a different dependence of the resistivity on the ATO concentration is found. In these series the decrease of the resistivity is more or less exponential and is spread out over a much wider concentration range. A curve with this shape will further on be referred to as type II. It is also remarkable that in the latter three series the resistivity does not depend anymore on the MPS to ATO ratio. It should be noted that the MPS to ATO ratio refers to the amount of MPS added to the ATO during the grafting procedure; however, only a part of the MPS is really grafted on the ATO (see chapter 2). In figure 5.3b the actual amount of grafted MPS for different MPS to ATO ratios is shown; the remaining part of added

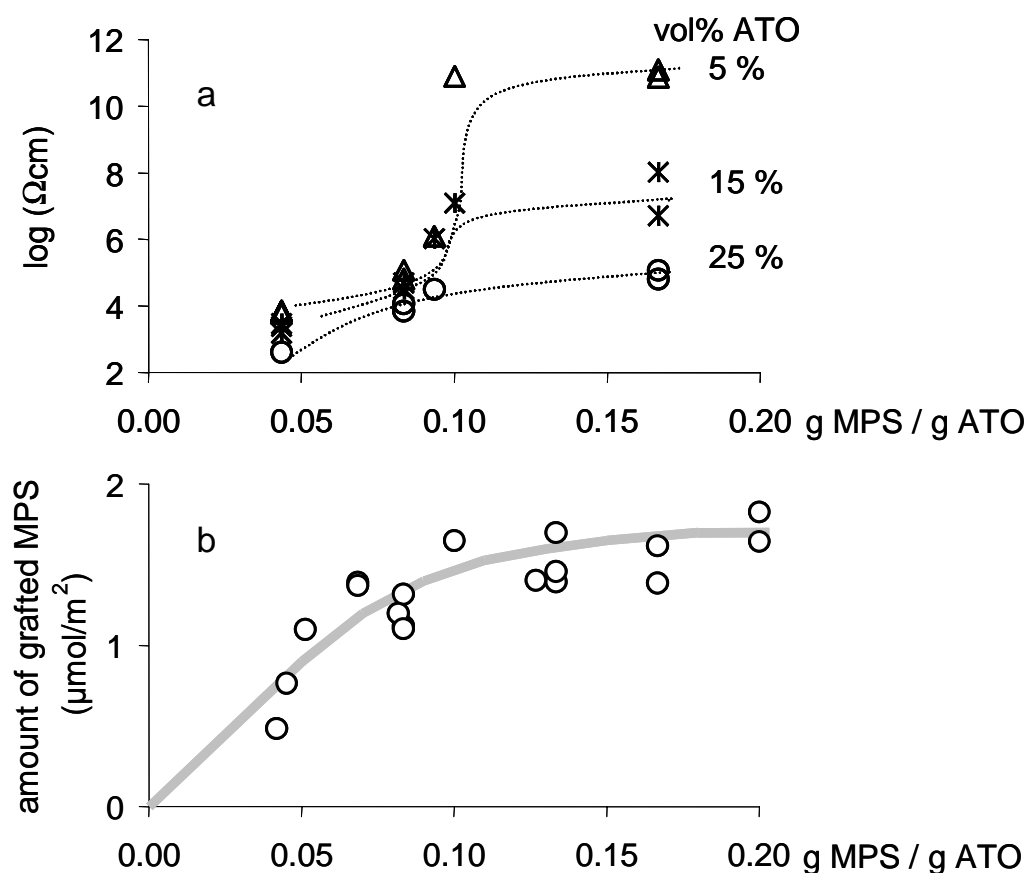


Figure 5.3 *a: Effect of MPS to ATO ratio on resistivity at fixed ATO concentrations. b: Amount of grafted MPS as function of MPS to ATO ratio.*

MPS that is not grafted on the ATO may be dissolved in the acrylate. The amount of grafted MPS may be more relevant for the coating resistivity than the overall amount of MPS added to the ATO. This becomes clearer by comparing the amount of grafted MPS for different MPS to ATO ratios with the coating resistivity for different MPS to ATO ratios, as shown in figure 5.3. At low MPS to ATO ratios curves of type I are found, thus the resistivity is low even at a filler fraction of only 5 vol%. In the same MPS to ATO range, the MPS layer on the ATO particles is not completely filled. The rapid increase of the resistivity for a filler fraction of 5 vol% between 0.08 and 0.10 g MPS / g ATO marks the transition to curves of type II. This transition matches the range where the amount of grafted MPS on ATO reaches its upper limit. Increasing the MPS to ATO ratio beyond 0.10 g MPS / g ATO does not result in more grafted MPS, which may explain the overlapping of the type II curves for different MPS to ATO ratios.

For the PEGDA coatings the trends are similar to those of the Ebecryl 745 coatings. With a MPS to ATO ratio below 0.10 g/g the resistivity versus ATO concentration curves have similar shape (type I) and similar resistivity levels as found for the Ebecryl 745 equivalents (see figure 5.4). With a MPS to ATO ratio higher than 0.10 g/g curves of type II are found. However, at low filler fractions the resistivity is considerably lower than for the corresponding Ebecryl 745 composites; this may be attrib-

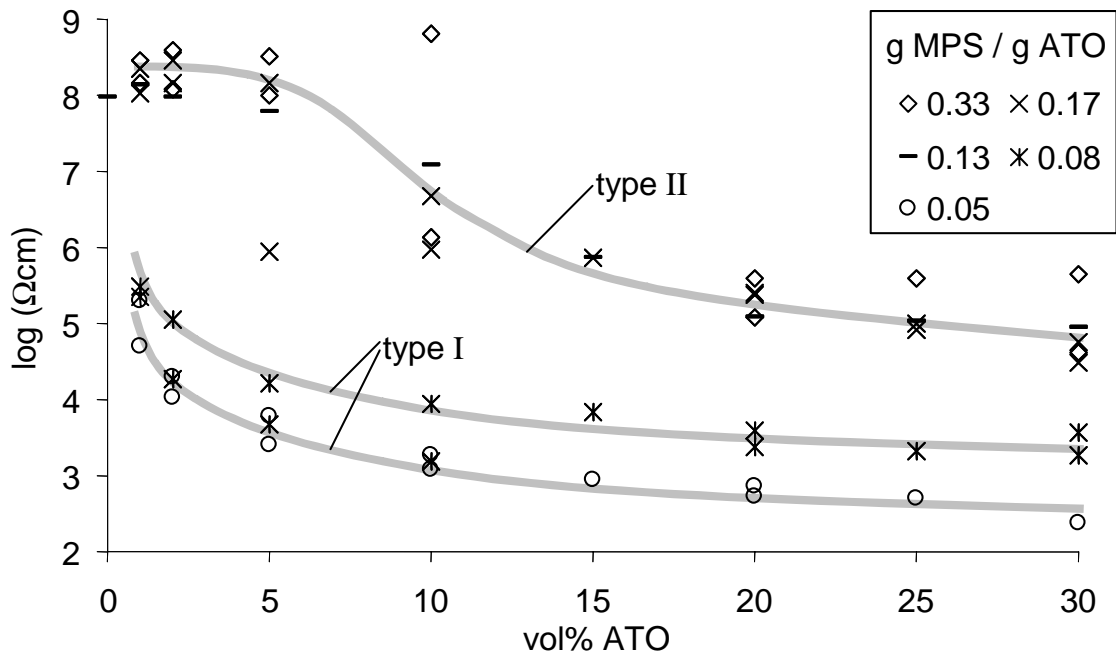


Figure 5.4 Resistivity of PEGDA coatings filled with ATO treated with 0.05 to 0.33 g/g MPS. Lines are guides to the eye.

uted to the large difference in resistivity of the matrix materials.

The compatibility of the MPS treated ATO particles with the TMPTA matrix appears to be lower than with the other two tested acrylate resins. In a TMPTA matrix the ATO particles have, especially at low MPS to ATO ratios, a strong tendency to segregate from the matrix and it appears difficult to make homogeneous coatings. With a MPS to ATO ratio of 0.04 g/g (the lowest used for the other acrylates) no homogeneous coating is made and with higher MPS to ATO ratios the reproducibility is poor. Figure 5.5 shows that most electrical resistivity versus ATO concentration curves show type I behaviour, also at MPS to ATO ratios higher than 0.10 g/g. At a MPS to ATO ratio of 0.25 g/g a type II curve is observed. The series at higher MPS to ATO ratios do not have exclusive type I or type II behaviour; a part of the data points appear on the type I curve found for low MPS to ATO ratios and the remainder of the data points appear on the type II curve found for the 0.25 g MPS / g ATO series.

To analyse the distribution of filler in the matrix TEM images were taken. Figure 5.6a shows a TEM image of a TMPTA coating filled with 1 vol% ATO (0.08 g/g MPS) that has a relative low resistivity and originates from a type I series. The filler particles are aggregated in rather open flocs. Figure 5.6b shows the same coating at a higher magnification; the pattern is similar to that of figure 5.6a, which is typical for a

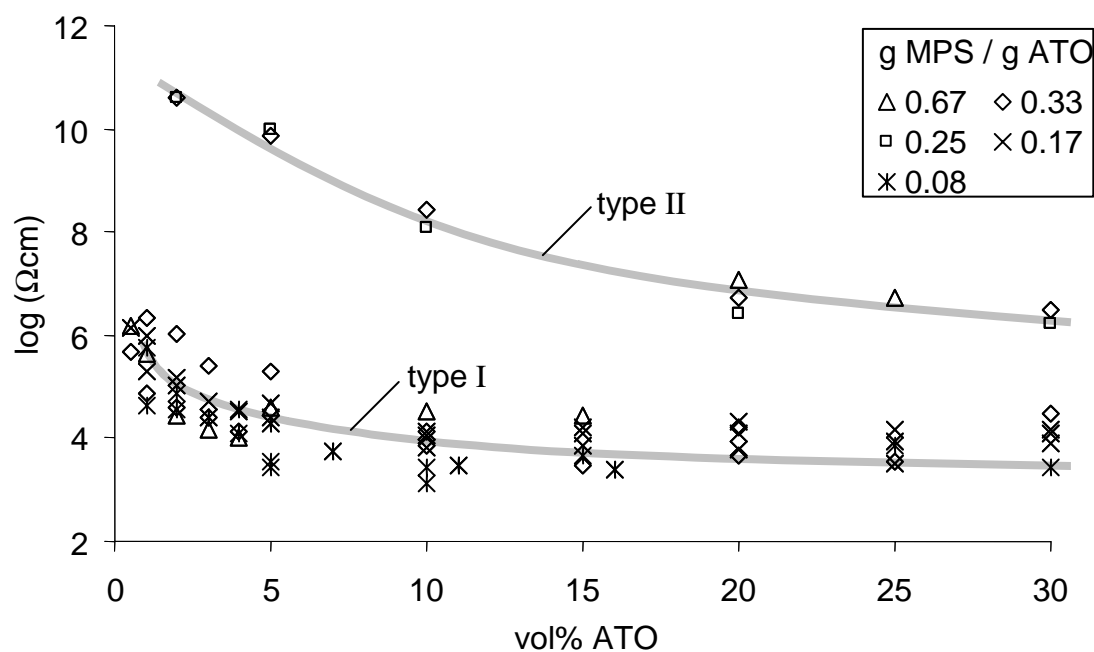


Figure 5.5 Resistivity of TMPTA coatings filled with ATO treated with 0.05 to 0.67 g/g MPS. Lines are guides to the eye.

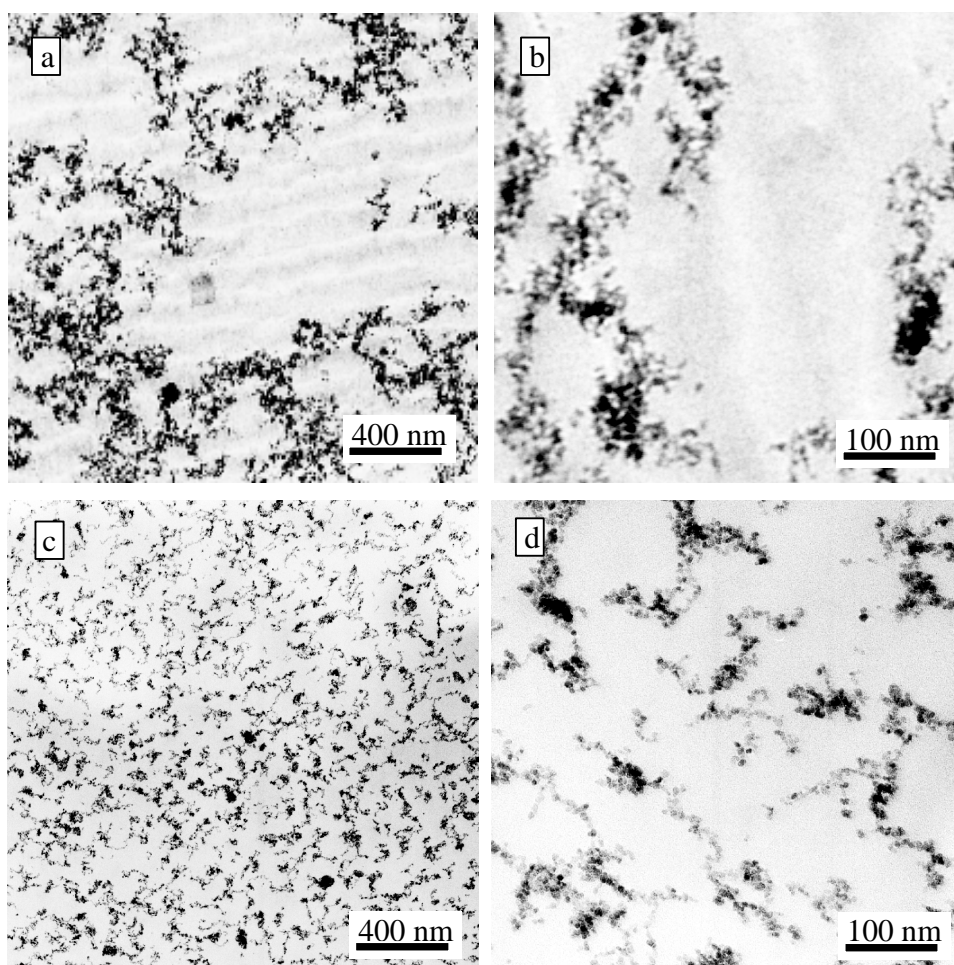


Figure 5.6 TEM images of: a, b; 1 % ATO (0.08 g MPS / g ATO) in TMPTA, curve type I, $\sim 10^5 \Omega\text{cm}$; c, d; 2 % ATO (0.33 g MPS / g ATO) in Ebecryl 745, curve type II, $\sim 10^{11} \Omega\text{cm}$.

fractal type distribution. In figure 5.6c and 5.6d an Ebecryl 745 coating with 2 vol% ATO (0.33 g/g MPS) is shown; this coating has a high resistance and originates from a type II series. At a length scale of a few micrometers the coating is homogeneous, but at smaller length scales small aggregates are visible. A continuous network like in the TMPTA coating is less evident. The small aggregates do not necessarily indicate aggregation in the coating mixture. Light scattering data indicate that small aggregates are already formed before or during the grafting of the silane coupling agents. After this procedure the small aggregates may not break up anymore and will also be found in the later coating mixture, but they may also have gained sufficient colloidal stability to prevent further aggregation in the coating mixture.

5.3.2. Electrical resistivity of tin oxide filled coatings

Although pure tin oxide has a higher resistivity than ATO, for some applications it is still more interesting as its transmittance for visible light is much higher. With tin oxide the same experiments were carried out as with ATO.

With Ebecryl 745 as matrix material all series followed type II behaviour (see figure 5.7), irrespective of the MPS to tin oxide ratio. The obtained resistivities are higher than found for the corresponding type II ATO-Ebecryl 745 coatings; the lowest obtained resistivity was $10^8 \Omega\text{cm}$. Also for PEGDA a type II resistivity versus filler fraction curve is found. With a PEGDA matrix addition of 25 vol% tin oxide resulted in resistivities of 10^6 - $10^7 \Omega\text{cm}$. With TMPTA as matrix the reproducibility was too low to draw any conclusion. The TEM images of a TMPTA coating with 1 vol% tin oxide (0.3 g/g MPS) were also not very conclusive (figure 5.8). At the highest magnification aggregates of a few hundred nanometer are visible that are close to each other, but it is not clear whether they form a continuous network or not. At a lower magnification the aggregates are distributed homogeneously, like in the high resistivity ATO coating. Already before the surface modification the starting tin oxide dispersion is opaque, which is a strong indication of the presence of aggregates. Hence, also in this case the aggregates in the coatings may be formed before or during the grafting procedure and may not indicate colloidal instability in the coating formulation.

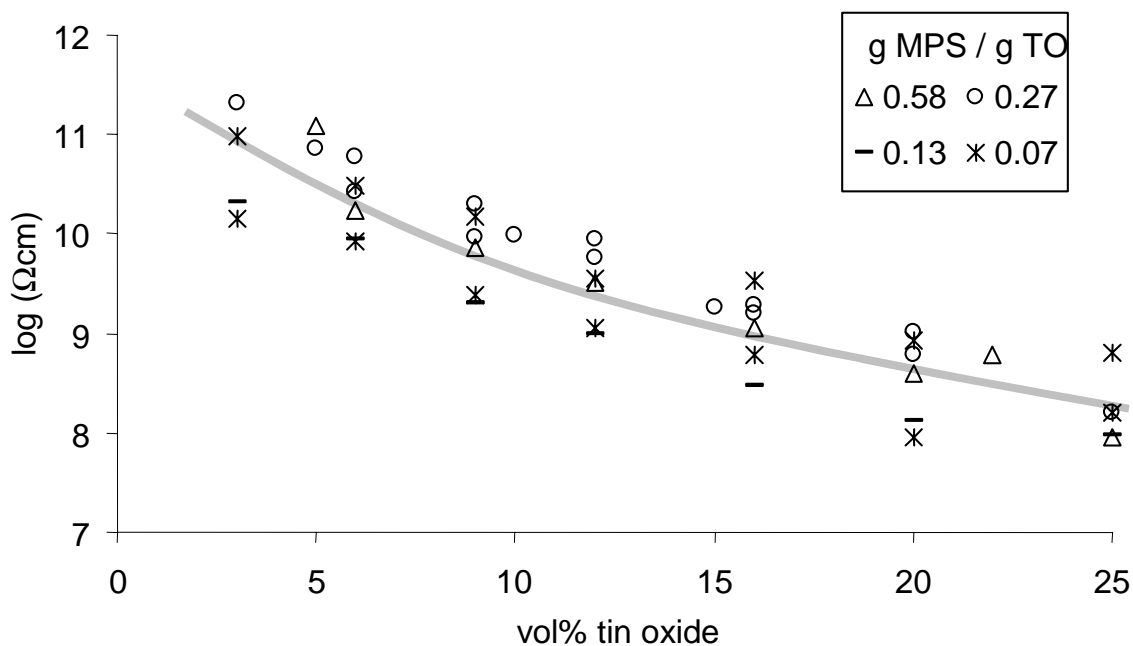


Figure 5.7 Resistivity of Ebecryl 745 coatings filled with tin oxide treated with 0.07 to 0.58 g/g MPS. Line is guide to the eye.

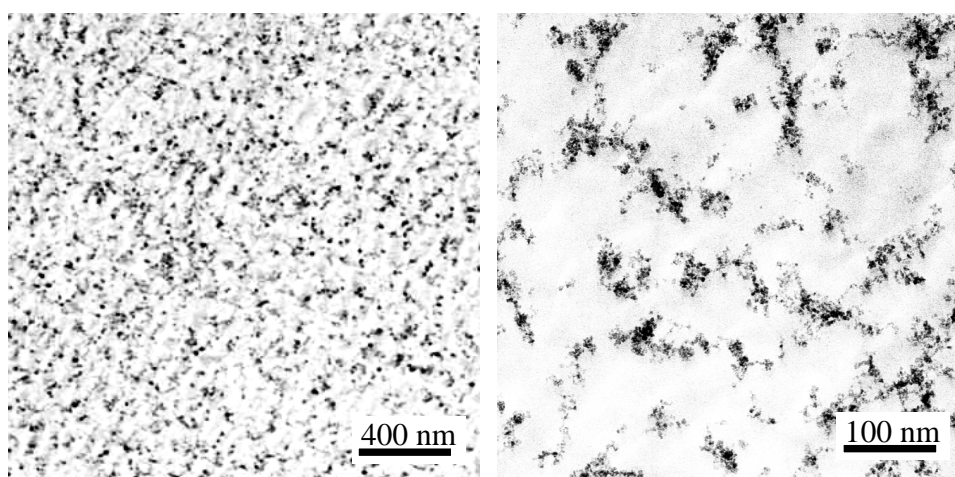


Figure 5.8 TEM images of 1 % tin oxide (0.4 g MPS / g tin oxide) in TMPTA

5.4. Models for the resistivity of composite materials

In the experiments two distinct shapes for the electrical resistivity versus filler fraction curves were found: type I and type II. Curves with an intermediate shape were not found. Given the clear distinction a separate theoretical evaluation will be given for both curve shapes.

5.4.1. Model for type I behaviour

The TEM image of a coating from a series with type I behaviour (figure 5.6a) indicates that a continuous particle network is already formed at a filler fraction of 1 vol%. This network resembles the continuous particle networks with fractal morphology that are found in experimental studies and computer simulations of particle aggregation due to colloidal instability⁽⁹⁻¹²⁾. The fractal morphology of the network can be used to model the electrical resistance (R) as function of filler fraction (ϕ) and the fractal dimension (D) of the network. As the electrical resistance in the filler network is expected to be much lower than the resistance in the matrix, the latter is ignored for the modelling of the resistivity of the composite.

The fractal scaling of the particle network enables a comprehensive mathematical description of the number of connecting paths as function of the filler fraction⁽⁹⁾. The volume (V) of a solid body relates to its radius (r) according to:

$$V \propto r^3 \quad [1]$$

For a fractal structure with a radius considerably larger than the radius of a single particle (a), the number of particles (n) is dependent on the fractal dimension (D) according to:

$$n \propto (r/a)^D \quad [2]$$

Assuming the volume of a particle to be a^3 , the volume fraction (ϕ) of the particles within a fractal structure is:

$$\phi \propto \frac{n \cdot a^3}{V} \propto \frac{(r/a)^D \cdot a^3}{r^3} \propto \frac{(r/a)^D}{(r/a)^3} \propto (r/a)^{(D-3)} \quad [3]$$

A particle network is build with stacked fractal aggregates. The average size of these building blocks is named the correlation length. Knowing the relationship between ϕ , D , and r , we can also calculate the correlation length (ξ) as function of the volume fraction:

$$\xi \propto a \cdot \phi^{\left(\frac{1}{D-3}\right)} \quad [4]$$

Thus the number of such building blocks (N_1) along a line with length l is:

$$N_1 \propto \frac{l}{\xi} \quad [5]$$

The number of building blocks (N_3) that are needed to fill a container with size $l \cdot w \cdot h$ is:

$$N_3 \propto \frac{l}{\xi} \cdot \frac{w}{\xi} \cdot \frac{h}{\xi} \propto \frac{lwh}{\xi^3} \quad [6]$$

and, assuming that each building block has one connecting point with any adjacent aggregate, the number of paths (P) between the walls $w \cdot h$ is:

$$P \propto \frac{N_3}{N_1} \propto \frac{lwh}{\xi^3} / \frac{l}{\xi} \propto \frac{wh}{\xi^2} \propto \frac{wh}{a^2 \cdot \phi^{2\left(\frac{1}{D-3}\right)}} \propto \frac{wh}{a^2} \cdot \phi^{\left(\frac{2}{3-D}\right)} \quad [7]$$

This relationship was used by Bremer⁽⁹⁾ to correlate the modulus of a particle gel to the filler fraction. He found a good agreement between the model and experimental data.

The resistance in one path is the number of particles in the path (Q_p) times the electrical resistance between two aggregated particles (R_f). The number of particles that form the conducting path can be calculated by multiplying the number of building

blocks (N_1) by the number of particles that form the connecting path within one building block (Q_b). For a straight connecting path the relationship would be:

$$Q_p \propto N_1 \cdot Q_b \propto \frac{l}{\xi} \cdot \frac{\xi}{a} \propto \frac{l}{a} \quad [8]$$

However, typically the connecting path is somewhat curved and a larger number of particles is needed. The number of particles in the connecting path within one building block is estimated by⁽¹³⁾:

$$Q_b \propto \left(\frac{\xi}{a}\right)^{1+x} \quad [9]$$

where x is a constant with a value typical between 0 and 0.4. Hence, the number of particles in one connecting path (Q_p) is:

$$Q_p \propto N_1 \cdot Q_b \propto \frac{l}{\xi} \cdot \left(\frac{\xi}{a}\right)^{1+x} \propto \frac{l}{a^{1+x}} \cdot \xi^x \propto \frac{l}{a} \cdot \phi^{\left(\frac{x}{D-3}\right)} \quad [10]$$

Assuming that the electrical resistance between two aggregated particles is the same for each pair of aggregated particles and is independent on the filler fraction or the shape of the network, the resistance of one path becomes:

$$R_p \propto R_f \cdot Q_p \propto R_f \cdot \frac{l}{a} \cdot \phi^{\left(\frac{x}{D-3}\right)} \quad [11]$$

Assuming that all parallel paths have an equal resistance, the bulk resistance (R_b) of the network can be calculated by dividing the electrical resistance of one path (R_p) by the number of paths:

$$R_b \propto \frac{R_p}{P} \propto \frac{R_f \cdot \frac{l}{a} \cdot \phi^{\left(\frac{x}{D-3}\right)}}{\frac{wh}{a^2} \cdot \phi^{\left(\frac{2}{3-D}\right)}} \propto R_f \cdot \frac{al}{wh} \cdot \phi^{\left(\frac{2+x}{D-3}\right)} \quad [12]$$

The resistance of a sample is converted in the specific resistance, or resistivity (R_s), by:

$$R_s = R_b \cdot \frac{wh}{l} \propto R_f \cdot a \cdot \phi^{\left(\frac{2+x}{D-3}\right)} \propto C \cdot \phi^{\left(\frac{2+x}{D-3}\right)} \quad [13]$$

where C is a constant that is proportional to the electrical resistance between two contacting filler particles. It should be noted that the mathematics of the fractal concept describes the aggregates as continuous structures, instead as the granular structures that

they really are. At low filler fractions, where the correlation length is considerably larger than the diameter of the primary particles, this approach is reasonably accurate. However, at high volume fractions, where the correlation length is only a few times the particle diameter, the continuous description may be very inaccurate.

For the fitting of the theoretical model only the experimentally determined resistivities for filler fractions below 5 % are used. The resulting values for D and C are given in table 5.2 (see also figure 5.9); variation of x within reasonable limits (0-0.4)⁽¹³⁾ does not result in large variations of the values for D . All values for D are within the range that is mentioned in the literature concerning particle aggregation. In computer simulations D varies from 1.7 to 2.5, depending on the conditions chosen^(5,9,10,14). When the first contact between two particles results in a rigid bond (rapid aggregation) the lowest values for D are found, but when reorientation of the bonds is introduced, or when only part of the contacts result in a bond, higher values are found. In experimental studies typically values from 1.8 to 2.1 are found, where the lower values are found for the more rapidly aggregating systems^(5,9,10).

The value for C increases with increasing MPS to ATO ratio. This indicates that the electrical resistance in a connecting path increases with an increased amount of grafted MPS. It is unlikely that the number of particles in a path will change dramatically due to increased MPS grafting, and a tenfold increase can be regarded as impossible. Hence the increase of the resistance in a path has to be attributed to an increase of the electrical resistance between two aggregated particles. This increase of resistance between the particles is already expected as the amount of insulating MPS on the particles is increased. The matrix does not have a significant effect on C : this confirms

MPS/ATO	matrix	$D (-)$ $x = 0.0$	$D (-)$ $x = 0.2$	$D (-)$ $x = 0.4$	C (Ωcm)
0.04 g/g	Ebecryl 745	2.2	2.2	2.1	$2 * 10^0$
	PEGDA	2.0	1.9	1.8	$9 * 10^0$
0.08 g/g	Ebecryl 745	2.3	2.3	2.2	$3 * 10^1$
	PEGDA	1.9	1.8	1.8	$7 * 10^1$
	TMPTA	2.0	1.9	1.8	$5 * 10^1$
0.17 g/g	TMPTA	1.9	1.8	1.7	$2 * 10^2$
0.33 g/g	TMPTA	2.0	1.9	1.8	$4 * 10^2$

Table 5.2 Resulting fractal dimension (D) and constant (C) after fitting of Eq. 12 to type I experimental data.

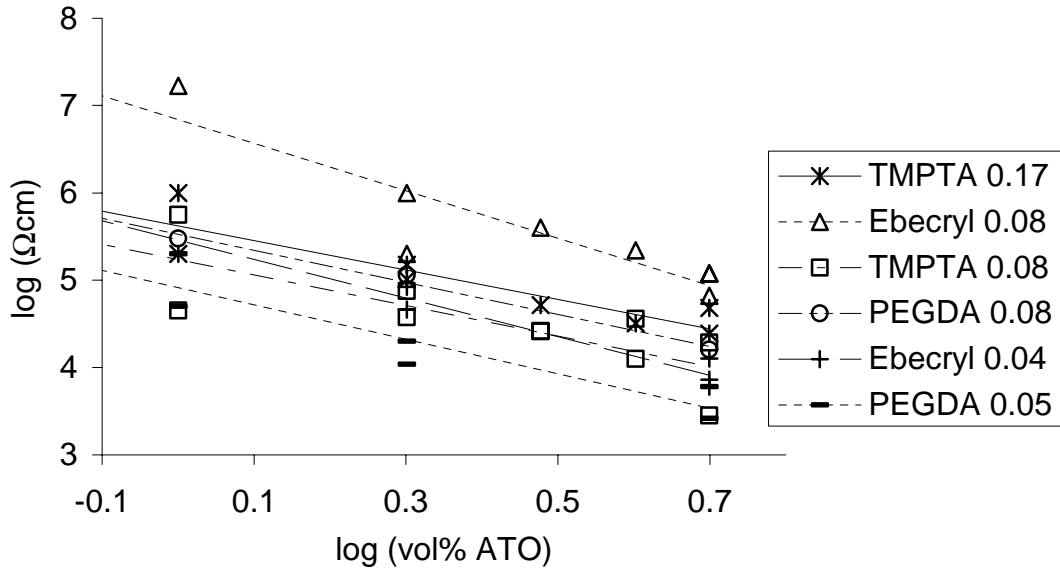


Figure 5.9 Fit of Eq. 12 to experimental series with type I behaviour, dashed lines are the fitted curves; the resulting values for D and C are presented in table 5.1.

that the electrical conduction mainly takes place in the filler network. Despite the simplicity of the model and the large variance in the measured data the fits give values for D that are comparable with literature and a reasonable trend for C .

5.4.2. Type II behaviour

Fitting the model of section 5.4.1 to the Ebecryl 745 coatings filled with ATO with 0.17 g MPS / g ATO would result in $D = 2.8$ and $C = 2 \Omega\text{cm}$. For the other series with type II behaviour similar values are found. For a filler fraction of 5 vol% this would lead to a correlation length of 1 mm, which should be visible with the naked eye. However, the coatings are very homogeneous, also when observed with an optical microscope. Furthermore the values for D and C are not in line with the results in section 5.4.1 and the TEM images of coatings of type II (figure 5.6c and 5.8a) do not show fractal aggregation on a large length scale. Thus describing the filler distribution with a fractal geometry leads to wrong results and another type of particle arrangement has to be considered to describe the type II curves.

Due to the grafting of a MPS layer on the filler surface the attraction between the filler particles may be reduced resulting in a repulsive net interaction between the particles and aggregation may be prevented⁽¹⁵⁾. The presence of small aggregates in the TEM images is not in contradiction with this hypothesis as these aggregates may al-

ready have been formed before or during the MPS grafting procedure. It is also possible that aggregation still occurs, but at a much lower rate so network formation may not be completed in the time span before the cross-linking of the matrix. These small aggregates may in a coating behave as stable particles. At low filler fractions a continuous filler network can be expected to be absent and consequently the electrical current has to flow through the matrix material that separates the particles. At higher filler fractions the average distance between the particles is smaller and due to geometrical constraints more contacts between the particles are established. At a certain filler fraction, the so-called critical volume fraction, the number of such formed contacts is large enough to form a continuous particle network. The location of the critical volume fraction depends on the shape of the filler particles, their relative size towards the matrix material, and the particle-particle and particle-matrix interactions.

At filler fractions below the critical volume fraction the electrical resistance is mainly determined by the distances between the particles⁽¹⁶⁾. The TEM image of a high resistivity coating with 2 vol% ATO (figure 5.6d) shows typical distances of 10-50 nm between the small filler aggregates. It can be expected that with increasing filler fraction the distance between aggregates becomes smaller and, at the upper end of the experimental range (30 vol%), the typical separation is probably no more than a few nanometers. At such short distances electron tunnelling notably enhances the electron transport and the electrical resistance is considerably lower than expected on basis of the bulk resistivities of the pure matrix materials^(1,2,16). Unfortunately the irregular structure of the aggregates and possible repulsive or attractive interactions make it impossible to construct a realistic model for the effective separation distance between the aggregates as function of the filler fraction. Considerations regarding the effects that electron tunnelling may have on the resistivity of the coatings are given in Appendix II.

5.5. Conclusions

By adding ATO particles with grafted MPS the electrical resistivity of acrylate coatings can be lowered to about 10^2 - 10^3 Ωcm ; with tin oxide with grafted MPS resistivity values of 10^6 - 10^8 Ωcm can be reached. For the ATO filled coatings the grafting density of MPS has a large influence on the obtained resistivity values. With an incomplete MPS grafting the colloidal stability of the ATO in the acrylate resins is low with aggregation of the ATO as a result. This aggregation results, already for ATO fractions as low as 1 vol%, in the formation of a continuous network of filler particles,

which is very beneficial for the lowering of the electrical resistance. With a maximal grafting density the ATO is more easily dispersed in the acrylate matrix, which favours a more homogeneous distribution in the final coatings. For the resistivity as function of filler fraction two different curve types are found, one (type I) is associated with coatings with aggregated particles and the other (type II) is associated with homogeneously dispersed particles. It is generally found that networks of aggregated nanoparticles have a fractal morphology. The fractal concept is used to make a comprehensive model for the resistivity as function of the filler fraction. Fitting of this model to experimental series that show type I behaviour gives values for the fractal dimension that compare well to literature values. The fitting results also indicate that increasing MPS grafting density results in a higher electrical resistance between aggregated particles. Fitting the same model to the experimental series that show type II behaviour gives unrealistic values for the fractal dimension and the correlation length, hence this model is not applicable for type II curves. Another accurate model for the resistivity as function of the filler fraction that is applicable for type II curves is not obtained, but a reasonable explanation for the experimentally determined relationship can be given. At low volume fractions the filler does not form a continuous network and the electrical resistivity is determined by the bulk resistivity of the polymer. Increasing the filler fraction results in a decrease of the distance between the particles and when the interparticle spacing becomes less than approximately 10 nm the composite resistivity decreases considerably due to electron tunnelling. At high volume fractions the distance between the aggregates is very small and the tunnelling resistivity becomes smaller than the resistivity of the filler. Hence at high filler fractions the bulk resistivity is mainly determined by the resistivity of the filler.

Reference List

1. R. Strumpler, J. Glatz-Reichenbach, *Journal of Electroceramics*, 3(4), 329-346 (1999).
2. R. D. Sherman, L. M. Middleman, S. M. Jacobs, *Polymer Engineering and Science*, 23(1), 36-46 (1983).
3. V. E. Gul, *Structure and properties of conducting polymer composites* (VSP BV, Zeist 1996).
4. B. W. Ninham, *Advances in Colloid and Interface Science*, 83, 1-17 (1999).
5. V. I. Roldughin, V. V. Vysotskii, *Progress in Organic Coatings*, 39, 81-100 (2000).

6. A. M. Kulkarni, C. F. Zukoski, *Langmuir*, 18, 3090-3099 (2002).
7. F. Lux, *Journal of Materials Science*, 28, 285-301 (1993).
8. F. Carmona, J. Ravier, *Carbon*, 40, 151-156 (2002).
9. L. Bremer, Fractal Aggregation in Relation to Formation and Properties of Particle Gels, thesis, LU Wageningen, (1992).
10. E. Dickinson, *Journal of Colloid and Interface Science*, 225, 2-15 (2000).
11. D. F. Evans and H. Wennerstroem, The colloidal domain: where physics, chemistry, biology, and technology meet (VCH, New York, 1994).
12. R. J. Hunter, Introduction to modern colloid science (Oxford University Press, Oxford, ed. Repr. with corr., 1996).
13. W. H. Shih, W. Y. Shih, S. I. Kim, J. Liu, I. A. Aksay, *Physical Review A*, 42, 4772-4780 (1990).
14. M. Kolb, *Advances in Solid State Physics*, 41, 381-389 (2001).
15. K. T. Miller, C. F. Zukoski, in Studies in Surface Science and Catalysis, 103(Semiconductor nanoclusters) 23-55, (Elsevier, Amsterdam, 1996).
16. S. Radhakrishnan, *Polymer Communications*, 26, 153-157 (1985).

Chapter 6

Mechanical properties of the coatings

Synopsis

In this chapter the mechanical properties of the nanocomposite coatings are discussed. The hardness and E-modulus of the coatings were measured by microindentation. It was found that the hardness and E-modulus both increase with increasing filler fraction. These effects were much larger for coatings with a (rubbery) PEGDA matrix than for coatings with a (glassy) TMPTA matrix. Also the amount and type of silane coupling agent used for the surface modification of the fillers was found to have a strong influence on hardness and E-modulus; the increase was largest when MPS was grafted on the fillers. After indentation the deformation of the coatings recovered for the greater part; PEGDA coatings with MPS grafted on the fillers even recovered fully. The abrasion resistance of the coatings increased with increasing silica fraction; at high silica fractions the performance was excellent.

6.1. Introduction

The use of fillers to improve the mechanical properties of polymeric materials is common practice. The fillers may significantly improve properties like modulus, yield strength, impact resistance, and abrasion resistance⁽¹⁻¹²⁾. For example, Ou et al.⁽¹³⁾ demonstrated that the addition of 5 w% of silica (50 nm) to nylon-6 resulted in increases in tensile strength (15%), strain-to-failure (150%), Young's modulus (23%), and impact strength (78%). At higher filler levels the Young's modulus further increased whereas the other values decreased. Mammeri et al.⁽¹⁴⁾ filled PMMA coatings with up to 100 % in situ formed silica, which resulted in an increase of the coating hardness from 180 MPa for the pure PMMA coating, to 540 MPa for a 53 mol% PMMA coating and 1400 MPa for a pure silica coating. Vu et al.⁽¹⁵⁾ showed that incorporation of 23 vol% silica in UV-curable acrylate coatings can give a 2.5-fold increase of the E-modulus and higher abrasion resistance. Silica nanoparticles can be found in many performance materials like car tyres and scratch and abrasion resistant coatings^(4,8,9,16-22).

The properties of a composite are not simply the sum of the properties of its components. The composite properties are also determined by the size, shape, and spatial distribution of the filler in the matrix and by the forces acting between the components^(8,11,12,22-24). It has been found that decreasing the average size of the fillers from a few micrometers to a few nanometers can result in a higher gain in yield stress and modulus⁽²²⁻²⁸⁾. The larger effect of nanoparticles is attributed to their larger surface area. The surface area is an important parameter as interactions between the filler and the matrix are very important for the composite properties. For a wide range of polymer matrices it is observed that near the filler surface the glass transition temperature (T_g) is shifted by tens of degrees^(7,17,23,24,29-32). Moving away from the filler surface, the T_g returns to the bulk value in a gradient that may stretch over tens of nanometers^(24,32-34). The size and the direction of this T_g shift are determined by the interactions between the polymer and the filler. In the case of strong interactions, like strong physical or covalent bonding, a strong increase of the T_g will be found whereas very weak interactions may result in a decrease of the T_g ^(32,35,36). Hence, modifications of the filler surface may affect the composite properties. For example, for silica-acrylate composites it has been shown that the T_g increases when 3-methacryloxypropyltrimethoxysilane is grafted on the silica surface, whereas with grafted acetoxypolypropyltrimethoxysilane the T_g decreases⁽³⁶⁾. Shifting of the T_g affects the mechanical properties, especially when a rubbery polymer becomes glassy or vice versa. If near the filler surface

the T_g of a rubbery polymer is raised above ambient temperature, a shell of glassy polymer round the filler is formed. This shell has a much higher E-modulus than the bulk rubber, consequently the modulus of the composite increases. The thickness of such a shell can be in the order of a few nanometers^(17,21,30,31,33,34); for nanocomposites this shell may contain a major part of the matrix and large changes in the mechanical properties may be expected. For glassy polymer matrices a similar increase of the T_g will have a smaller effect on the mechanical properties as no glass transition will take place. Literature examples indeed show that fillers that give strong reinforcement in rubbers have far less effect in glassy polymers^(26,37). For glassy polymers the addition of fillers may improve the toughness and impact resistance^(5,35). This improvement is especially obtained when a filler with weak interactions with the polymer is used.

6.2. Experimental

As matrix material for the coatings either PEGDA (polyethyleneglycoldiacrylate Mw 575, Aldrich) or TMPTA (trimethylolpropanetriacrylate, UCB) was used. 3-Methacryloxypropyltrimethoxysilane (MPS; ABCR) and octyltrimethoxysilane (OTS; Aldrich) were used to modify the silica, tin oxide, and ATO fillers following the procedure as described in chapter 2. 2-Hydroxy-2-methylpropiophenone (Aldrich) was used as photoinitiator. All materials were used as received. The coating materials were mixed with the aid of a water-propanol solvent mixture. The coatings were applied on a polycarbonate substrate (Lexan 9030; GE plastics) after which the samples were placed during 30-90 minutes in a well-ventilated place to allow the solvents to evaporate. Subsequently the coatings were cured by exposure to UV in an UVACUBE (Dr. Hönle), which is equipped with a nitrogen flushed sample compartment with a quartz window, a timed shutter, and a H-lamp (Dr. Hönle) with an intensity in the UV-A region of 25 mW/cm². The typical thickness of the cured coatings is 5-30 μm .

Microindentation measurements were performed with a Fischerscope 100C with a Vickers indenter. The measurements were performed in the controlled load mode, in which the load was increased and decreased following a quadratic function in time. For coatings with a TMPTA matrix the load was increased from 0.4 mN to 10 mN and for coatings with a PEGDA matrix from 0.4 mN to 2 mN. The maximum displacement (h) under these loads ranged roughly between 0.4 μm for coatings with a high filler content and 4 μm for coatings without filler, which corresponds to 3 to 12 % of the coating thickness. The starting load of 0.4 mN is the minimum force that can be measured by this equipment. The load was increased in a period of 20 seconds, and after 5 sec-

onds at the maximum value, the load was decreased to 0.4 mN in a period of 20 seconds.

The abrasion resistance was tested with a Taber abrader equipped with CS-10F wheels and 500 gram loads (ASTM standard D-1044A). The ranking between different samples was performed on basis of visual judgement. Attempts were done to quantify the results by measuring the loss of transmission of a laser beam, but, as the loss of transmission for the best coatings is considerably smaller than the variation of transmittance within one sample, this method is not very accurate.

6.3. Hardness and elasticity

With microindentation a pyramid shaped indenter is pushed with a controlled load in a sample and the resulting displacement of the indenter is measured⁽¹⁾. During loading, penetration of the indenter results in a deformation of the sample, which is composed of plastic, elastic, and visco-elastic components. During unloading the elastic deformation recovers instantly whereas the visco-elastic deformation may recover gradually and the plastic deformation is permanent.

The resistance against penetration can be expressed by the universal hardness HU . The HU is the force that is used for driving the indenter in the sample divided by the projected contact area. Mathematically this is expressed in equation 1:

$$HU = \frac{F}{A(h)} = \frac{F}{\alpha \cdot h^2} \quad [1]$$

where F = applied force, A = contact area, h = displacement, and $\alpha = 26.43$, which is a constant determined by the shape of the Vickers indenter. This equation implies that as long as HU is independent from penetration depth, the h vs. $F^{1/2}$ plot should be a straight line starting from the origin. In the measurements, however, extrapolation of the h vs. $F^{1/2}$ curve to $F^{1/2} = 0$ results in a small negative displacement value. For the localisation of the surface of the sample, the indenter is slowly lowered until it registers a minimal force. This force is already high enough for a small penetration of the indenter in the sample, which results in a small error in the determination of $h = 0$. The real displacement (h) is calculated by adding the negative displacement of the extrapolated h vs. $F^{1/2}$ line at $F^{1/2} = 0$ to the measured displacement. This real value for h is used for the calculation of HU . The HU can also be calculated from the slope (s) of the h vs. $F^{1/2}$ plot. In this case an erroneous h value is automatically corrected. For this calculation equation 2 is used:

$$HU = \frac{1}{\alpha \cdot s^2} \quad [2]$$

In most of the cases the h vs. $F^{1/2}$ plot shows a straight line. With thin coatings, where the indentation is considerably more than about 10% of the coating thickness, the h vs. $F^{1/2}$ plot is curved. This curve can be explained by the fact that the measured mechanical properties are a combination of the mechanical properties of the coating and the substrate. Upon increasing indentation depth the substrate increasingly contributes to the measured mechanical properties. For coatings that are harder than the substrate, this results in an upward curvature of the h vs. $F^{1/2}$ plot and for coatings that are softer than the substrate this results in a downward curvature.

The unloading data are used to calculate the E -modulus (E) of the sample following the method of Oliver and Pharr^(1,38):

$$E = \frac{\sqrt{\pi}}{2 \cdot \beta \cdot \sqrt{A}} \cdot \frac{dF}{dh} \quad [3]$$

where β is a constant determined by the shape of the indenter and A is the projected contact area; for dF/dh and A the values at maximum indentation are used⁽³⁸⁾.

The h vs. $F^{1/2}$ plot for the polycarbonate substrate is shown in figure 6.1. The arrows indicate the direction in which the plot develops during the measurement. The unloading curve is less steep than the loading curve and the sample only partly recovers, thus the deformation appears to be partly plastic and partly elastic. As time-dependent measurements were not performed the visco-elastic component is unknown. The HU calculated from this measurement is 0.13 GPa and the E -modulus is 3.0 GPa. These values are higher than the values indicated by the manufacturer (0.095 and 2.35 GPa); the discrepancy may be due to the aging of the material and differences between the test methods^(1,39). A typical load displacement plot for a tested coating is also shown in figure 6.1. Here the difference between the loading and the unloading curve is much smaller, which indicates that the deformation of these materials is mainly elastic. This behaviour is found for both TMPTA based and PEGDA based coatings; for several PEGDA coatings the loading and the unloading curve even match completely.

A complete overview of the hardness and E -modulus values for the nanocomposite coatings is given in table 6.1. The hardness and the E -modulus show similar trends; further on the results are discussed only on basis of the hardness, bearing in mind that for the E -modulus the discussion would be the same.

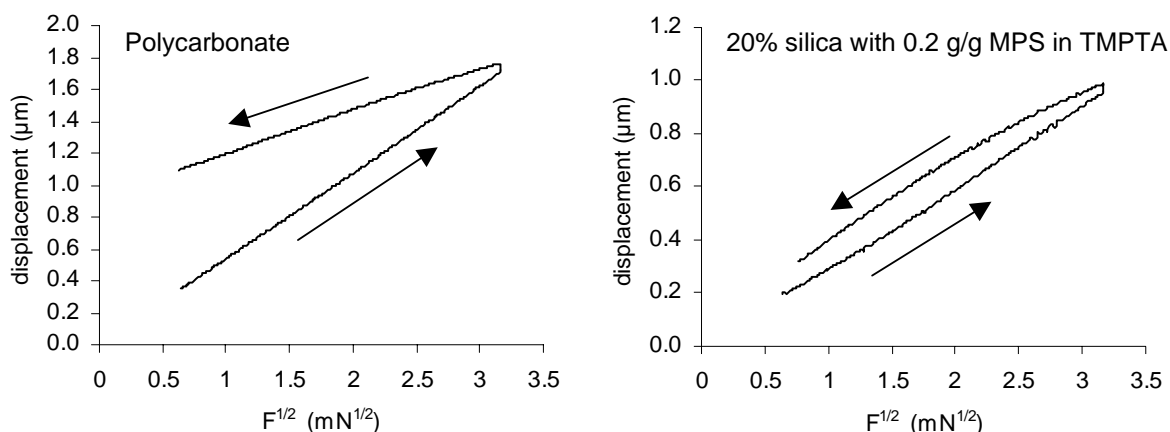


Figure 6.1 Load displacement plots resulting from micro-indentation of polycarbonate and of a typical coating.

6.3.1. Coatings with a PEGDA matrix

PEGDA coatings consist of cross-linked polymers with a T_g well below room temperature ($-30\text{ }^{\circ}\text{C}$), which classifies them as rubbers. A small indentation load already resulted in a relatively large displacement, but after releasing the load the sample fully recovered. The maximum force that was used on these samples was 2 mN, which is only five times higher than the minimum force that the equipment can apply. Even at this low force the penetration was up to 4 μm. For the 0 % and 10 % filled PEGDA coatings extra thick coatings ($> 40\text{ }\mu\text{m}$) were prepared for an accurate measurement without the influence of the substrate.

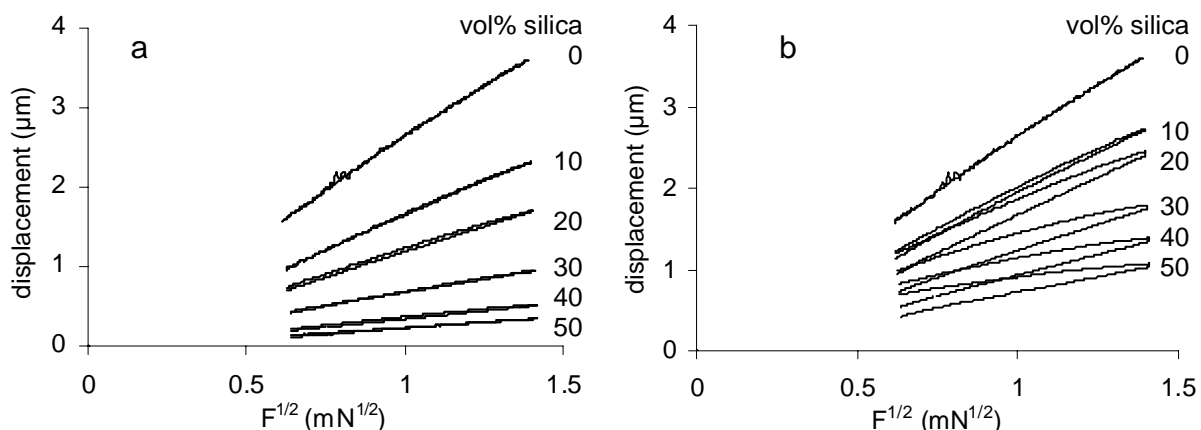


Figure 6.2 Load displacement curves for PEGDA coatings with various silica contents, a: 0.2 g MPS / g silica, b: 0.2 g OTS / g silica.

Figure 6.2a shows the h vs. $F^{1/2}$ plots for a series of PEGDA coatings with a silica filler with 0.2 g MPS / g silica. In these samples the silica and the PEGDA are chemically linked through the MPS⁽⁴⁰⁾. Increasing the silica fraction in the coatings results in a smaller indentation depth, which indicates a higher hardness. During the release of the indenter, the sample recovered almost completely, thus the deformation was mainly elastic. A corresponding series with silica treated with OTS (0.2 g/g), is shown in figure 6.2b. Contrary to MPS, OTS cannot establish a chemical link between the filler and the matrix. Also with OTS an increase of the silica concentration resulted in a smaller indentation depth, but the effect was smaller. Moreover, in this case the unloading curve did not follow the loading curve as seen for the samples with MPS, thus the deformation had a more plastic or visco-elastic character.

The universal hardness HU as function of silica concentration is shown in figure 6.3a. The surface treatment of silica appears to have a large effect on the HU . Filling PEGDA coatings with 50 vol% of OTS treated silica increased the HU by roughly ten times. At the same concentration of MPS treated silica, the HU increased by roughly hundred times. Samples with untreated silica have a lower HU than samples with MPS treated silica, but a higher HU than samples with OTS treated silica. Modification of the silica with smaller amounts of MPS resulted in hardness values closer to the unmodified silica, but a similar decrease of the amount of OTS had virtually no effect (table 6.1).

The found effects of the surface treatment on the HU of the composite coatings make sense. PEGDA and untreated silica are both rather polar, thus one may expect strong physical interactions. Treatment of the silica with OTS decreases the polarity of

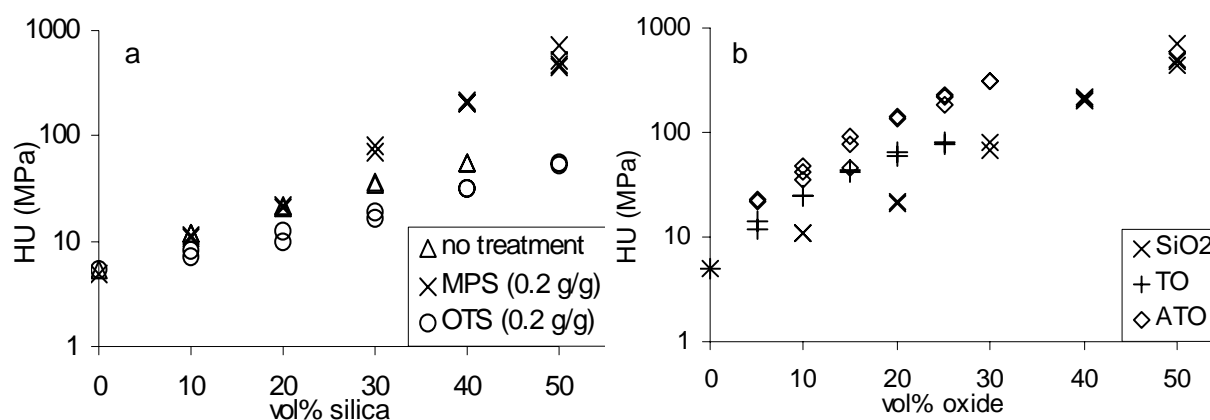


Figure 6.3 Hardness of filled PEGDA coatings. a: effect of surface modification, b: effect of type of filler (all with 0.2 g/g MPS).

Filler modification (g/g oxide)	Amount filler (vol%)	Hardness (MPa)	E-modulus (GPa)	Filler modification (g/g oxide)	Amount filler (vol%)	Hardness (MPa)	E-modulus (GPa)
PEGDA without filler				PEGDA – ATO			
--	--	5.1	0.12		5	17	0.30
PEGDA – silica					10	20	0.37
without silane coupling agent	10	12	0.24	MPS (0.05)	15	35	0.67
	20	21	0.45		20	52	1.0
	30	36	0.81		25	84	1.6
	40	56	1.3		30	1.2 *10 ²	2.2
MPS (0.05)	10	8.5	0.17	MPS (0.08)	5	11	0.22
	20	19	0.33		10	20	0.36
	30	33	0.62		15	38	0.75
	40	75	1.4		20	60	1.1
	50	2.3 *10 ²	3.8		25	1.0 *10 ²	1.8
MPS (0.1)	20	23	0.45	MPS (0.17)	30	1.6 *10 ²	2.7
	30	67	1.3		5	22	0.26
	40	1.3 *10 ²	2.4		10	42	0.59
	50	2.7 *10 ²	4.5		15	72	0.95
MPS (0.2)	10	11	0.20	20	1.4 *10 ²	1.6	
	20	22	0.47	25	2.1 *10 ²	2.6	
	30	74	1.1	30	3.0 *10 ²	3.8	
	40	2.1 *10 ²	4.1	TMPTA without filler			
	50	5.4 *10 ²	5.7	--	--	2.9 *10 ²	4.6
OTS (0.1)	10	8.7	0.15	TMPTA – silica			
	20	10	0.22	10	3.7 *10 ²	5.6	
	30	15	0.35	20	4.7 *10 ²	7.1	
	40	24	0.59	MPS (0.2)	30	6.6 *10 ²	9.1
50	50	1.2	40		1.0 *10 ³	13	
OTS (0.2)	10	7.3	0.16	50	1.3 *10 ³	17	
	20	9.8	0.22	OTS (0.2)	10	3.3 *10 ²	5.3
	30	16	0.37		20	3.6 *10 ²	5.7
	40	28	0.70		30	4.0 *10 ²	6.0
	50	55	1.2		40	3.9 *10 ²	6.1
			50		3.8 *10 ²	6.1	
PEGDA – tin oxide				TMPTA –tin oxide			
MPS (0.1)	10	41	0.85	5	3.2 *10 ²	5.3	
	20	86	2.1	MPS (0.2)	10	3.6 *10 ²	6.1
	30	1.2 *10 ²	2.8		15	3.9 *10 ²	6.6
5	17	0.39	20		4.4 *10 ²	7.1	
MPS (0.2)	10	38	0.83	TMPTA - ATO			
	20	1.0 *10 ²	2.4	5	2.3 *10 ²	4.4	
				10	2.2 *10 ²	4.3	
				MPS (0.2)	15	2.6 *10 ²	4.6
					20	2.6 *10 ²	4.4
					25	2.7 *10 ²	5.2
					30	3.4 *10 ²	6.7

Table 6.1 Hardness and E-modulus of PEGDA and TMPTA coatings with various fillers.

the silica surface, and may weaken the interactions with the PEGDA. Silica that is treated with MPS is believed to be linked to the PEGDA by covalent bonds, thus has stronger interactions than untreated silica. Strong interactions between the filler and the matrix lead to an increase of the T_g near the filler surface^(21,31,34,41). The higher T_g may imply that near the filler surface the PEGDA is no longer a rubber but a glass, with a much higher hardness and E -modulus. Preliminary DSC and solid state NMR experiments on PEGDA coatings filled with MPS treated silica indeed showed that a considerable part of the organic matrix was immobilised. These experiments are not presented here as the amount of collected data is too small to be conclusive. With weaker interactions the T_g near the filler surface will be lower. Consequently one may expect that the amount of matrix material in the glassy state is also lower, leading to a lower HU of the whole composite.

Besides silica (SiO_2) also tin oxide (TO) and antimony doped tin oxide (ATO) were used as filler. The results for these fillers treated with 0.2 g MPS / g oxide are shown in figure 6.3b. The sizes of the silica, TO, and ATO particles are approximately 15, 5, and 7 nm, respectively. Based on the filler-matrix interface area one would expect that the largest increase in HU would be obtained in TO filled coatings, and the smallest increase would be obtained with silica filled coatings. However, the strongest increase was found with ATO. This may indicate that the interactions between the matrix and the different oxides are not equal in strength. It may also indicate differences in the structure of the polymer network. This is not unlikely as tin oxide was found to slow down the curing of the matrix, possibly due to excessive termination of propagating chains.

6.3.2. Coatings with a TMPTA matrix

Pure TMPTA coatings are much harder than pure PEGDA coatings. To compensate for the higher hardness the maximum applied force in the indentation experiments was increased to 10 mN. This force resulted in an indentation depth of 0.5 to 1.2 μm . With a typical coating thickness of 10-20 μm the influence of the substrate is expected to be small.

The fillers and their surface treatment were the same as used for the PEGDA coatings. Figure 6.4a shows the h vs. $F^{1/2}$ plots for TMPTA coatings that are filled with various amounts of MPS treated silica (0.2 g MPS / g silica). With increasing silica concentration the indentation depth at constant load decreased. Moreover, the deformation became more elastic. The series with silica that was treated with OTS (0.2 g/g) is

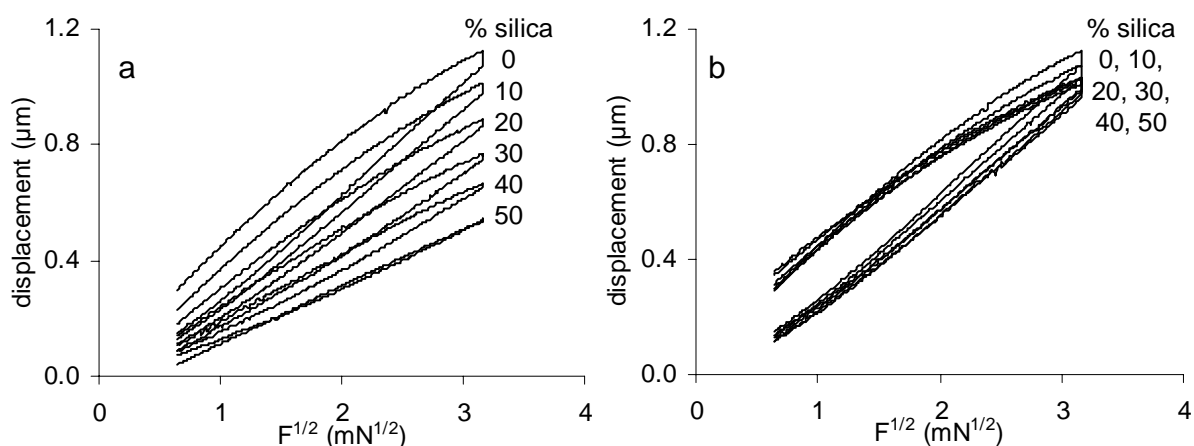


Figure 6.4 Load displacement plots for TMPTA coatings with various silica contents. *a*: 0.2 g MPS / g silica, *b*: 0.2 g OTS / g silica.

shown in figure 6.4b. With increasing silica fraction only a small decrease in indentation depth was found. Also differences in the shape of the h vs. $F^{1/2}$ plots were negligible.

The HU of the TMPTA coatings with silica is shown in figure 6.5a. Like in the experiments with PEGDA it shows that chemical linkage between the filler and the matrix increased the hardness. Unlike in the experiments with PEGDA no difference between silica and TO was found (see figure 6.5b). For the differences in relative performance of silica, TO, and ATO in PEGDA and TMPTA no explanation is found. A direct comparison between the silica filled PEGDA and TMPTA coatings is given in

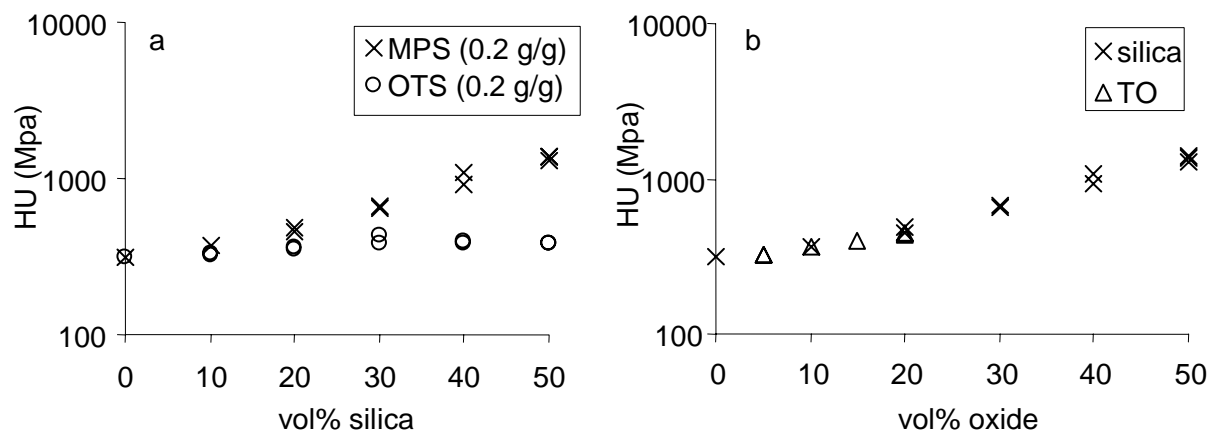


Figure 6.5 Hardness of filled TMPTA coatings. *a*: effect of surface modification, *b*: effect of type of filler (both with 0.2 g/g MPS).

figure 6.6. The effect of silica on the hardness is much larger for the rubbery PEGDA matrix than for the glassy TMPTA matrix. This is in line with literature examples where filler reinforcement in rubbery and glassy polymers are compared⁽²⁶⁾. The *HU* and *E*-modulus of PEGDA with 50 vol% MPS treated silica are almost the same as the *HU* and *E*-modulus of TMPTA with 50 vol% MPS treated silica. This may be explained by a virtually complete transition of the PEGDA matrix to the glass state, which is not unlikely as at this high filler level virtually all matrix material is within a few nm from a filler surface. The much larger differences between the mechanical properties of PEGDA and TMPTA coatings filled with 50 vol% OTS treated silica does not contradict with this explanation. The interactions of PEGDA with OTS treated silica are weaker than the interactions with MPS treated silica, hence probably the layer of PEGDA in the glass state is thinner and a considerable part of the PEGDA is still in the rubber state.

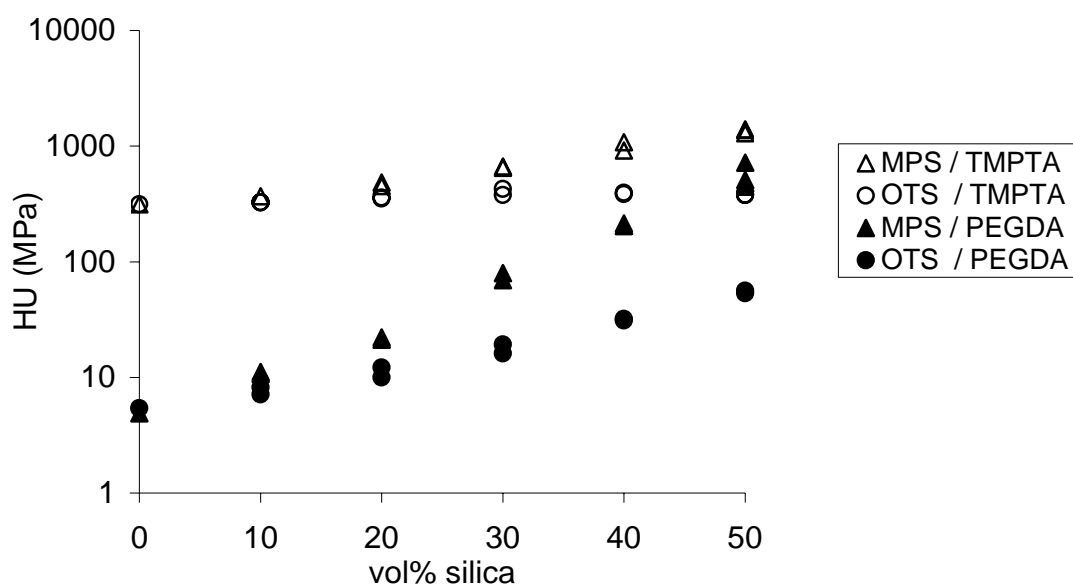


Figure 6.6 *Hardness of PEGDA and TMPTA coatings with MPS and OTS modified silica.*

6.4. Abrasion resistance

The variation in abrasion resistance for the different coatings was very large. The worst coating, pure PEGDA, was already badly damaged after ten passes of the abrading wheels whereas the best coating, TMPTA with 50 vol% silica, was virtually undamaged after 1000 passes of the abrading wheels. The abrasion resistance is found to be dependent on the composition of the coatings, but also on the coating thickness and

adhesion. Coatings that were too thin initially gave a reasonable protection, but even with a minor damage to the coating the substrate was exposed and upon further abrading action the damaged spot grew quickly. Similar problems arose with coatings with a very weak adhesion; these coatings delaminated due to the forces developed during the abrading action. No general values for the required coating thickness and adhesion can be given as these strongly depend on the properties of the coatings themselves. Microscope images of some tested coatings are shown in figure 6.7.

As expected, changing the composition of the coatings had an effect on the abrasion resistance. The most important component for the properties of the coating was the matrix material. Pure PEGDA was an absolute inferior material for the protection against abrasion but pure TMPTA performed already quite good. For both matrix materials, addition of silica (with MPS modification) resulted in an improved abrasion resistance, for instance on a TMPTA coating with 30 vol% silica the wear track could

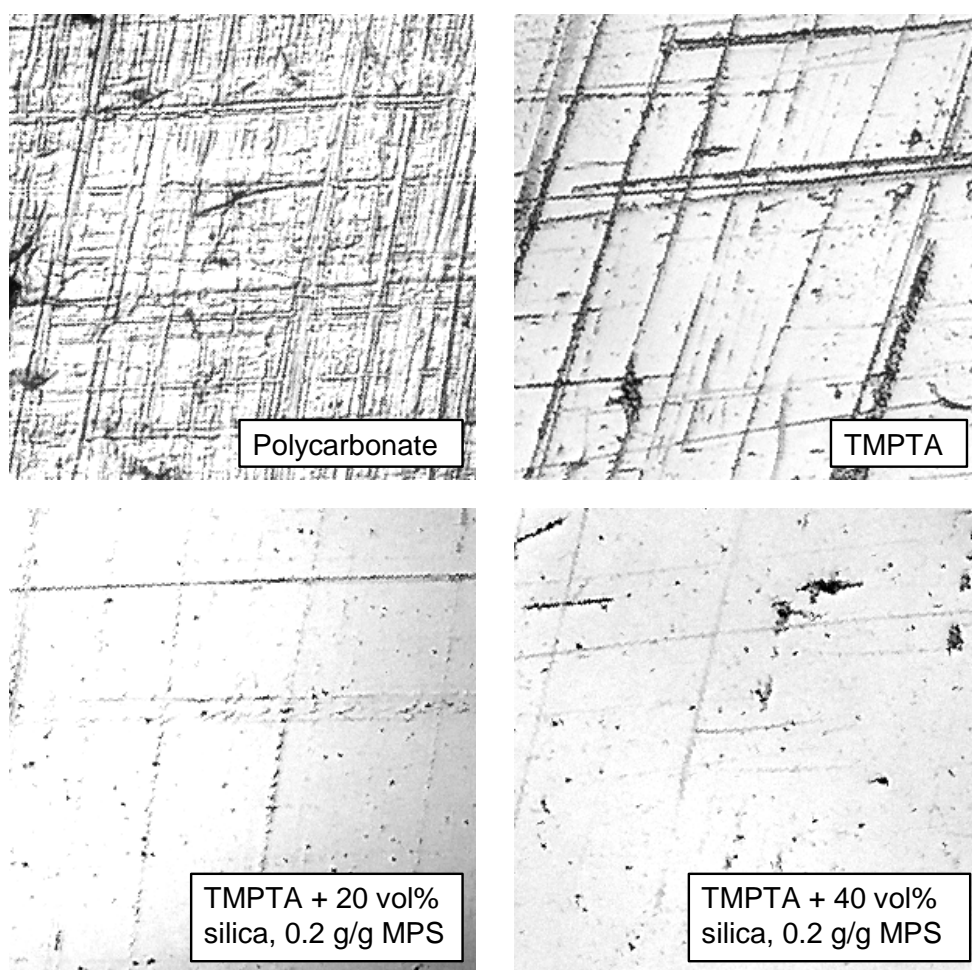


Figure 6.7 Appearance of substrate and coatings after Taber abrasion test (100 cycles, CS-10F wheels, 500g loads).

hardly be seen by the naked eye, even after 500 cycles. The modification of the particles with MPS had a positive effect on the abrasion resistance. The coatings in which silica was modified with 0.2 g/g MPS performed better than the samples in which silica was modified with 0.1 g/g MPS. The abrasion resistance followed the general trend of the hardness and E -modulus of the coatings; the higher these values, the better the abrasion resistance. However, this was only the general trend and coatings with equal hardness did not necessarily have the same abrasion resistance. For instance, PEGDA with 40 vol% silica with MPS modification had a hardness slightly below the hardness of pure TMPTA, but it had a higher abrasion resistance. Even stronger this was seen in the comparison between the coatings and the polycarbonate substrate. The polycarbonate is harder and has a much higher E -modulus than the PEGDA coatings with a filler content of 20 or 30 vol%, but the abrasion resistance is far worse. Evidently other factors also play a significant role. One factor may be the recovery after deformation. In the indentation tests the recovery of the PEGDA-silica coatings were complete whereas the recovery of the TMPTA coating and especially of the polycarbonate was incomplete.

6.5. Conclusions

The fillers can induce a large increase of the hardness and E -modulus of the coatings. The magnitude of the increase depends on the type of matrix material, the type of filler, and on the groups present on the surface of the filler. The reinforcing effect of the fillers is much larger for PEGDA than for TMPTA. The large reinforcing effect for PEGDA may be explained by an increase of the T_g of the PEGDA near the filler surface, which induces a transition from the rubber into the glass state for the PEGDA near the filler surface. For TMPTA this effect does not play a role as it is already in the glass state. The reinforcing effect of silica is enhanced after surface modification of the silica with MPS; this may be explained by stronger interactions between the filler and the matrix as physical bonds are replaced by chemical bonds. The surface modification of silica with OTS decreases its reinforcing effect; this may be explained by weaker interactions between the filler and matrix as the physical interactions between the acrylate matrices and the OTS are weaker than the physical interactions of the acrylate matrices with the silica. The abrasion resistance of the nanocomposite coatings with a high filler fraction is very good. The good abrasion resistance is believed to be due to the high hardness of the coatings and the highly elastic recovery after deformation.

Reference List

1. V. A. Soloukhin, Nanocomposite Hybrid Coatings on Polycarbonate, thesis, TU Eindhoven (2003).
2. F. Bauer, H. J. Glasel, U. Decker, H. Ernst, A. Freyer, E. Hartmann, V. Sauerland, R. Mehnert, *Progress in Organic Coatings*, 47, 147-153 (2003).
3. V. A. Soloukhin, W. Posthumus, J. C. M. Brokken-Zijp, J. Loos, G. de With, *Polymer*, 43, 6169-6181 (2002).
4. J. Gilberts, A. H. A. Tinnemans, *RAD news*, 24, 7-10 (1998).
5. B. Wetzel, F. Hauptert, M. Q. Zhang, *Composites Science and Technology*, 63, 2055-2067 (2003).
6. M. Q. Zhang, M. Z. Rong, S. L. Yu, B. Wetzel, K. Friedrich, *Wear*, 253, 1086-1093 (2002).
7. N. S. Enikolopyan, M. L. Fridman, I. O. Stalnova, V. L. Popov, *Advances in Polymer Science*, 96, 1-67 (1990).
8. R. Rothon, Particulate-filled polymer composites (Longman Scientific & Technical, Harlow, 1995).
9. S. Frings, Organic-Inorganic Hybrid Coatings, thesis, TU Eindhoven (1999).
10. M. W. Ellsworth, D. L. Gin, *Polymer News*, 24(10), 331-341 (1999).
11. A. Ciesielski, An introduction to rubber technology (Shawbury, 1999).
12. B. Pukanszky, E. Fekete, *Advances in Polymer Science*, 139, 109-153 (1999).
13. Y. Ou, F. Yang, Z. Yu, *Journal of Polymer Science Part B: Polymer Physics*, 36, 789-795 (1998).
14. F. Mammeri, L. Rozes, C. Sanchez, E. Le Bourhis, *Journal of Sol-Gel Science and Technology*, 26, 413-417 (2003).
15. C. Vu, O. LaFerte, A. Eranian, *European Coatings Journal*, 64, 66-70 (2002).
16. S. Sepeur, N. Kunze, B. Werner, H. Schmidt, *Thin Solid Films*, 351(1,2), 216-219 (1999).
17. C. G. Reid and A. R. Greenberg, *Journal of Applied Polymer Science* 39, 995-1014 (1990).
18. H. Fukushima, O. Takemoto, M. Tamuraand, K. Yonekura, Coating composition forming wear-resistant coat and article covered with the coat. Mitsubishi Rayon Company, WO9711129, (1998).
19. H. J. Glasel, F. Bauer, H. Ernst, M. Findeisen, E. Hartmann, H. Langguth, R. Mehnert, R. Schubert, *Macromolecular Chemistry and Physics*, 201(18), 2765-2770 (2000).
20. M. Misra, A. Guest, M. Tilley, *Surface Coatings International*, 594-595 (1998).

21. J. W. ten Brinke, V. M. Litvinov, J. E. G. J. Wijnhoven, J. W. M. Noordermeer, *Macromolecules*, 35, 10026-10037 (2002).
22. M. van Es, Polymer-Clay Nanocomposites, thesis, TU Delft (2001).
23. J. B. Donnet, *Composites Science and Technology*, 63, 1085-1088 (2003).
24. H. Van Damme and A. Burr, *Macromolecular Symposia*, 194, 1-11 (2003).
25. R. P. Singh, M. Zhang, D. Chan, *Journal of Materials Science*, 37, 781-788 (2002).
26. Z. S. Petrovic and W. Zhang, *Materials Science Forum*, 352, 171-176 (2000).
27. D. Gersappe, *Physical Review Letters*, 89, 058301-1-058301/4 (2002).
28. M. Sumita, H. Tsukihi, K. Miyasaka, K. Ishikawa, *Journal of Applied Polymer Science*, 29, 1523-1530 (1984).
29. A. Yim, R. S. Chanal, L. E. S. Pierre, *Journal of Colloid and Interface Science*, 43, 583-590 (1973).
30. P. S. Theocaris, *Colloid and Polymer Science*, 263, 863-872 (1985).
31. B. J. Ash and R. W. Siegel, *Materials Letters*, 55, 83-87 (2002).
32. J. Berriot, H. Montes, F. Lequeux, D. Long, P. Sotta, *Macromolecules*, 35, 9756-9762 (2002).
33. J. Berriot, F. Lequeux, H. Montes, H. Pernot, *Polymer*, 43, 6131-6138 (2002).
34. J. Berriot, H. Montes, F. Lequeux, D. Long, P. Sotta, *Europhysics Letters*, 64, 50-56 (2003).
35. B. J. Ash, R. W. Siegel, L. S. Schadler, *Macromolecules*, 37, 1358-1369 (2004).
36. C. Becker, H. Krug, H. Schmidt, *Materials Research Society Symposium Proceedings*, 435, 237-242 (1996).
37. E. Reynaud, C. Gauthier, J. Perez, *La Revue de Metallurgie-CIT/Science et Genie des Matériaux*, 96(2), 169-176 (1999).
38. W. C. Oliver, G. M. Pharr, *Journal of Materials Research*, 7, 1564-1583 (1992).
39. G. M. Swallowe, *Mechanical properties and testing of polymers: an A-Z reference* (1999).
40. Chapter 4, this thesis (2004).
41. H. Montes, F. Lequeux, J. Berriot, *Macromolecules*, 36, 8107-8118 (2003).

Epilogue

7.1. Aims of this study

The project was started with the aim to develop organic-inorganic nanocomposite coatings with good scratch and abrasion resistance and with anti-static properties. The objective of this study was to get insight in what determines these properties rather than producing ‘the perfect coating’. For the properties not only the type and relative amounts of the organic and inorganic components used, but also the interactions between the components and the distribution of the components were expected to be essential. As the distribution of the components and their interactions are established during the preparation of the coatings, studying the processes in the preparation stage was as important as studying the final properties of the coatings.

7.2. Preparation and composition of the coatings

The preparation of the coatings starts with the grafting of silane coupling agents on the metal oxide fillers. A complicating factor in this study was the desire to maintain colloidal stability of the nanoparticles, especially as the stability of the particles changed during the grafting procedure. As a consequence, important parameters for the grafting reactions, like pH and solvent composition, were not optimised for the grafting reactions themselves but for maintaining colloidal stability. The resulting reaction conditions nevertheless were adequate to graft the major part of the added silane coupling agents on the particles.

The next steps in the coating preparation procedure are the mixing of all components, application of the coating formulation on the substrate, and drying of the coatings. As supplied, the nanoparticles can only be dispersed in polar media, thus not in most acrylate resins. After the grafting of silane coupling agents on the nanoparticles, dispersions in media with a lower polarity were possible. Dispersing the nanoparticles in pure acrylate resins was still rarely possible (for the desired filler fractions), but with the aid of small amounts of solvents homogeneous coating formulations with a rheology suitable for coating application could be prepared. During the solvent evaporation after application of the coating formulation colloidal stability of the nanoparticles could be lost. However, aggregation of the nanoparticles in these formulations did not

result in segregation on a macroscopic scale but resulted in the formation of a fractal type continuous particles network.

The last step of the coating preparation was the UV curing of the matrix. In this step chemical bonds between the matrix and the filler should be formed by copolymerisation of the acrylate matrix with MPS that was grafted on the particles. Real-time monitoring of the UV curing showed that the acrylate and the MPS copolymerised as intended. It was expected that the filler particles would absorb UV light, but would not strongly affect the UV curing otherwise. For silica and ATO this expectation was correct, but for tin oxide a strong retardation of the UV curing was found. To explain this retardation, a mechanism for (meth)acrylate radical consumption by tin oxide is proposed that effectively corresponds to catalysis of termination of the free radical polymerisation by disproportionation.

7.3. Properties of the coatings

The introduction of nanoparticles in the acrylate resins resulted in a higher hardness and Young's-modulus of the coatings and in an improved abrasion resistance. Especially for the rubbery PEGDA matrix large increases of these values were found. In comparison with silica, tin oxide and ATO gave harder coatings. It was anticipated that the formation of a chemical bond between the matrix and the filler would be beneficial for mechanical properties of the composite. Indeed this was found, for coatings with chemical bonds between the filler and the matrix higher values for hardness and Young's-modulus were found than for analogues coatings without these chemical bonds. Also the elastic recovery after deformation was enhanced by the chemical bonds.

Beforehand it was uncertain whether the chosen concept for lowering of the electrical resistivity of the coatings would be successful. It was expected that the grafting of an insulating layer of silane coupling agents on the ATO particles would increase the electrical resistance between the particles, perhaps preventing a significant lowering of the electrical resistivity of the composite. Indeed a rise of the coating resistivity with increasing amount of silane coupling agents was found, but within acceptable limits. However, the occurrence of two types of resistivity vs ATO concentration curves, depending on the grafting density, was a surprise. An explanation for the occurrence of two curve types was found in a difference between coatings with aggregated particles and coatings with well-dispersed particles. For the coatings with aggre-

gated particles a good match between the experimental data and a theoretical model was found.

7.4. Suggestions for further research

One of the most surprising results of this study was the retardation of the curing of the coatings by tin oxide. A mechanism explaining this retardation was proposed, but not verified. The relative redox potentials of the (meth)acrylate radicals and of the tin oxide are crucial for this mechanism. The retardation should only occur if the redox potential of the (meth)acrylate radicals is between the valence band and the conduction band of the semiconductor. It might be useful for verification of this mechanism to carry out free radical polymerisations with other monomer semiconductor combinations that fulfil this requirement.

The adhesion of the nanocomposite coatings was found to strongly decrease with increasing filler fraction. This may be linked to a more limited penetration of the acrylate in the polycarbonate substrate. Measurements with a confocal Raman microscope or with ATR-IR spectroscopy may be useful to obtain quantitative data regarding the acrylate diffusion.

In this thesis the chemical structure of the nanocomposite coatings is described. The physical interactions between the different components, however, are not elucidated. Preliminary solid state NMR relaxation measurements and DSC (ΔC_p) measurements indicate that the acrylate polymer has a lower mobility near the filler matrix interface than in the bulk. As in nanocomposites with a high filler fraction virtually all matrix material is within a few nm of the fillers, the fraction of the acrylate that is immobilised can be very high. The properties of this immobilised layer may be substantially different from the bulk acrylate, and may be very important for the mechanical properties of the composite. To understand the mechanical properties of the nanocomposite coatings a further study of this immobilised layer, depending on surface treatment of the filler, type of acrylate, and type of filler, would be useful.

The colloidal stability of the nanoparticles in apolar media played an important role in this study, but the coating formulations contained too many components to study the colloidal stability adequately. Control over the colloidal stability is especially important for the preparation of anti-static coatings with a low fraction of conductive filler. A good electrical conductivity at low filler fractions can only be reached when the conductive filler is organised in a continuous network. Such a network is only formed when an initially stable dispersion of conductive particles becomes unstable

and the particles aggregate. Although the general trends that determine the colloidal stability are known, a better understanding of the colloidal stability is strongly desired to improve the control over the properties of the coatings. This may only be possible by making a step backwards, and to gather information regarding the colloidal stability of the nanoparticles (with grafted silane coupling agents) in different single component solvents. Emphasis may be laid on the difference in the surface energies of the dispersing medium and of the particles, as this is thought to be a dominant factor for colloidal instability.

Appendix I

Derivation of the curing rate equation

By approximation the curing rate is determined by the propagation rate R_p for the polymerisation of the (meth)acrylate groups. This propagation rate is determined by the chance that the radical and a (meth)acrylate group meet and the chance that this encounter results in a reaction:

$$R_p = k_p \cdot [M] \cdot [R^*] \quad [A1]$$

where k_p is the propagation rate constant in $\text{mol}^{-1} \text{L s}^{-1}$, $[M]$ is the concentration of (meth)acrylate in mol/L , and $[R^*]$ is the radical concentration in mol/L . The number of free radicals in the system is determined by the rate at which they are generated and the rate at which they are consumed. The radicals are generated by illumination of the photoinitiator. The rate of this process depends on the number of photons that are absorbed by the photoinitiator and the efficiency with which the absorption of a photon results in the formation of initiating radicals:

$$R_i = 1000 \cdot \Phi \cdot I_a \quad [A2]$$

where R_i is the rate of radical generation in $\text{mol radicals L}^{-1} \text{s}^{-1}$, Φ is the efficiency of the photoinitiator in $\text{radicals photon}^{-1}$, and I_a is the amount of absorbed light in a certain volume in $\text{einstein cm}^{-3} \text{s}^{-1}$. For a system where the light is only absorbed by the photoinitiator the amount of absorbed light can be calculated by:

$$I_a = I_0 \cdot \left(1 - 10^{-\varepsilon[PI] \cdot d}\right) \cdot \frac{A}{V} \quad [A3]$$

where I_0 is the flux of incident light through a certain area in $\text{einstein cm}^{-2} \text{s}^{-1}$ (note that the dimensions of I_a and I_0 are not equal), ε is the extinction coefficient of the photoinitiator in $\text{L mol}^{-1} \text{cm}^{-1}$, $[PI]$ is the photoinitiator concentration in mol/L , A is the to the light exposed area of the sample in cm^2 , and V is the volume of the sample in cm^3 , and d is the thickness of the sample in cm .

The main process for radical consumption is the reaction between two radicals; the two radicals may form a new covalent bond or one hydrogen atom may be transferred from one radical to the other. The rates of both reactions scale with the probab-

ity that two radicals meet and the chance that such an encounter results in either reaction. In a simplified form the radical consumption is expressed by:

$$R_t = k_t [R^*]^2 \quad [A4]$$

where R_t is the rate of radical consumption in $\text{mol L}^{-1} \text{s}^{-1}$ and k_t is the termination rate constant in $\text{mol}^{-1} \text{L s}^{-1}$.

During curing the radical concentration rapidly changes until the rate of radical consumption is in equilibrium with the rate of radical generation (steady state approximation):

$$R_t = R_i, \text{ therefore: } k_t [R^*]^2 = 1000 \cdot \Phi \cdot I_a \quad [A5]$$

leading to,

$$[R^*] = \sqrt{1000 \cdot \Phi \cdot I_a / k_t} = \sqrt{1000 \cdot \Phi \cdot I_0 \cdot (1 - 10^{-\varepsilon [PI] \cdot d}) \cdot A / (k_t \cdot V)} \quad [A6]$$

It should be noted that due to the light gradient in the coating there is also a gradient for the radical concentration and the calculated $[R^*]$ is an averaged value. This averaged value should only be used if the light absorbance is small as this implies that also the gradient of the light intensity and hence the gradient of the radical concentration will be small.

Combining [A6] with [A1] and $V/A = d$ the expression for the curing rate becomes:

$$R_p = k_p \cdot [M] \cdot \sqrt{1000 \cdot \Phi \cdot I_0 \cdot (1 - 10^{-\varepsilon [PI] \cdot d}) / (k_t \cdot d)} \quad [A7]$$

Appendix II

Electron tunneling

Electron tunnelling is a very complex process that depends on a large number of variables like distance, dielectric constant, applied voltage, filler shape, temperature, effective electron mass, etc. Radhakrishnan⁽¹⁾ presented equations for several electron transport mechanisms between filler particles that are not in direct contact. He showed that the separation between the particles together with the applied voltage and the temperature determine which transport mechanism prevails. Unfortunately, his equations contain several parameters that cannot easily be evaluated numerically, which limits the application of these equations. Sherman *et al.*⁽²⁾ derived a model for the tunneling component of the resistivity of a conductor filled polymer. By restricting the validity of the model with limiting conditions for temperature and applied voltage they could omit some of the electron transport mechanisms that are incorporated in the model of Radhakrishnan. The limiting conditions are met by the experiments described in this thesis. Another serious simplification of the model is the neglecting of interactions between the particles and size effects, which results in an inaccurate description for the particle distribution. However, the model is useful to get a better idea for how large the contribution of the electron tunnelling to the resistivity may be. Their final equation reads:

$$R_t = \frac{\pi \cdot h^2 \cdot L \cdot (L + d)}{6 \cdot e^2 \cdot \sqrt{2 \cdot m^* \cdot V} \cdot a_{ct}} \cdot \left(1 - \frac{\phi}{\phi_c}\right) \cdot e^{\frac{\pi^2}{h} \sqrt{2 \cdot m^* \cdot V} \cdot L} \quad [\text{AII-1}]$$

where R_t is the tunnelling resistivity for the composite, h is the Planck constant, L is the distance between adjacent particles, d is the diameter of the particles (for ATO 7 nm), e is the elementary charge, m^* is the effective electron mass, V is the barrier height, and a_{ct} is the effective tunnel junction cross-section area. Figure AII.1 shows the electrical resistivity as function of the distance between two filler particles according to Eq. [AII-1] with the estimated values^(2,3) $m^* = 5 \times 10^{-32}$ kg, $V = 1$ eV = 1.6×10^{-19} J, $a_{ct} = 4 \times 10^{-19}$ m² and $\phi/\phi_c = \{(d+L)/d\}^{1/3}$ (assuming that the particles are placed at the centre points in a regular lattice with a variable length unit of $d+L$). The dotted lines in the figure represent the resistivities of the matrix and the filler, which act as

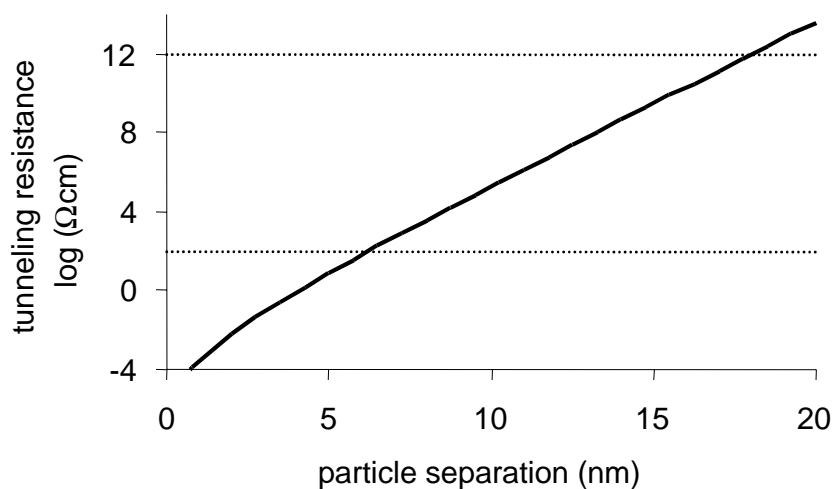


Figure AII.1 *Theoretical tunnel resistivity according to the model of Sherman et al. The dotted lines represent the estimated bulk resistivities of ATO particles (lower line) and Ebecryl 745 (upper line).*

limiting values beyond which the tunnelling resistivity is unimportant for the resistivity of the composite. When the tunnelling resistivity is higher than the bulk resistivity of the matrix material, electron transport in the matrix will take place by the ‘normal’ conduction mechanism and the tunnelling contribution can be ignored. When the tunnelling resistivity (in the matrix) is lower than the resistivity of the filler, the resistance within the filler will be the limiting factor for electric transport and the contribution of the resistance in the matrix material to the composite resistivity may be ignored.

Using the model of Radhakrishnan, a particle separation of 18 nm results in a tunnel resistivity of 10^{12} Ωcm, which is about the resistivity that is measured for Ebecryl 745 coatings with an ATO fraction of 5 vol%. As the separations for a filler fraction of 2 vol% are about 10-50 nm (see figure 5.6d), a particle separation of 18 nm for coatings with a filler fraction of 5 vol% is reasonable. Hence, electron tunnelling might in this case be the determining factor for the resistivity of the composite, though the significance of this match is not very high as it is based on crude estimates of several variables. With increasing volume fractions the distances between the particles decrease and a gradual decrease of the resistivity is expected.

The resistivity of type II coatings with an ATO fraction of 30 vol% is about 10^5 Ωcm; in the model of Radhakrishnan this corresponds to a tunnelling distance of about 10 nm. Moreover, the model also indicates that for particle separations less than 6 nm the tunnel resistivity is smaller than 10^2 Ωcm, which is the estimated resistivity of a

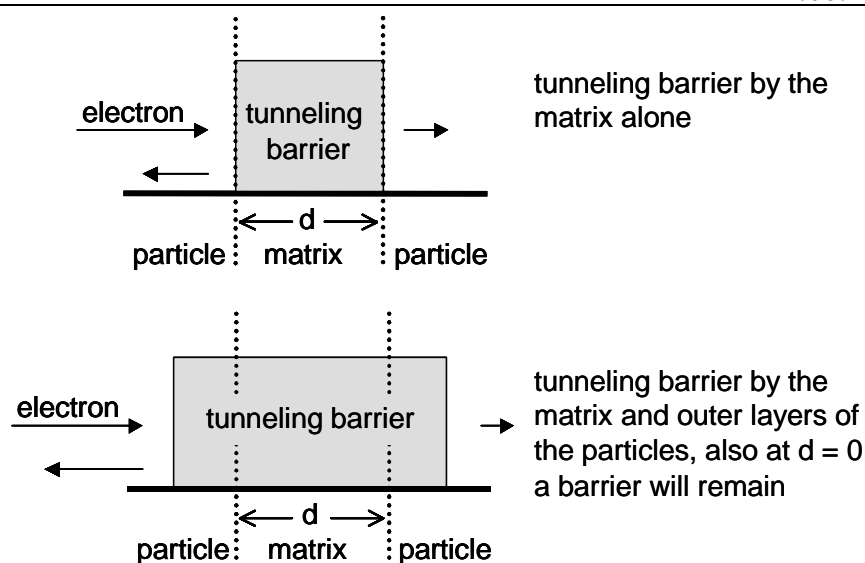


Figure AII.2 Schematic representation of the tunneling barrier.

coating consisting only of ATO particles (estimated on basis of the resistivities of type I coatings with a high fraction of aggregated ATO particles). These values for the particle separations are unrealistic high; probably the tunnelling barrier is larger than estimated. To obtain a resistivity of $10^2 \Omega\text{cm}$ (lowest experimental resistivity) at a more realistic 1 nm (aggregated particles), the combined term Vm^* has to be 86 times higher, which is not realistic. The problems with the fitting of the model to the experimental data may be due to the neglecting of the resistance within the filler. The outer layer of the ATO particles likely is enriched with antimony and consequently has a much higher resistance than the core of the particle⁽⁴⁾. Hence the outer layer of the particle may be part of the tunnel barrier; when the size of this additional barrier equals the barrier of a polymer layer with a thickness of a few nm (figure AII.2), it may explain the poor fitting of the resistivity at small particle separations. However, the high resistivities found for tin oxide cannot be explained with the same considerations. Here the high resistivity of bulk tin oxide may play a role.

Reference List

1. S. Radhakrishnan, *Polymer Communications*, 26, 153-157 (1985).
2. R. D. Sherman, L. M. Middleman, S. M. Jacobs, *Polymer Engineering and Science*, 23(1), 36-46 (1983).

Appendix II

3. A. Chatterjee and D. Chakravorty, *Journal of Physics. D: Applied Physics*, 23, 1097-1102 (1990).
4. M. J. van Bommel, W. A. Groen, H. A. M. van Hal, W. C. Keur, T. N. M. Bernards, *Journal of Materials Science*, 34(19), 4803-4809 (1999).

Summary

This thesis deals with the preparation and characterisation of UV-curable acrylate metal oxide nanocomposite coatings. The main topics of research are surface modification of metal oxide nanoparticles with silane coupling agents, the incorporation of these modified fillers in UV-curable acrylate matrices, the influence of the fillers on the UV curing, and the electrical and mechanical properties of the coatings. The coatings are composed of silica, tin oxide, or antimony doped tin oxide (ATO) as filler; 3-methacryloxypropyltrimethoxysilane (MPS) or octyltrimethoxysilane (OTS) as silane coupling agent; and polyethyleneglycoldiacrylate (PEGDA), trimethylolpropanetriacrylate (TMPTA), or Ebecryl 745 as acrylate matrix.

The silane coupling agents were grafted on the metal oxide nanoparticles to increase the compatibility of the particles with the acrylate matrix. The reactions involved in the grafting of MPS on the particles were followed with ^{29}Si -NMR. The hydrolysis of the methoxy groups of MPS is found to be the rate determining step. As the hydrolysis is base catalysed, the reactions proceed faster in dispersions with a high pH. The kinetics measurements also revealed that reaction of MPS with ATO is faster than homocondensation of the MPS. Solid state NMR revealed that chemical bonds are formed between the MPS and the particles. FTIR measurements revealed that the carbonyl group of the grafted MPS forms a hydrogen bond with the metal oxide surface. The maximum amount of MPS that can be grafted on the particles corresponds to one monolayer of MPS molecules with an orientation parallel to the metal oxide surface. If for the grafting an amount of MPS is used that is lower than the amount needed for monolayer coverage of the particles, the majority of the MPS is bonded to the particles.

The UV curing of the coatings was followed by real-time FTIR. Silica and ATO do not interfere directly with the curing reactions, although ATO can retard the curing due to strong absorption of the UV light. Tin oxide however interferes directly with the curing reactions, resulting in a strong retardation of the curing. It is suspected that tin oxide can catalyse termination of the radical polymerisation by disproportionation. In homopolymerisations the acrylate resins polymerise faster than MPS. However, during curing of the coatings the methacrylate groups of the MPS react faster than the acrylate

groups of the acrylate resin. This indicates that the MPS and the acrylate copolymerise, and consequently it indicates that a chemical link between the nanoparticles and the matrix is formed.

ATO and tin oxide are electrically conductive materials, hence when used as filler they lower the electrical resistivity of the composite. However, it was unknown whether the coating resistivity would be affected by the grafting of silane coupling agents on the particles. It is found that decreasing the amount of grafted MPS on ATO results in a decrease of the electrical resistance between the particles, and a lower resistivity of the composite. Furthermore the grafted MPS is found to have a strong effect on the distribution of the ATO particles in the acrylate matrix. With a large amount of grafted MPS, the ATO particles may have a good colloidal stability in an acrylate matrix, leading to a homogeneous distribution of the particles. With a small amount of grafted MPS, the ATO particles lack colloidal stability in an acrylate matrix and additional solvents need to be added for a stable dispersion. Upon drying of these dispersions, the ATO particles aggregate and under favourable conditions a fractal type ATO particle network can be formed. A coating with an ATO particle network has, especially at low-volume fractions, a much lower electrical resistivity than a coating with homogeneously distributed particles.

The hardness and E-modulus of the coatings were measured by microindentation. It was found that the hardness and E-modulus both increase strongly with the filler fraction. Also the amount and type of silane coupling agent grafted on the filler particles were found to have a strong influence on hardness and E-modulus. The increase of the hardness and E-modulus was largest with a large amount of grafted MPS. Moreover, when MPS was grafted on the fillers, the coatings showed more elastic recovery after the indentation than when OTS was grafted on the fillers. Tests with a Taber abrader revealed that the abrasion resistance is strongly enhanced by the nanoparticles.

Samenvatting

In dit proefschrift wordt het maken en de karakterisering van UV-uithardende acrylaat metaal oxide nanocomposiet coatings beschreven. De belangrijkste onderdelen van dit onderzoek zijn de oppervlakte modificatie van de metaaloxide nanodeeltjes met silanen, het dispergeren van deze gemodificeerde deeltjes in de acrylaat matrix, de invloed van de vulstoffen op de UV-uitharding, en de elektrische en mechanische eigenschappen van de coatings. De coatings zijn opgebouwd uit silica, tin oxide, of antimoon gedoopt tin oxide (ATO) als vulstof; 3-methacryloxypropyltrimethoxysilaan (MPS) of octyltrimethoxysilaan (OTS); en polyethyleenglycoldiacrylaat (PEG-DA), trimethyloltriacrylaat (TMPTA) of Ebecryl 745 als matrix.

Om de compatibiliteit van de metaaloxide nanodeeltjes met de acrylaat matrix te verbeteren werd het metaaloxide oppervlak gemodificeerd door reactie met MPS of OTS. Het verloop van de reactie van MPS met de deeltjes werd gevolgd met ^{29}Si -NMR. De snelheidsbepalende stap voor deze reactie is de hydrolyse van de methoxy groep van MPS. De hydrolyse wordt gekatalyseerd door basen, dus de reacties verlopen sneller bij een hogere pH. Uit de experimenten bleek dat de condensatie van MPS met ATO sneller is dan de homocondensatie van MPS. Met vaste stof NMR werd vastgesteld dat er een chemische binding tussen de MPS en de deeltjes wordt gevormd. Met FTIR werd vastgesteld dat de carbonylgroep van MPS een waterstof brug vormt met het metaal oxide oppervlak. De maximum hoeveelheid MPS dat aan de deeltjes gebonden wordt komt overeen met een monolaag van parallel aan het metaal oxide oppervlak georiënteerde MPS moleculen.

De UV-uitharding van coatings werd gevolgd met FTIR. ATO, en in mindere mate tin oxide, absorberen UV licht. Hierdoor is de hoeveelheid gevormde radicalen lager en is de uitharding trager. De directe invloed van silica en ATO op de uithardingsreacties is gering. Tin oxide daarentegen heeft een grote invloed op de uithardingsreacties; bij direct contact tussen de tin oxide en de matrix danwel MPS wordt de uitharding sterk vertraagd. Mogelijkerwijs wordt terminatie door disproportionering gekatalyseerd door tin oxide. In homopolymerisaties is de omzetting van de acrylaten sneller dan van MPS, echter in een copolymerisatie van een acrylaat met MPS is de omzetting van MPS sneller. Ook tijdens de uitharding van de nanocomposiet coatings wordt het

MPS dat op de deeltjes verankerd zit sneller omgezet dan het acrylaat. Dit duidt op copolymerisatie van het MPS met het acrylaat, dus het is aannemelijk dat de deeltjes chemisch verbonden worden met de matrix.

ATO en tin oxide hebben een goede elektrische geleidbaarheid, dus bij gebruik als vulstof verlagen ze de elektrische weerstand van het composiet. De invloed van de op de deeltjes verankerde silanen op de elektrische weerstand van het composiet was onbekend. Het bleek dat de vermindering van de hoeveelheid MPS op de ATO deeltjes resulteert in een lagere elektrische weerstand tussen de deeltjes, en dus in een lagere weerstand van het composiet. Bovendien heeft het MPS een grote invloed op de verdeling van de ATO deeltjes in de matrix. Met een maximale MPS bedekking kan de ATO een goede colloïdale stabiliteit in de acrylaat matrix hebben, zodat de ATO deeltjes homogeen verdeeld zijn. Met een onvolledige MPS bedekking is colloïdale stabiliteit van de ATO deeltjes in de acrylaat matrix alleen niet mogelijk, voor een goede stabiliteit is de toevoeging van oplosmiddelen vereist. Na het aanbrengen van een dergelijke coating formulering verdampen de oplosmiddelen en vindt aggregatie van de ATO deeltjes plaats. Onder gunstige omstandigheden resulteert dit in een fractaal netwerk van ATO deeltjes. Een coating met een fractaal ATO deeltjes netwerk heeft een veel lagere elektrische weerstand dan een coating met homogeen verdeelde ATO deeltjes.

De hardheid en de E-modulus van de coatings werd gemeten met microindentatie. Zowel de hardheid als de E-modulus stijgen sterk bij verhoging van de fractie vulstof. Daarnaast worden de hardheid en E-modulus beïnvloed door de hoeveelheid en type van het silaan dat gebruikt is voor de oppervlaktemodificatie van de vulstof. De grootste stijging van de hardheid en E-modulus werd gevonden bij een volledige bedekking van de deeltjes met MPS. Daarnaast is de elastische terugvering na de indentatie hoger wanneer de deeltjes bedekt zijn met MPS dan wanneer ze bedekt zijn met OTS. Testen met een Taber Abrader lieten zien dat de slijt en kras bestendigheid van de coatings sterk verbetert door de toevoeging van nanodeeltjes.

Dankwoord

Tijdens het onderzoek en het schrijven van dit proefschrift heb ik op de steun van veel mensen kunnen rekenen, op inhoudelijk en organisatorisch vlak, maar ook op het meer persoonlijke vlak. Bij deze wil ik hen daarvoor bedanken.

Allereerst wil ik mijn promotor, professor Rob van der Linde, bedanken voor de vrijheid die ik gekregen heb om zelf invulling aan mijn onderzoek te geven, maar ook voor de kritische noten wanneer dit nodig was. Ook de rollen van mijn tweede promotor Bert de With en mijn begeleiders José Brokken en Louis Tinnemans waren zeer belangrijk. Hun opmerkingen hebben een positieve invloed op mijn bewijsvoering gehad. Ik wil graag mijn waardering uitspreken naar Mariëlle Wouters en Joris Gilberts voor hun praktische hulp bij experimenten en bij het schrijven. Ik ben zeer erkentelijk aan Jos Laven voor de tijd die hij heeft vrijgemaakt om diverse onderwerpen met mij te bespreken.

Een bekend gezegde luidt: eerst zien, dan geloven. Dit geldt zeker voor wetenschappelijk onderzoek; de uitvoering van de diverse analytische methoden en de juiste interpretatie van de resultaten is dus cruciaal. Ik wil dan ook graag mijn waardering uitspreken voor de mensen die mij hierbij hebben geholpen. Pieter Magusin, Marcel van Genderen, Eugene van Oers, Otto van Asselen, Joachim Loos, Anne Spoelstra, Paulien Smit, Wieb Kingma, Niek Lousberg en Marco Hendrix, bedankt.

Naast de voorgenoemde mensen heb ik bijna iedereen binnen SPC en SVM wel eens lastiggevallen met een vraag of een klein probleempje. De bereidheid om te helpen was altijd groot; deze goede collegialiteit waardeer ik in hoge mate. Onderzoek gaat gepaard met successen en met frustraties, en voor beide is het prettig om ze met iemand te kunnen delen. Hiervoor wil ik in het bijzonder Vincent, Delphine, Marshall, Auke, Gabriëlle, Okan, Nathalie, Francis en Robert bedanken.

Curriculum Vitae

Willem Posthumus was born on the 5th of December 1972 in Wijnjeterp. In 1991 he completed secondary education (VWO) at the Ichthus College in Drachten. In the same year he started studying chemistry at the Rijksuniversiteit Groningen. As part of this study he did two research projects: in the group of professor Engberts he studied solvent effects on the aggregation of surfactants and in the group of professor Ahlberg at Göttenborgs Universitetet he did synthetic work. In 1997 he graduated with as specialization organic chemistry. Besides studying, he worked from 1994 to 1997 for the foundation for housing of exchange students in Groningen as student manager. From 1998 to 1999 he worked for Philips CFT. In the end of 1999 he started his PhD in the Coatings Technology group of professor Van der Linde at the Technical University of Eindhoven, which has resulted in this thesis.